

## 4.2.2 1/3.5 Scale Test

### 1) Objectives

The ACC design uses an anti-vortex cap at the top of the standpipe to prevent the formation of a vortex as the flow drains from the tank such that the flow will only switch from a high flow to a lower flow when the level in the ACC drops below the top of the standpipe.

Without the anti-vortex cap it is possible for supercritical flow to form at the standpipe inlet as the water level approaches the top of the standpipe. Under these conditions and gas could be entrained, and the flow rate would not switch smoothly. The purpose of these experiments was to demonstrate that the inclusion of the anti-vortex cap will promote smooth flow switching as the tank water level decreases.

The test was conducted to confirm the flow behavior and potential for vortex formation in the ACC and to confirm the effect of the anti-vortex cap.

### 2) Test Apparatus

The outline drawing of the test facility is shown in Fig. 4.2.2-1. The test apparatus consists of the standpipe, test tank, pump, and piping. The anti-vortex cap that is installed at the top of the standpipe was made of transparent acrylate such that the flow can be observed at the standpipe inlet. The scale of the standpipe inlet is 1/3.5 of the actual standpipe design.



**Fig. 4.2.2-1 Outline Drawing of 1/3.5 Scale Test Apparatus**



### 3) Testing Method

(1) The experiment was scaled using the Froude Number as the basis since there was an open tank with a fluid surface. The relationship between the model tank ( $m$ ) and the actual accumulator ( $p$ ) is given below assuming the Froude Number is defined as

$$Fr = \frac{V}{(g \cdot L)^{0.5}} \quad (4-2)$$

And  $Fr_p = Fr_m$  (4-3)

$$Q_p = \left( \frac{L_p}{L_m} \right)^{2.5} \cdot Q_m \quad (4-4)$$

$$V_p = \left( \frac{L_p}{L_m} \right)^{0.5} \cdot V_m \quad (4-5)$$

$$t_p = \left( \frac{L_p}{L_m} \right)^{0.5} \cdot t_m \quad (4-6)$$

where

$Fr$	:	Froude number
$L$	:	Typical dimension
$Q$	:	Typical flow rate
$V$	:	Typical velocity
$t$	:	Time
$p$	:	Subscript denoting the actual ACC
$m$	:	Subscript denoting the 1/3.5 scale model

(2) The flow rate was measured by an ultrasonic flow meter and the tank water level was measured by the level marking on the sidewall of the tank.

### 4) Test Conditions

The test conditions are shown in Table 4.2.2-1. Two types of standpipe inlet (with the anti-vortex cap and without it) were tested. The tests were performed using two flow rates in which the test and actual ACC Froude numbers were preserved. The flow rates were [ ] and [ ]. These cover the expected flow rates at flow switching for minimum and maximum initial gas pressures, respectively. The injection characteristics with test flow rates are shown in Figs. 4.2.2-2 to 4.2.2-5.

**Table 4.2.2-1 Test Conditions**

Test Number	Test Condition			Remarks	Corresponding Actual Condition	
	Anti-vortex Cap	Flow Characteristics	Flow Rate just before switching (gpm (l/sec))		Initial Gas Pressure (psig (MPa(g)))	Flow Rate just before switching (gpm (m <sup>3</sup> /h))
1-1	No	Fig. 4.2.2-2	[ ]	Froude number is preserved.	[ ]	[ ]
1-2	Yes	Fig. 4.2.2-3	[ ]		[ ]	[ ]
2-1	No	Fig. 4.2.2-4	[ ]		[ ]	[ ]
2-2	Yes	Fig. 4.2.2-5	[ ]		[ ]	[ ]

## 5) Parameters and Measuring Equipment

Flow rate and water level were measured to confirm the conditions during flow switching. The flow rate was measured using an ultrasonic flow meter and the tank water level was measured by the level markings on the sidewall of the tank.

## 6) Test Results and Consideration

Test results are summarized in Table 4.2.2-2. The flow at the inlet for various conditions is shown in Photos. 4.2.2-1(1/2), (2/2) through 4.2.2-2(1/2), (2/2). The following observations were made during the test.

- (1) In the case of the standpipe inlet without the anti-vortex cap, a slight surface dimple appeared above the inlet and the initiation of supercritical flow developed when the water level began to decrease. When the water level decreased further, the supercritical flow condition was apparent and the surface dimple reached into the standpipe, and gas entrainment occurred. (Photo. 4.2.2-1(1/2), (2/2))
- (2) Below the water level where the supercritical flow condition becomes apparent, the critical depth became smaller consistent with the water level reduction. This resulted in a lower flow rate and a slower reduction of the water level.
- (3) The condition described in (2) above is apparent in the wave pattern. For example, in Fig. 4.2.2-2, supercritical flow was apparent, gas entrainment started 26 seconds after initiation of the test, and the variation of the flow rate became larger. As the flow rate became smaller, it took as long as 5 seconds before the flow rate into the standpipe became zero.
- (4) This qualitative condition appeared in the case of both the minimum initial gas pressure of [ ] and the maximum initial gas pressure of [ ] without any significant differences.
- (5) In the case of the standpipe inlet with the anti-vortex cap, a slight disturbance appeared on the water surface as the water level decreased from just above the upper end of the cap to the lower end of the cap. However, neither a vortex nor a supercritical flow occurred, and the flow rate switched sharply over a short period of time. (Photos. 4.2.2-2(1/2), (2/2))

This condition is apparent in the wave pattern. For example, in Fig. 4.2.2-3, the flow rate into the standpipe became zero in approximately 1 second. The flow rate switched much more quickly than the case without the anti-vortex cap (which was approximately 5 seconds in Fig. 4.2.2-2).

- (6) Based on the data and visual observations described above, the desired effects of the anti-vortex cap were confirmed.

**Table 4.2.2-2 Summary of Test Results**

Test Number (T. No)	Test Condition		Test Results		
	Flow Characteristics	Anti-vortex Cap	Vortex Formation	Time to finishing switching (sec)	Remark
1-1	Fig. 4.2.2-2	No	Yes	Approx. 5	Photo. 4.2.2-1(1/2), (2/2)
1-2	Fig. 4.2.2-3	Yes	No	Approx. 1	Photo. 4.2.2-2(1/2), (2/2)
2-1	Fig. 4.2.2-4	No	Yes	[       ]	-
2-2	Fig. 4.2.2-5	Yes	No	[       ]	-

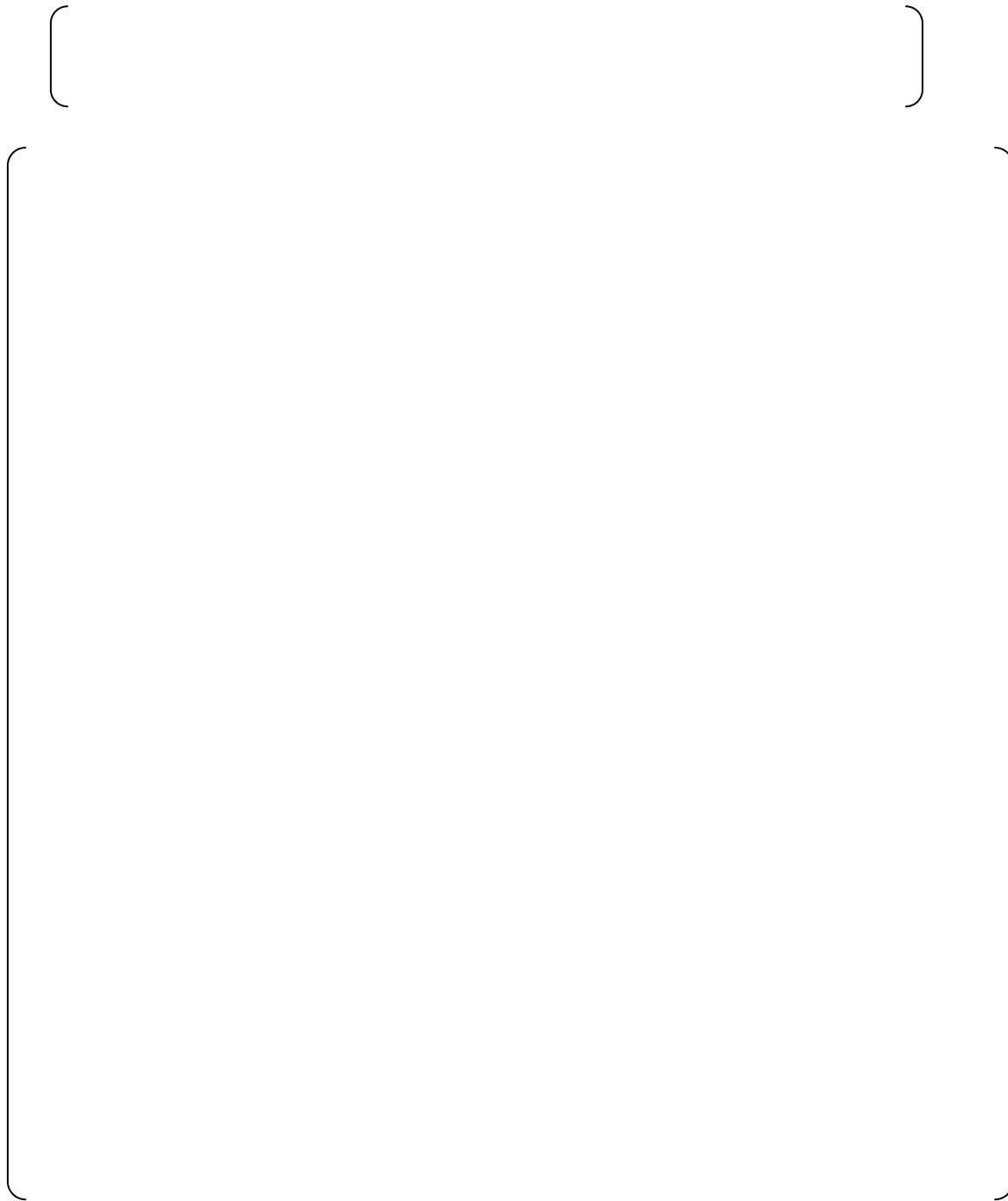


**Photo. 4.2.2-1 (1/2) Visualization of Flow without Anti-Vortex Cap (T. No. 1-1) 1/2**

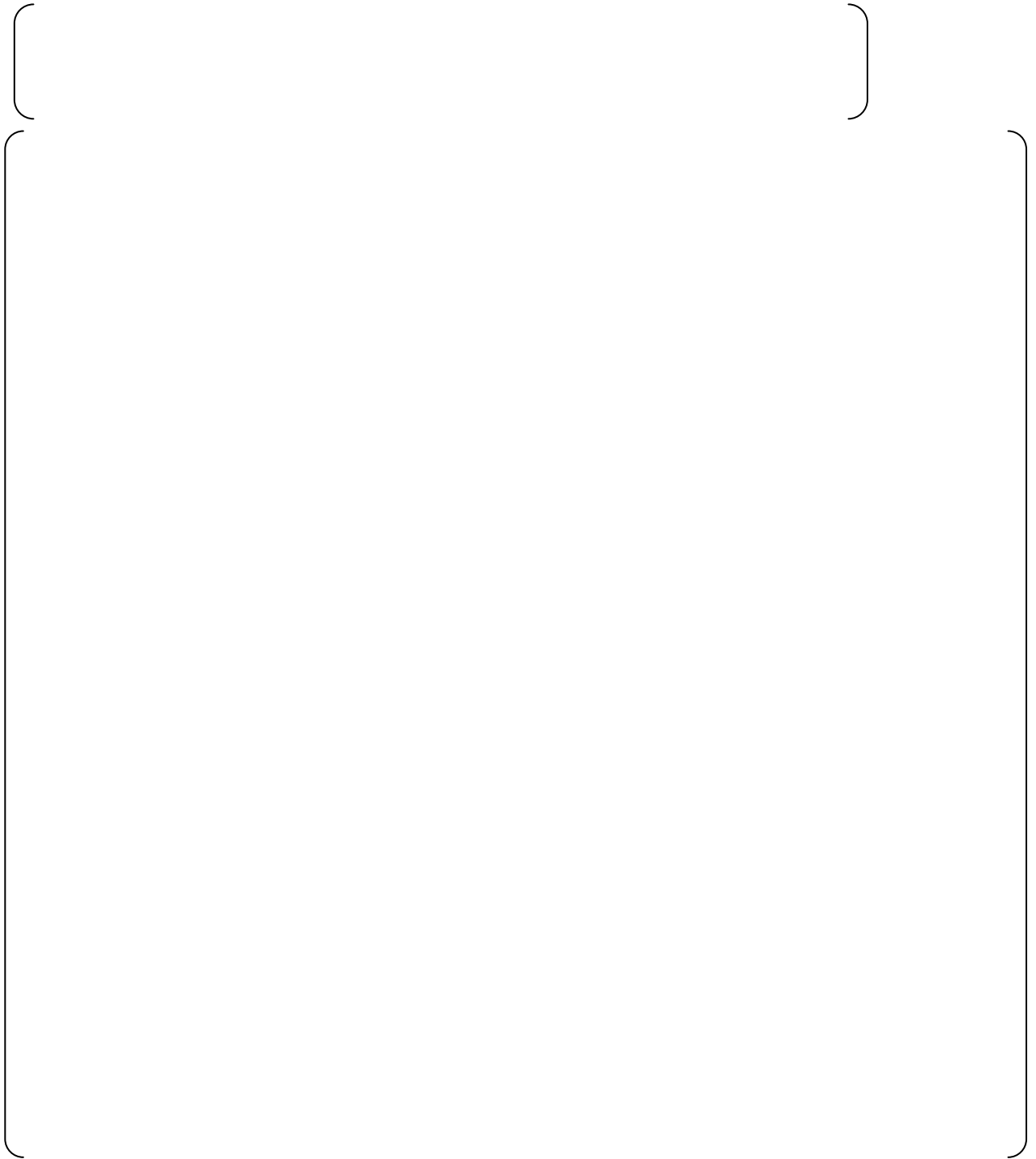


**Photo. 4.2.2-1 (2/2) Visualization of Flow without Anti-Vortex Cap (T. No. 1-1) 2/2**

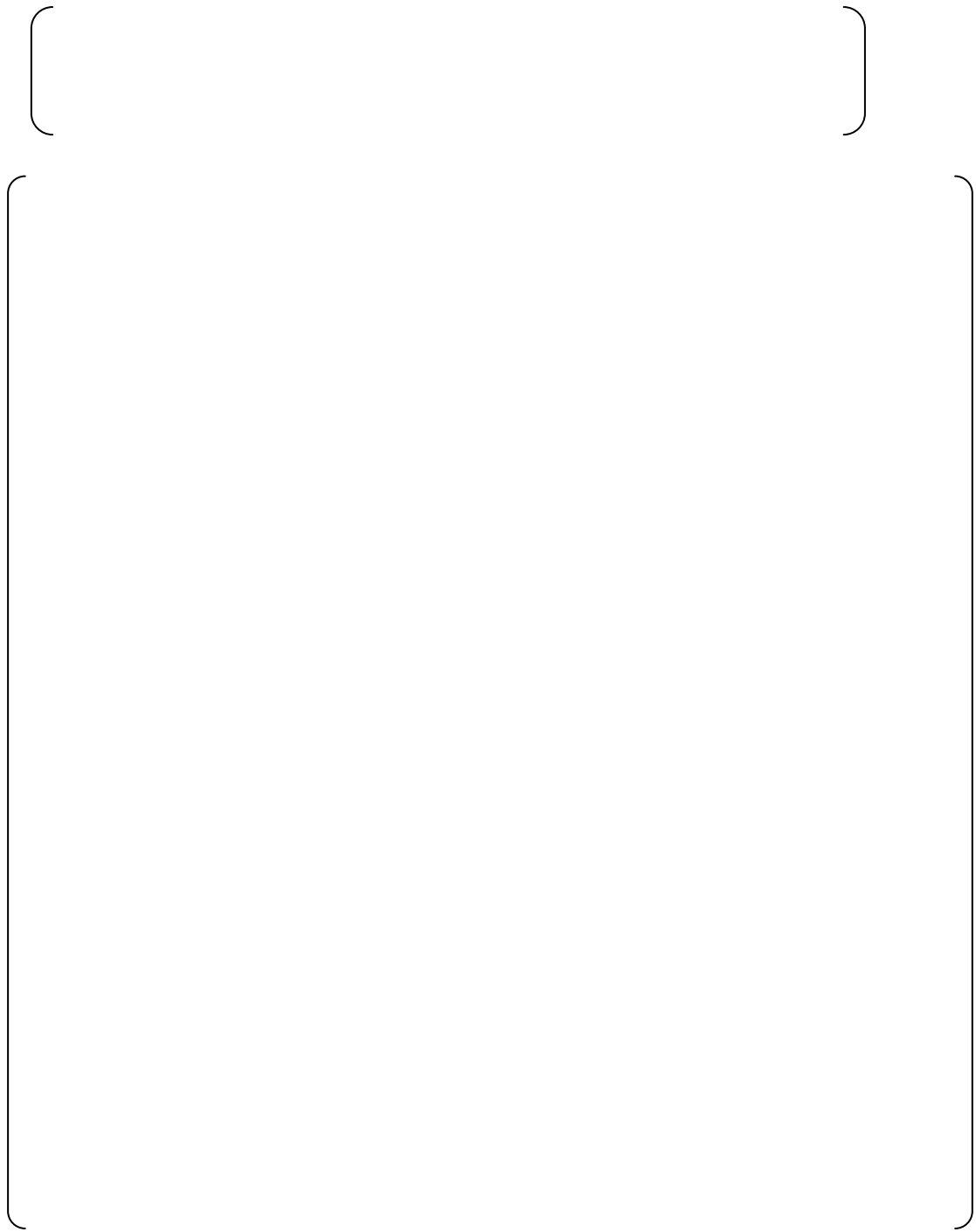


**Photo. 4.2.2-2 (1/2) Visualization of Flow with Anti-Vortex Cap (T. No. 1-2) 1/2**

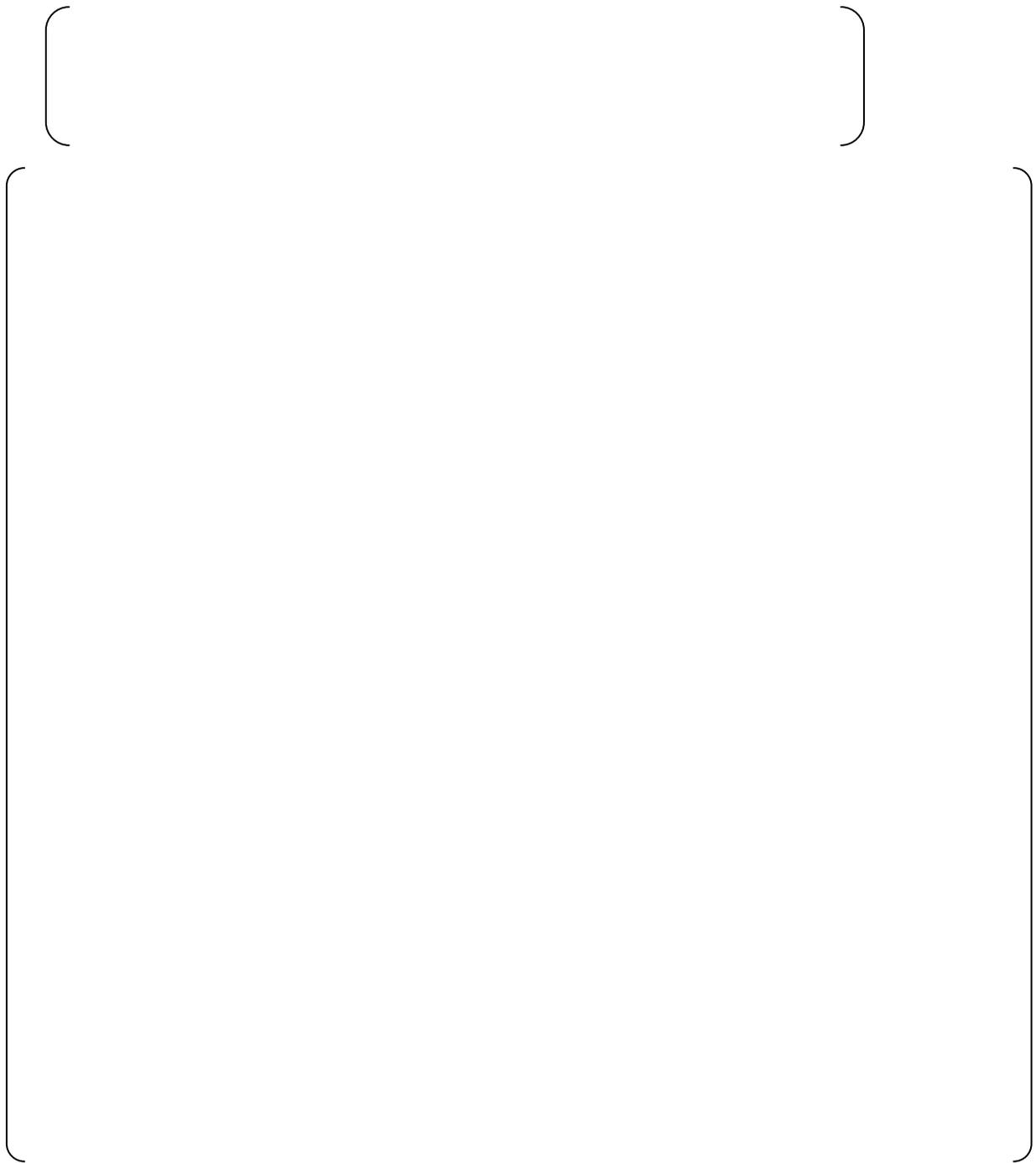


**Photo. 4.2.2-2(2/2) Visualization of Flow with Anti-Vortex Cap (T. No. 1-2) 2/2**

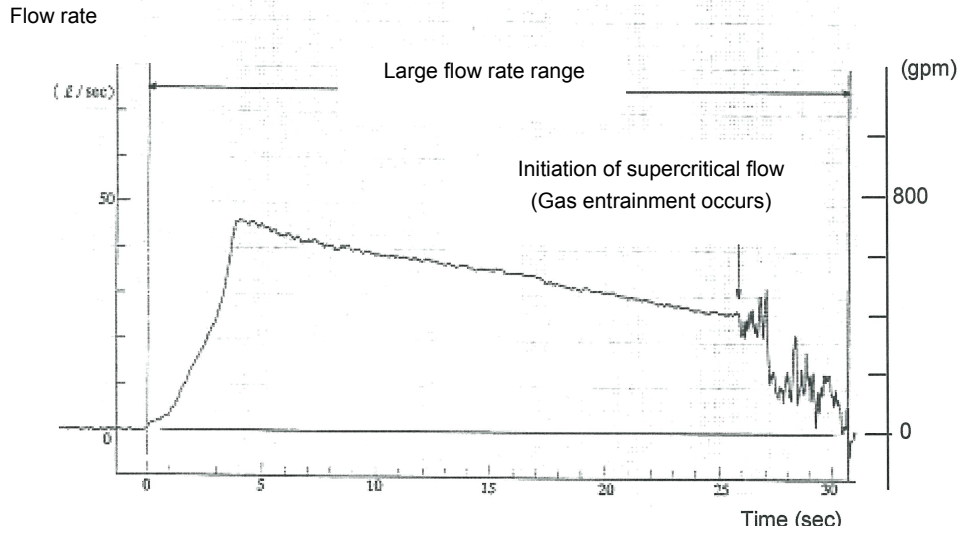


**Fig. 4.2.2-2 Test Flow Characteristics without Anti-Vortex Cap (T. No. 1-1)**

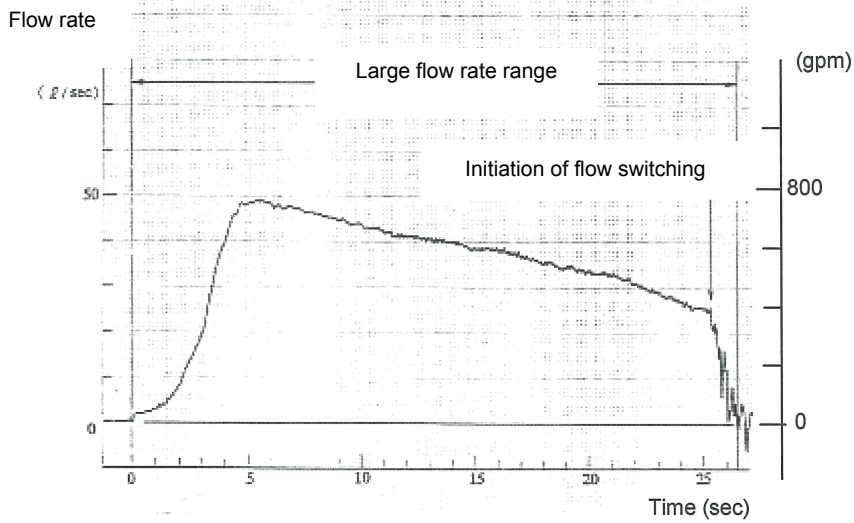


Fig. 4.2.2-3 Test Flow Characteristics with Anti-Vortex Cap (T. No. 1-2)



**Fig. 4.2.2-4 Test Flow Characteristics without Anti-Vortex Cap (T. No. 2-1)**



**Fig. 4.2.2-5 Test Flow Characteristics with Anti-Vortex Cap (T. No. 2-2)**

### 4.2.3 1/5-Scale Test

#### 1) Objectives

##### (1) Confirm the operational characteristics of the flow damper

Observe the flow in the flow damper during large and small flow, large to small flow switching, and confirm the expected behavior of the flow.

##### (2) Confirm the performance characteristics during large and small flow by measurement

The cavitation factor and flow rate coefficient were measured and confirmed to be similar to the expected ACC performance. The flow characteristics obtained by this test are compared with the results of the full height 1/2-scale test later in this report.

#### 2) Test Apparatus

The outline drawings of the test apparatus is shown in Fig. 4.2.3-1. The test facility consists of a test tank, flow damper, standpipe, injection piping, and exhaust tank. The flow damper is made of transparent acrylate to allow the fluid characteristics in the flow damper to be observed. A ball valve (nominal diameter is [                      ]) is provided on the injection line as the isolation valve and a gate valve (nominal diameter is [                      ]) is also provided on the injection line to control the flow resistance.



**Fig. 4.2.3-1 Outline Drawing of the Visualization Test Apparatus**

The specifications of the test facility are as follows:

(1) Test tank

Design Pressure : [ ]  
 Diameter : [ ]  
 Height : [ ]  
 Volume : [ ]

(2) Flow damper and standpipe (1/5-scale actual size)

Diameter of vortex chamber : [ ]  
 Height of vortex chamber : [ ]  
 Shape of standpipe : [ ]

(3) Injection piping

Inner diameter : [ ]  
 (Simulating the pressure drop)

(4) Exhaust tank

Design Pressure : [ ]  
 Diameter : [ ]  
 Height : [ ]  
 Volume : [ ]

### 3) Testing Method

(a) Visualization test method

- (1) Visualization tests were conducted for three cases: (i) examining flow characteristics during large flow injection and flow switching by setting the initial pressure at [ ], which is the maximum design pressure of the test tank; (ii) examining flow characteristics during small flow injection by setting the initial pressure at [ ] for an extended small flow injection time, and (iii) examining flow characteristics during flow switching by setting the initial pressure at [ ], which has the same Froude number as that of the actual plant condition.
- (2) The flow characteristics in the flow damper were recorded and observed using a video camera, as shown in Fig. 4.2.3-1.
- (3) The characteristics of the flow in the vortex chamber were observed using blue ink as a flow tracer.

## (b) Low pressure injection testing method

(1) The test tank pressure, test tank water level, damper outlet pressure, and exhaust tank pressure were measured and input into a PC to calculate the flow rate coefficient and the cavitation factor.

(2) The flow rate coefficient and cavitation factor were obtained by the following equations:

Flow rate coefficient:  $C_V$

$$C_V = \frac{1}{\sqrt{K_D}} \quad (4-7)$$

$$K_D = \frac{(P_A + \rho g H) - (P_D + \rho V_D^2 / 2 + \rho g H')}{\rho V_D^2 / 2} \quad (4-8)$$

Cavitation factor:  $\sigma_v$

$$\sigma_v = \frac{P_D + P_{at} - P_v}{(P_A + \rho g H) - (P_D + \rho V_D^2 / 2 + \rho g H')} \quad (4-9)$$

Where

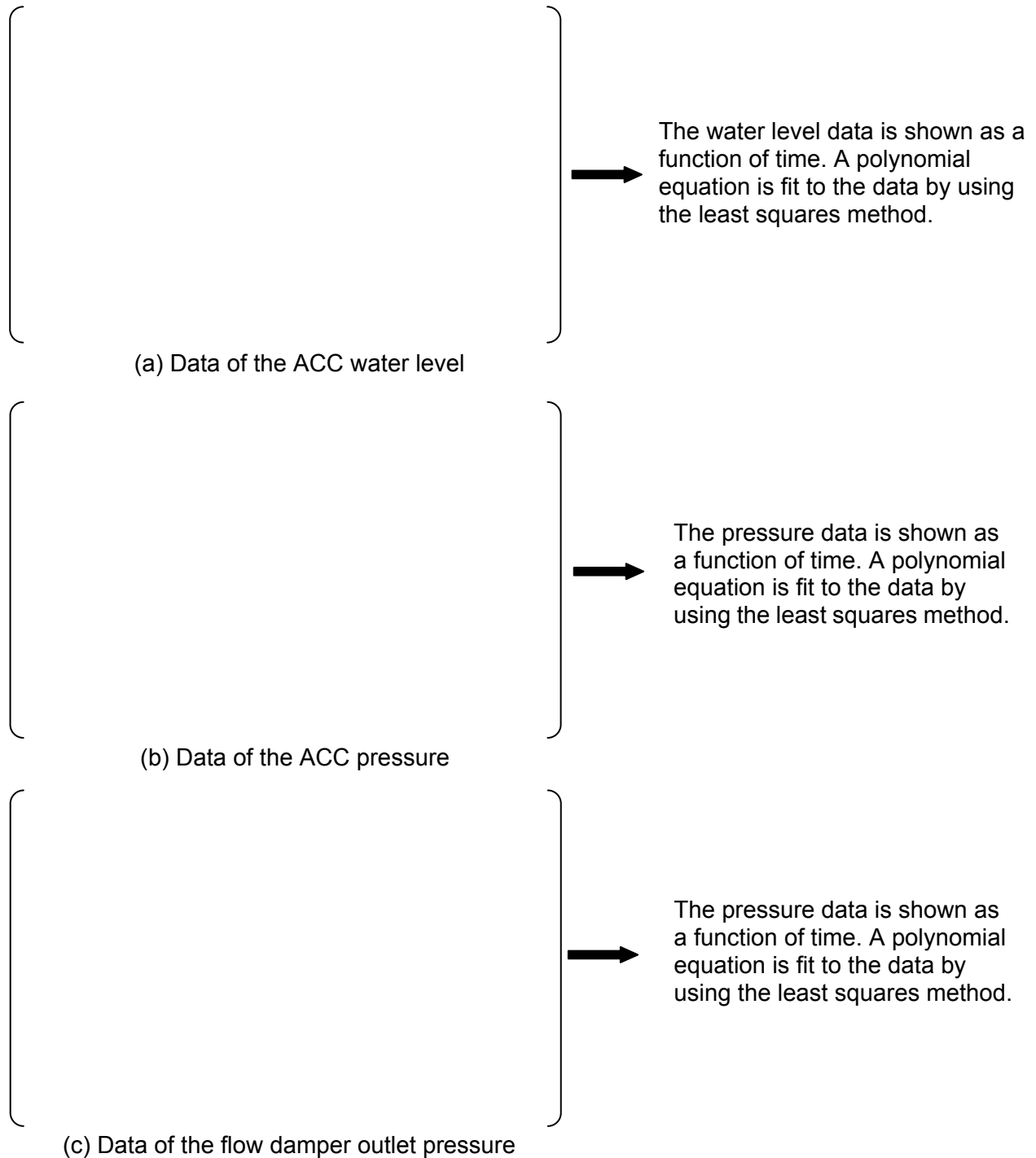
- $K_D$  : Resistance coefficient of flow damper
- $P_A$  : Test tank pressure [gage]
- $\rho$  : Density of water
- $g$  : Acceleration of gravity
- $H$  : Distance between test tank water level and vortex chamber
- $H'$  : Distance between outlet pipe and vortex chamber
- $P_{at}$  : Atmospheric pressure
- $P_v$  : Vapor pressure of water
- $P_D$  : Static pressure of flow damper outlet piping [gage] <sup>Note</sup>
- $V_D$  : Velocity in the flow damper outlet piping <sup>Note</sup>

Note: These parameters were the values converted to the scale of the actual ACC



### (3) Data Processing

Data smoothing techniques were utilized to eliminate noise from the data of the ACC water level, the ACC pressure, and the flow damper outlet pressure, the data processing method is discussed below.



#### 4) Test Conditions

##### Visualization Test Conditions

Visualization test conditions are shown in Table 4.2.3-1.

##### Low Pressure Injection Test Conditions

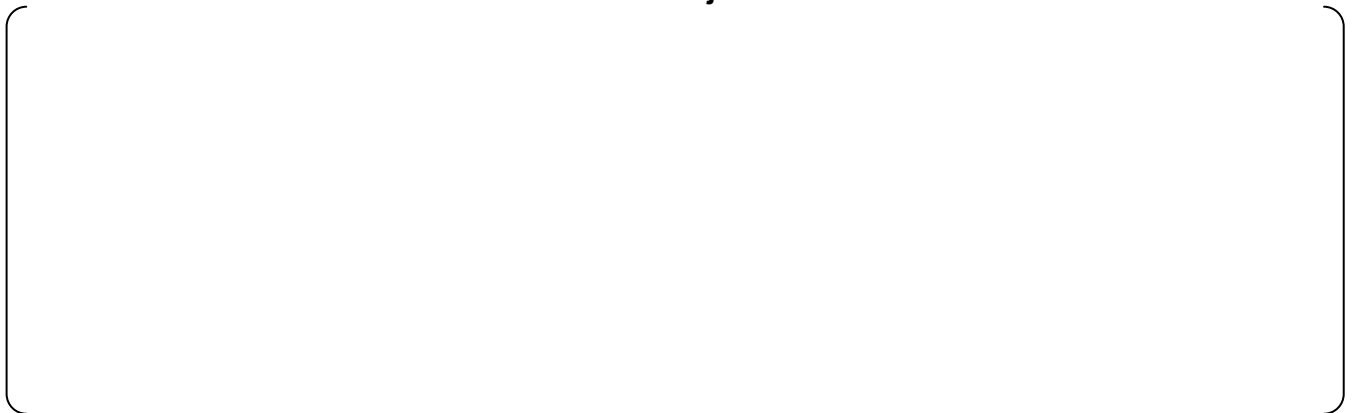
Low pressure test conditions are shown in Table 4.2.3-2.

The purpose of this test was to confirm the flow characteristics of the flow damper during large flow with wide variations of cavitation factors. The initial pressure conditions for the test tank and the exhaust tank were set at values that facilitated the testing.

**Table 4.2.3-1 Visualization Test Conditions**



**Table 4.2.3-2 Low Pressure Injection Test Conditions**



## 5) Parameters and Measuring Equipment

Pressure, water level, and temperature were measured to calculate cavitation factors and flow rate coefficients. The differential pressure transducer for measuring water level in the tank and the attachments for the pressure transducer are shown in Fig. 4.2.3-1.

## 6) Test Results and Consideration

### a) Visualization Test Results

The visualization test results are summarized in Table 4.2.3-3 and the flow in the vortex chamber during large flow, large/small flow switching, and small flow are shown in Photos. 4.2.3-1 to 4.2.3-3. The white lines are added in the photos to clearly show the tracer trajectories.

- (1) The characteristics of the large flow are shown in Photo. 4.2.3-1. Since the flow tracer traveled from the point of the flow from the standpipe directly to the flow damper exit following collision with the water from the small flow inlet, it was confirmed that a vortex was not formed in the vortex chamber during large flow injection.
- (2) The characteristics of the large / small flow switching are shown in Photo. 4.2.3-2. It shows the beginning of the formation of a vortex during flow rate switching. It was also confirmed that gas entrainment from the standpipe did not occur and the flow rate switched smoothly in a short time.
- (3) The characteristics of small flow are shown in Photo. 4.2.3-3. It was confirmed that the flow tracer swirled to the outlet, and a stable vortex was formed in the vortex chamber. No cavitation was observed at the center of the vortex.

**Table 4.2.3-3 Visualization Test Results**

Test Number (T. No.)	Initial Pressure (Test Tank)	Large Flow	Flow Rate Switching	Small Flow
1/5-1-1	[            ] [            ]	A vortex was not formed in the vortex chamber during large flow.	The flow rate switched smoothly in a short time.	-
1/5-1-2	[            ] [            ]	-	-	A stable vortex was formed in the vortex chamber.
1/5-1-3	[            ] [            ]	-	The flow rate switched smoothly in a short time.	-

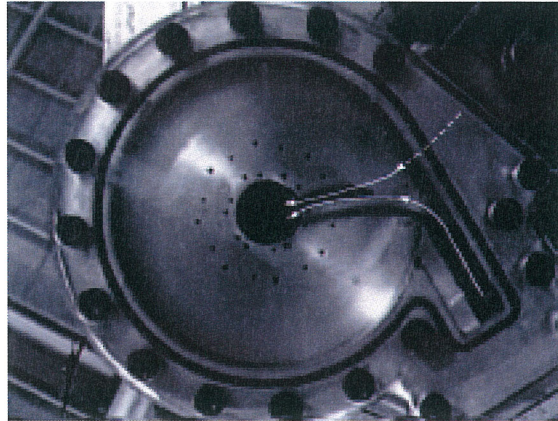


**Photo. 4.2.3-1 Large Flow**

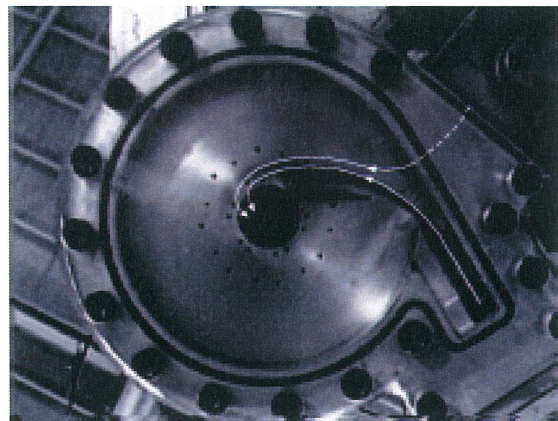


**Photo. 4.2.3-2 Switching Flow Rate**



**Photo. 4.2.3-3 Small Flow**

**b) Low Pressure Injection Test Results**

This test was conducted at low pressure using a 1/5-scale model and the following results were obtained.

- (1) The test tank pressure, water level, and the outlet pressure of the flow damper as a function of time are shown in Figs. 4.2.3-2 (1/2),(2/2) to 4.2.3-4 (1/2),(2/2). It was confirmed that the test tank water level decreased rapidly during large flow and decreased gradually after the flow rate switched to small flow.
- (2) The relationship between the flow rate coefficient and cavitation factor in the flow damper is shown in Figs. 4.2.3-2 (2/2) to 4.2.3-4 (2/2) <sup>Note</sup>. The behavior of large flow injection shows that the flow rate coefficient increased with the cavitation factor and then became almost constant when the cavitation factor was greater than [ ].

Note: The data is plotted near steady conditions.

- (3) The relationship between the flow rate coefficient and cavitation factor in the flow damper during small flow is also shown. The flow rate coefficient during small flow was constant and independent of the cavitation factor.

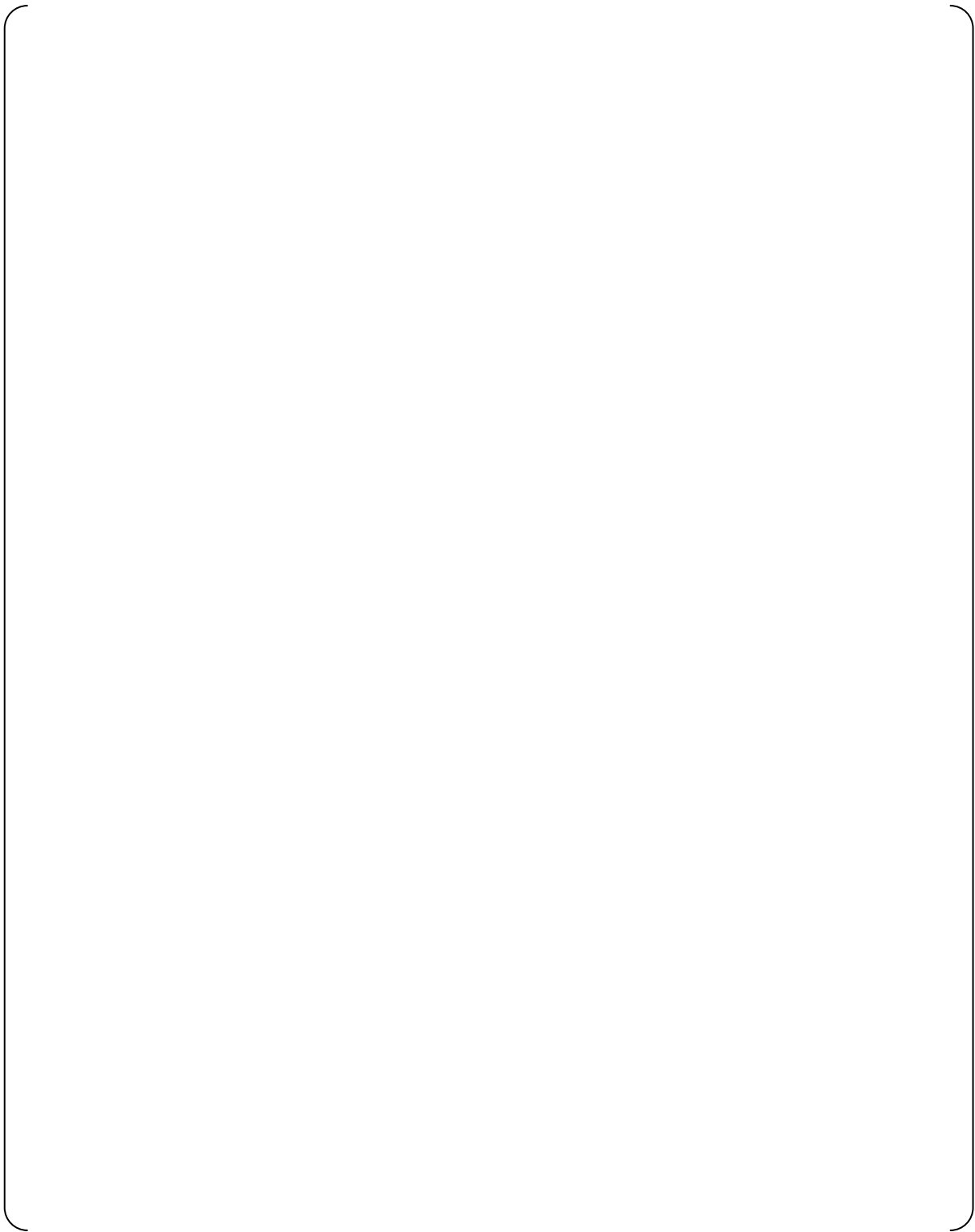


**Fig. 4.2.3-2 (1/2) Low Pressure Injection Test Results (T. No. 1/5-2-1) 1/2**

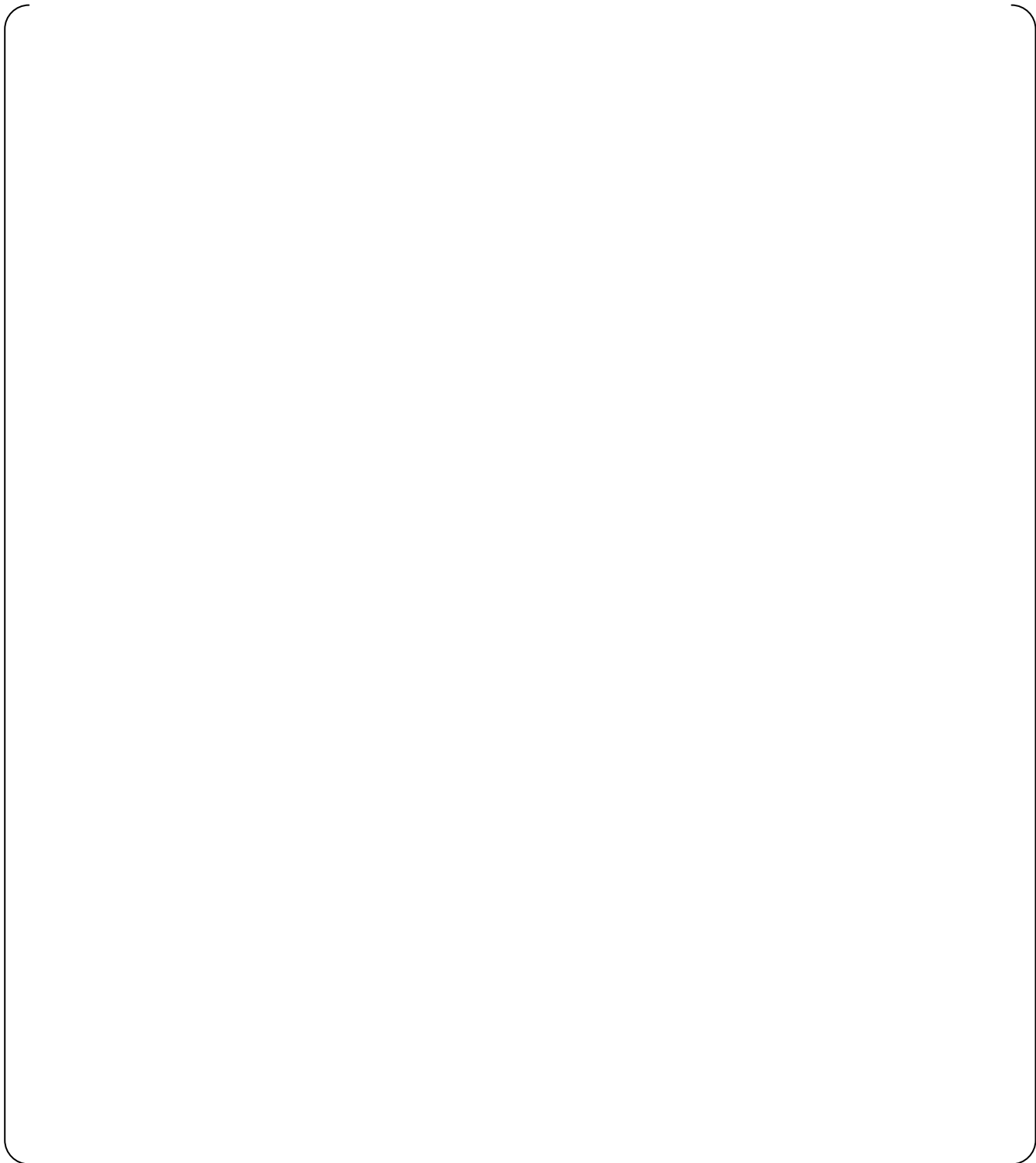


**Fig. 4.2.3-2 (2/2) Low Pressure Injection Test Results (T. No. 1/5-2-1) 2/2**

Large Flow Rate

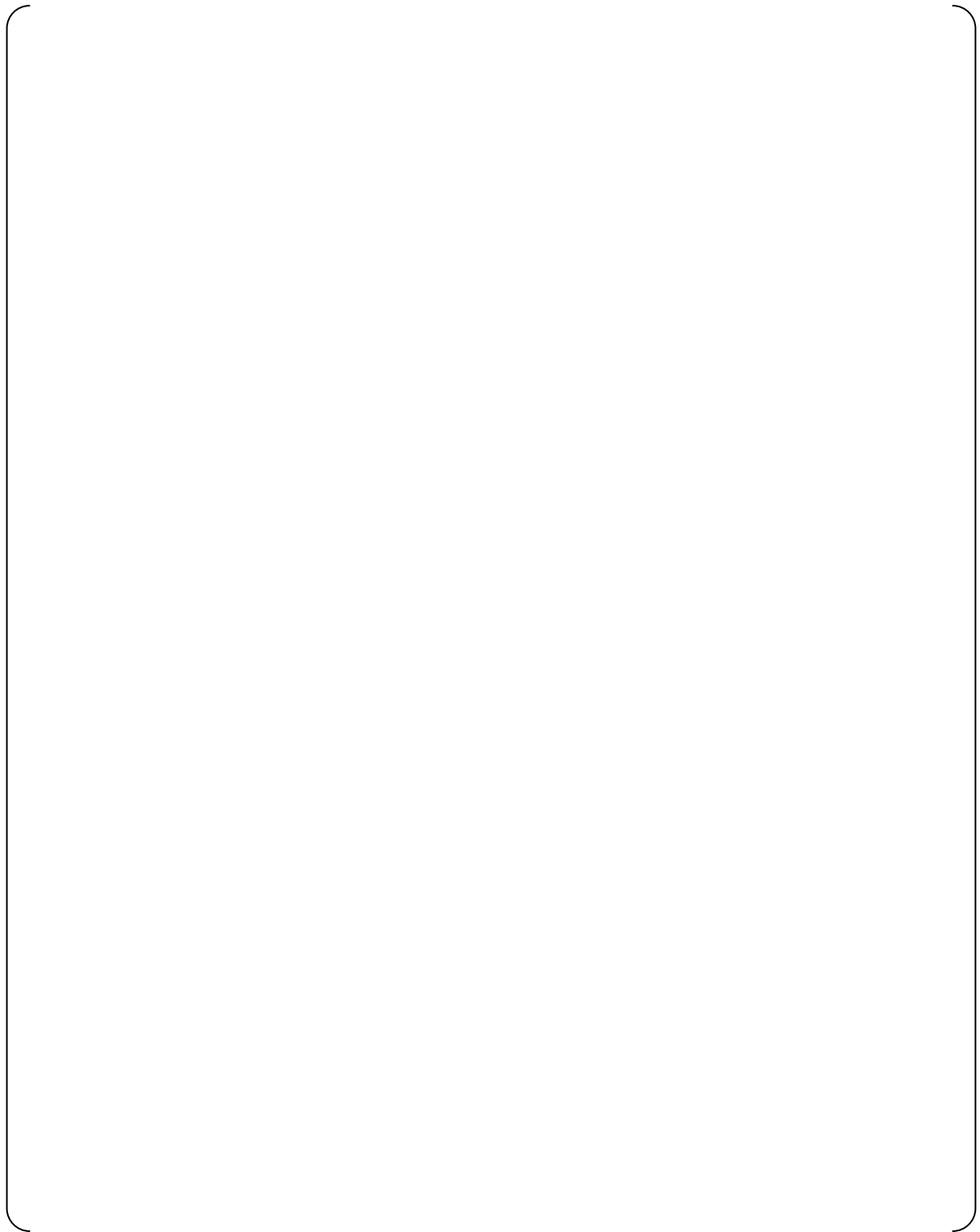


**Fig. 4.2.3-3(1/2) Low Pressure Injection Test Results (T. No. 1/5-2-2) 1/2**

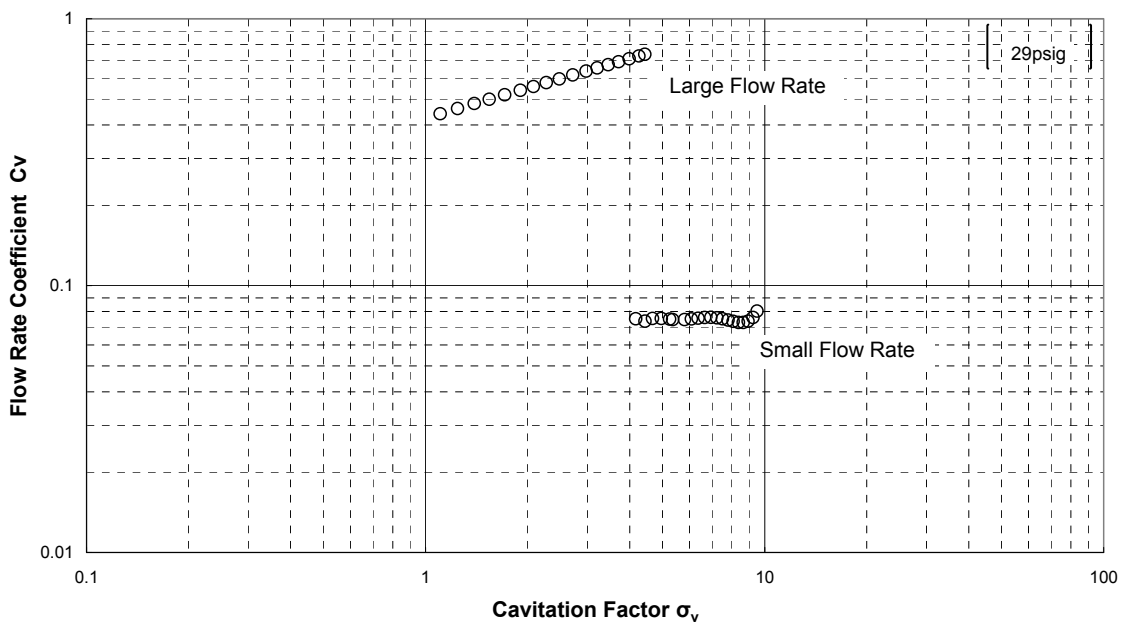
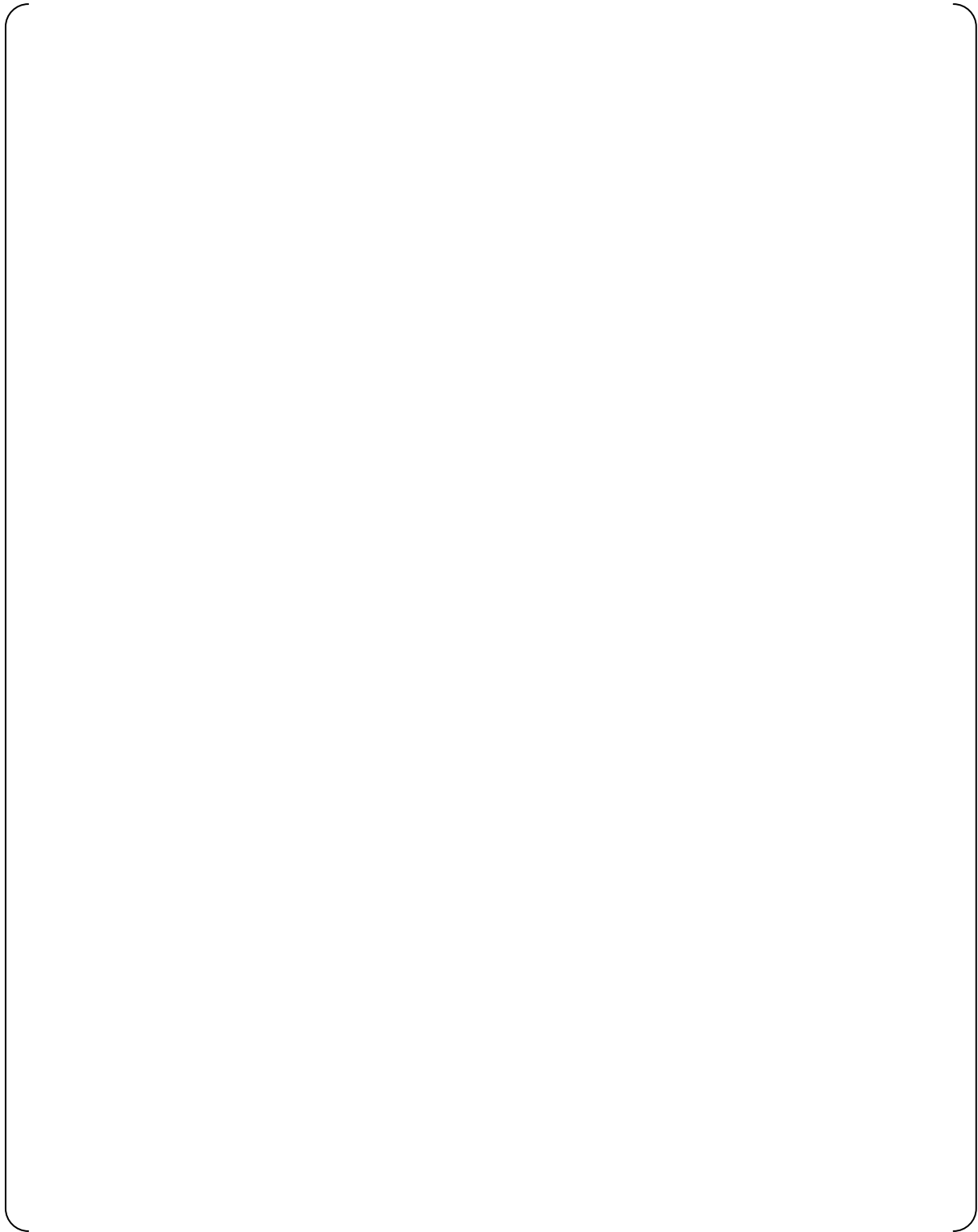


Fig. 4.2.3-3 (2/2) Low Pressure Injection Test Results (T. No. 1/5-2-2) 2/2



**Fig. 4.2.3-4 (1/2) Low Pressure Injection Test Results (T. No. 1/5-2-3) 1/2**

**Fig. 4.2.3-4(2/2) Low Pressure Injection Test Results (T. No. 1/5-2-3) 2/2**

#### 4.2.4 Full Height 1/2-Scale Test

##### 1) Objectives

- (1) Obtain the flow characteristics data and confirm no gas entrainment  
The test was conducted to obtain the flow characteristics data in the flow damper and to confirm that gas entrainment through the standpipe is prevented during flow switching and small flow injection.
- (2) Confirm that the flow characteristics can be characterized by dimensionless numbers (cavitation factor and flow rate coefficient)  
Since a throat was added at the vortex chamber outlet to form a strong vortex, it was assumed that cavitation might occur at the throat. The cavitation phenomenon is characterized by the cavitation factor which can be determined. It was confirmed by the test that the flow rate coefficient can be characterized as a function of the cavitation factor.
- (3) Confirm the flow switching water level  
The flow rate, as expected, switched from large flow to small flow when the water level decreased to the lower end of the standpipe cap. However, it is assumed that the water level for flow switching may vary in the actual accumulator. Therefore, the actual switching water level was confirmed.
- (4) Confirm the effect of dissolved nitrogen gas  
Since the accumulator is pressurized by nitrogen gas, it is assumed that nitrogen gas dissolves into the water. If the water contains dissolved nitrogen gas, the dissolved gas may come out of solution during injection and affect the flow characteristics of the flow damper. Therefore, the test was conducted to evaluate the effect of dissolved gas on the injection flow.

##### 2) Test Facility

The schematic and outline drawing of the test facility and the general flow path are shown in Fig. 4.2.4-1 and Fig. 4.2.4-2. The test facility consists of a test tank, flow damper, injection piping, and exhaust tank. The flow damper is installed in the test tank. The height of the test tank and the standpipe is the full-scale height and the inner diameter of the test tank is 1/2-scale (Fig. 4.2.4-3 and Fig. 4.2.4-4). Therefore, the water volume is 1/4 scale and the flow rate is also 1/4 scale. The test was conducted to simulate the actual injection time. In addition, the water level transient during flow switching in the standpipe can be observed to represent the level transient in the actual standpipe. A ball valve is provided on the injection line as the isolation valve and a gate valve is provided on the injection line to control flow resistance. A pressure control valve is provided on the upper side of the test tank to control the tank pressure during the test.

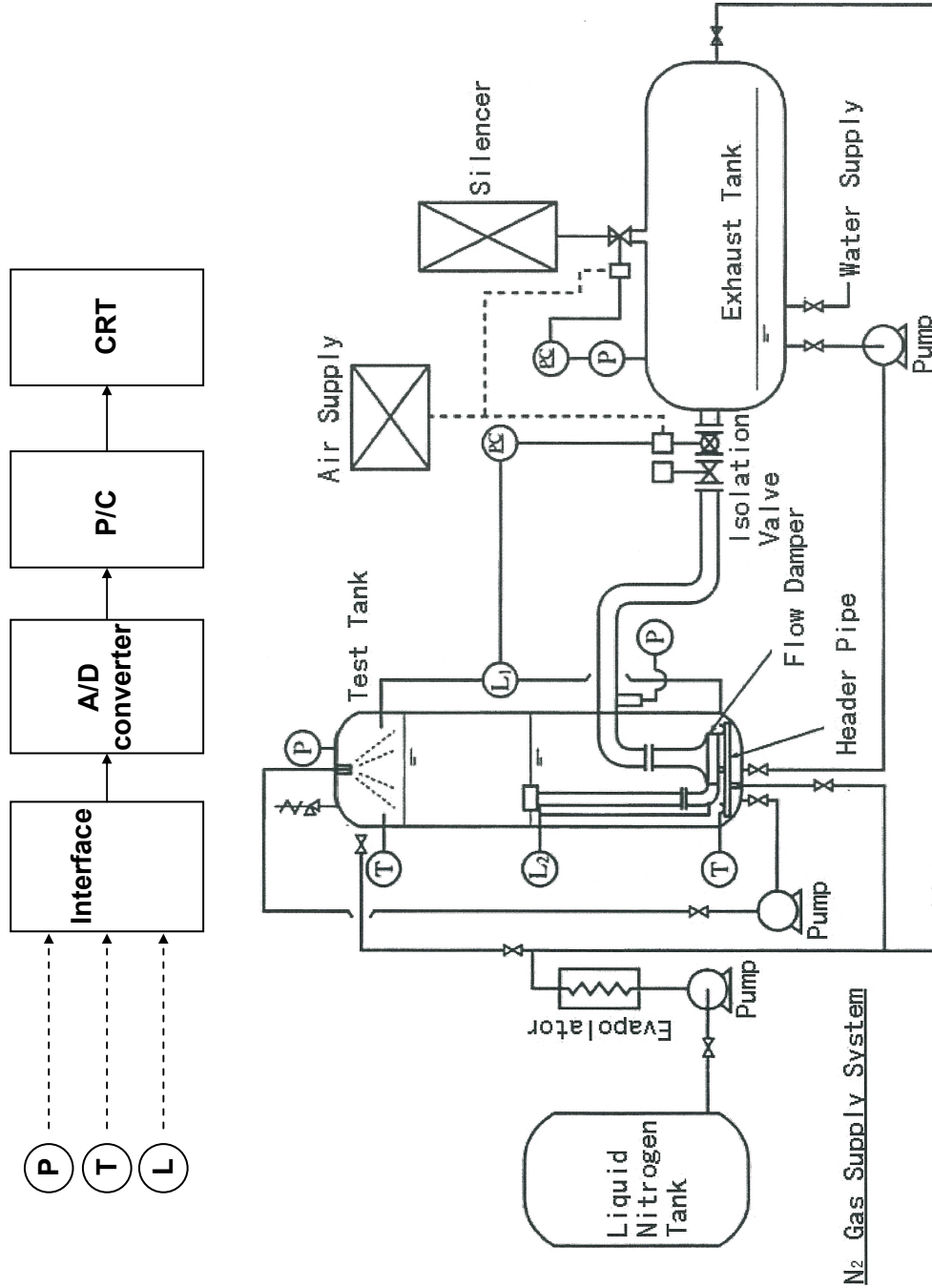
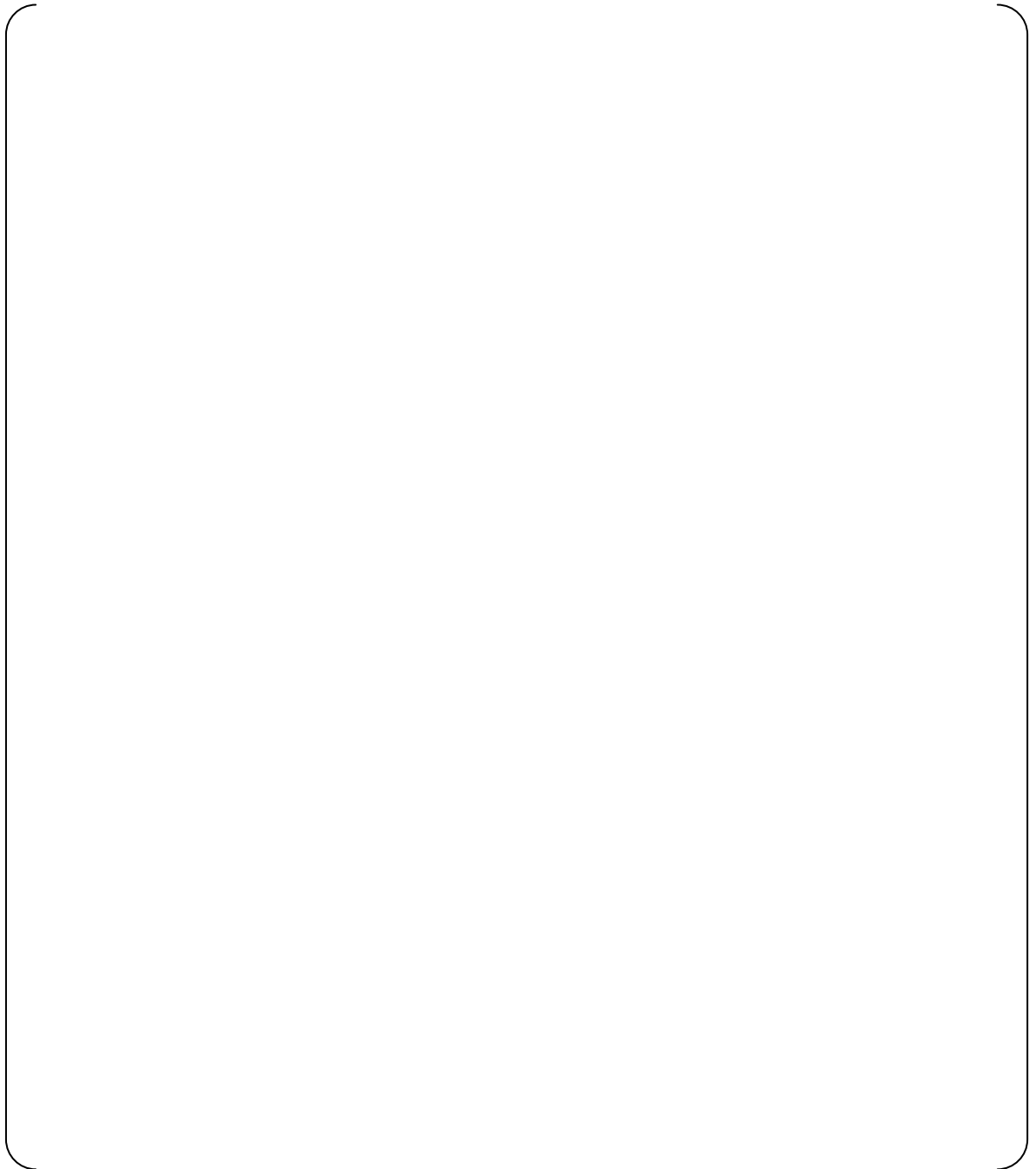


Fig. 4.2.4-1 Schematic Drawing of the Full Height 1/2-Scale Test Facility



**Fig. 4.2.4-2 Outline Drawing of the Full Height 1/2-Scale Test Facility**





**Fig. 4.2.4-3 Schematic Comparison of Actual Tank and Test Tank**



**Fig. 4.2.4-4 Outline Drawings of the Actual Flow Damper and the Test Flow Damper**

### 3) Test Conditions

Full height 1/2-scale test conditions are shown in Table 4.2.4-1. The following seven cases were tested for initial tank pressures that reflect the ACC operating conditions. The pressure of the exhaust tank corresponds to RCS pressure.

- Case 1: The initial test tank pressure was 586 psig (4.04MPa [gage]) simulating the condition for ECCS performance during a large LOCA.
- Case 2: The initial test tank pressure was 657 psig (4.53 MPa [gage]) to obtain design data for high pressure.
- Case 3: The initial tank pressure was 758 psig (5.23 MPa [gage]) to obtain design data for high pressure.
- The pressure in the exhaust tank was 14 psig (0.098 MPa [gage]) for Case 1, 2, and 3. since the pressure of the exhaust tank will become the same as the pressure of the containment vessel (C/V) after the blowdown phase of a large LOCA and the ECCS performance analysis uses approximately 14 psig (0.098 MPa [gage]).
- Case 4: The initial tank pressure was the same as Case 1. However, the pressure in the exhaust tank was maintained at 71 psig (0.49 MPa [gage]) to obtain data for a high back pressure case.
- Case 5: The test was conducted with water containing dissolved nitrogen by bubbling and showering to confirm the effect of dissolved nitrogen gas on flow characteristics.
- Case 6: The test was conducted with a small differential pressure between the test tank and the exhaust tank to take into account large cavitation factors.
- Case 7: The injection test was conducted with the initial tank pressure of [ ] to correspond to the pre-operational test conditions.
- The valve opening speed was set at [ ] seconds which is faster than the depressurization time during a LOCA in order to assure smaller cavitation factors.
- The resistance coefficient of the piping was controlled at the actual design condition [(6.5)] in order to confirm the injection time during the large flow injection period.

**Table 4.2.4-1 Test Conditions of Full Height 1/2-Scale Test**

	Test Tank Pressure psig [MPa [gage]]	Exhaust Tank Pressure psig [MPa [gage]]	Initial Gas Volume ft <sup>3</sup> [m <sup>3</sup> ]	Injection Water Volume		Objective
				Large Flow ft <sup>3</sup> [m <sup>3</sup> ]	Small Flow ft <sup>3</sup> [m <sup>3</sup> ]	
Case 1	586 (4.04)	14 (0.098)	[ ]	[ ]	[ ]	Obtain flow characteristics for ECCS performance evaluation during a large LOCA
Case 2	657 (4.53)	14 (0.098)	[ ]	[ ]	[ ]	Obtain flow characteristics for a high pressure design
Case 3	758 (5.23)	14 (0.098)	[ ]	[ ]	[ ]	Obtain flow characteristics for large differential pressures
Case 4	586 (4.04)	71 (0.49)	[ ]	[ ]	[ ]	Obtain flow characteristics for small differential pressures
Case 5	[ ]	[ ]	[ ]	[ ]	[ ]	Obtain flow characteristics to confirm the effect of dissolved nitrogen gas
Case 6	[ ]	[ ]	[ ]	[ ]	[ ]	Obtain flow characteristics for large cavitation factors
Case 7	[ ]	[ ]	[ ]	[ ]	[ ]	Obtain flow characteristics for the assumed pre-operational test conditions

#### 4) Parameters and Measuring Equipment

Pressure, water level, and temperature were measured by the instruments shown in Fig. 4.2.4-1 for all test cases and used to calculate the cavitation factor and the flow rate coefficient.

#### 5) Test Results and Conditions

The test results are shown in Figs. 4.2.4-5 to 4.2.4-11. The test results, such as injection flow rate, test tank pressure, test tank water level and the flow rate coefficients <sup>Note</sup> during both large and small flow for each test case, are shown in these figures. The conclusions for each test are described as follows.

Note: Plotted for near steady conditions.

##### [Case 1]

- It was confirmed that the injection flow rate smoothly switched from large flow to small flow, and small injection began after large flow injection. (Refer to Fig. 4.2.4-5(1/2))
- It was confirmed that the test tank pressure dropped quickly after initiating the test and dropped gradually after the flow rate switching at approximately 114 psig (0.8 MPa [gage]). (Refer to Fig. 4.2.4-5(2/2))
- It was confirmed that when the test tank water level was reduced to the flow switching level, the standpipe water level temporarily dropped to its low point level in about 1.7 seconds, recovered, and then continued to drop gradually during the small flow injection period. (Refer to Fig. 4.2.4-5(1/2))
- It was confirmed that the standpipe water level did not decrease to the top of the flow damper during flow switching. (Refer to Fig. 4.2.4-5(1/2))

##### [Case 2]

- Although the initial test tank pressure was 71 psi (0.49 MPa) higher than in Case 1, it was confirmed that the injection flow rate, test tank pressure, and water level as a function of time were the same as in Case 1. (Refer to Fig. 4.2.4-6 (1/2), (2/2))
- Since the initial test tank pressure was 71psi (0.49 MPa) higher than in Case 1, the range of the cavitation factor during large flow shifted slightly to the lower side. However, in the region where the cavitation factor was the same as in Case 1, the flow rate coefficient was also the same as in Case 1. Therefore, it was confirmed that the characteristics of the flow rate coefficient and the cavitation factor are the same even if the tank pressure was increased 71 psi (0.49 MPa). (Refer to Fig. 4.2.4-6(2/2))
- It was confirmed that the characteristics of the flow rate coefficient and the cavitation factor during small flow were the same as in Case 1. (Refer to Fig. 4.2.4-6(2/2))

##### [Case 3]

- Although the initial test tank pressure was 172 psi (1.19 MPa) higher than in Case 1, it was confirmed that the injection flow rate, test tank pressure, and water level as a function of time were the same as in Case 1. (Refer to Fig. 4.2.4-7(1/2), (2/2))
- In the performance range where the cavitation factor was the same as in Case 1, the flow rate coefficient was also the same as in Case 1. Therefore, it was confirmed that the characteristics of the flow rate coefficient and the cavitation factor are the same even if the tank pressure is increased by 172 psi (1.19 MPa). (Refer to Fig. 4.2.4-7(2/2))

- It was confirmed that the characteristics of the flow rate coefficient and the cavitation factor during small flow were the same as in Case 1. (Refer to Fig. 4.2.4-7(2/2))

**[Case 4]**

- Although the pressure of the exhaust tank was 71 psig (0.49 MPa [gage]) as opposed to 14 psig (0.098 MPa [gage]) in Case 1, it was confirmed that the injection flow rate, test tank pressure, and water level as a function of time were the same as in Case 1. (Refer to Fig. 4.2.4-8(1/2), (2/2))
- The flow characteristics data was obtained over a larger range of cavitation factors than Case 1 because of higher back pressure in the exhaust tank. (Refer to Fig. 4.2.4-8(2/2))

**[Case 5]**

- For this case, nitrogen gas was dissolved into the water. It was confirmed that the flow rate coefficient during large flow was smaller than that of the case where nitrogen was not dissolved. (Refer to Fig. 4.2.4-9(2/2))
- It was confirmed that the flow rate coefficient during small flow was essentially the same as in Case 1 and no change was caused by the dissolved nitrogen gas. (Refer to Fig. 4.2.4-9(2/2))

**[Case 6]**

- It was confirmed that the injection flow rate was switched from large flow to small flow smoothly, and small injection began after large flow injection. (Refer to Fig. 4.2.4-10(1/2))
- The flow characteristics data was obtained for a larger range of cavitation factors than in Case 1 since the initial test tank pressure was reduced. (Refer to Fig. 4.2.4-10(2/2))

**[Case 7]**

- Although Case 7 was a low-pressure injection test, it was confirmed that the test tank pressure and water level decreased rapidly during large flow and more gradually after flow rate switched to small flow, as in Case 1. (Refer to Fig. 4.2.4-11(1/2))
- It was confirmed that the flow characteristics of the flow damper during both large and small flow were consistent with those in other cases. (Refer to Fig. 4.2.4-11(2/2))

**Performance Confirmation During Large Flow**

In the case that simulates LOCA conditions, the resistance coefficient during large flow injection is less than [ ]. These results are generally consistent with the performance requirements.

**Performance Confirmation During Small Flow**

Measurements from the test results of Case 1 show that the flow rate before and after the flow switching was approximately 3170 gpm (approximately 720 m<sup>3</sup>/h) and approximately 652 gpm (approximately 148 m<sup>3</sup>/h), respectively. Therefore, the flow-switching ratio (3170/652 = 4.9) was less than [ ] and was consistent with the performance requirements.

**Flow Switching Water Level**

The measured flow-switching water level in each test case is shown in Table 4.2.4-2. The expected flow-switching water level was set at the lower end of the anti-vortex cap installed at the inlet of the standpipe. The actual flow-switching water levels were within the range from [ ] to [ ] of the expected flow switching water level.

Based on the above test results, it was confirmed that the variation of the flow-switching water level was limited to a sufficiently small range by the anti-vortex cap at the inlet of the standpipe.

**Table 4.2.4-2 Flow Switching Water Level**

	Initial tank pressure [psig (MPa [gage])]	Exhaust tank pressure [psig (MPa [gage])]	Flow switching water level [in (mm)] <sup>Note</sup>
Case 1	586 (4.04)	14 (0.098)	+0.16 (+4)
Case 2	657 (4.53)	14 (0.098)	+0.12 (+3)
Case 3	758 (5.23)	14 (0.098)	+0.91 (+23)
Case 4	586 (4.04)	71 (0.49)	+0.39 (+10)
Case 5	586 (4.04)	[ ]	+1.50 (+38)
Case 6	427 (2.94)	[ ]	-0.16 (-4)
Case 7	213 (1.47)	[ ]	+0.12 (+3)

Note: Reference point is the bottom of the anti-vortex cap. The upper is '+', and the lower is '-'.

#### **Water Level Reduction During Flow Switching**

It was confirmed that the reduction of the water level in each test during flow switching was less than the height of the standpipe and sufficient margin was provided to prevent gas entrainment. (Refer to Fig. 4.2.4-12)

#### **Effect of Dissolved Nitrogen Gas**

It was confirmed that, in the test with nitrogen saturated water (Case 5), the duration of large flow injection was slightly longer (approximately [ ]) than in Case 1. Since Case 5 was conducted with nitrogen-saturated water by bubbling and showering, and this condition is not expected in the actual accumulator, it is assumed that dissolved nitrogen has a smaller impact in the actual tank. (Refer to Fig. 4.2.4-9(2/2))

#### **Result of the Test Assuming Pre-operational Test Conditions**

The comparison between the characteristics of cavitation factor vs. flow rate coefficient measured in a LOCA simulation test (Case 1) and in this test is shown in Fig. 4.2.4-11. This comparison shows that the cavitation factor can be obtained from this test for a wider range than the LOCA simulation test (Case 1). (Refer to Fig. 4.2.4-11(2/2))

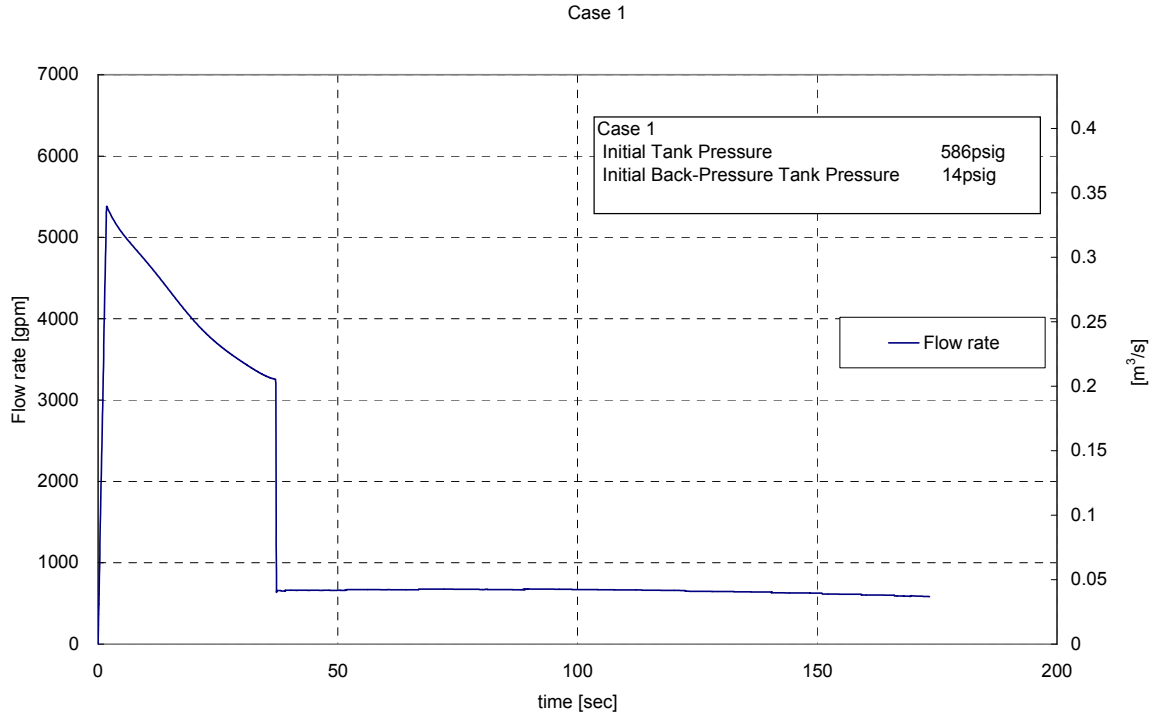
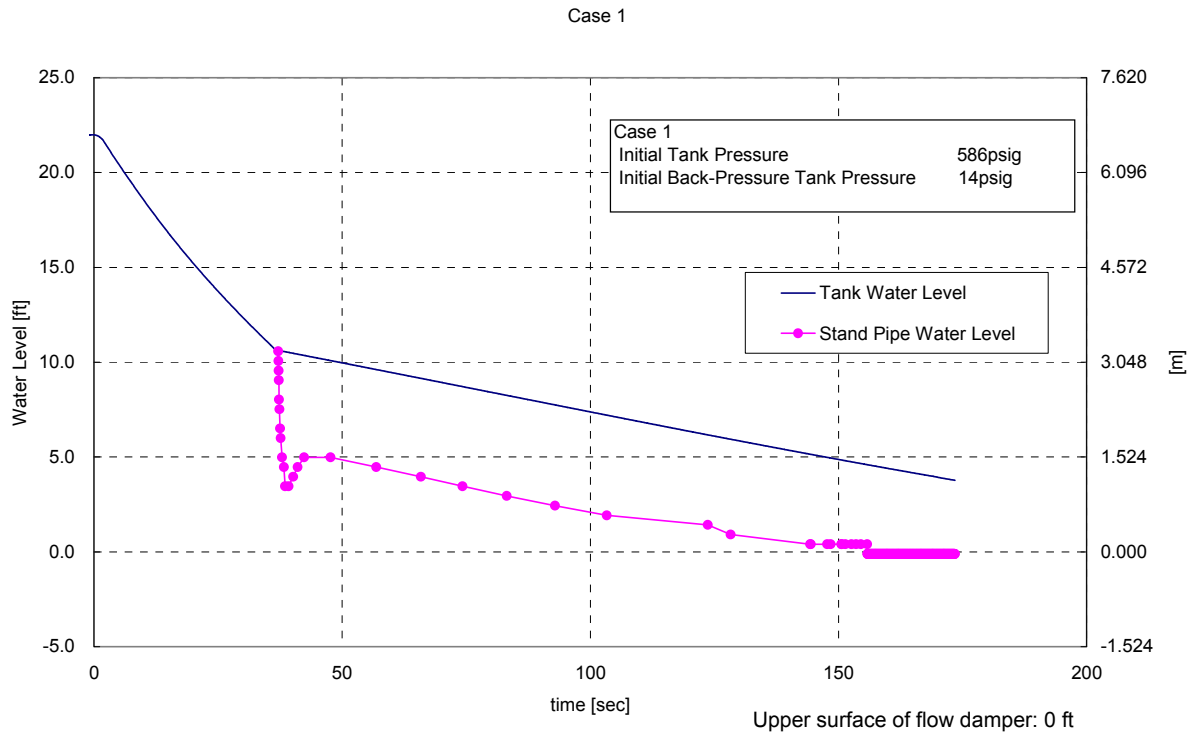


**Fig. 4.2.4-5 (1/2) Full Height 1/2-Scale Test Results (Case 1) 1/2**

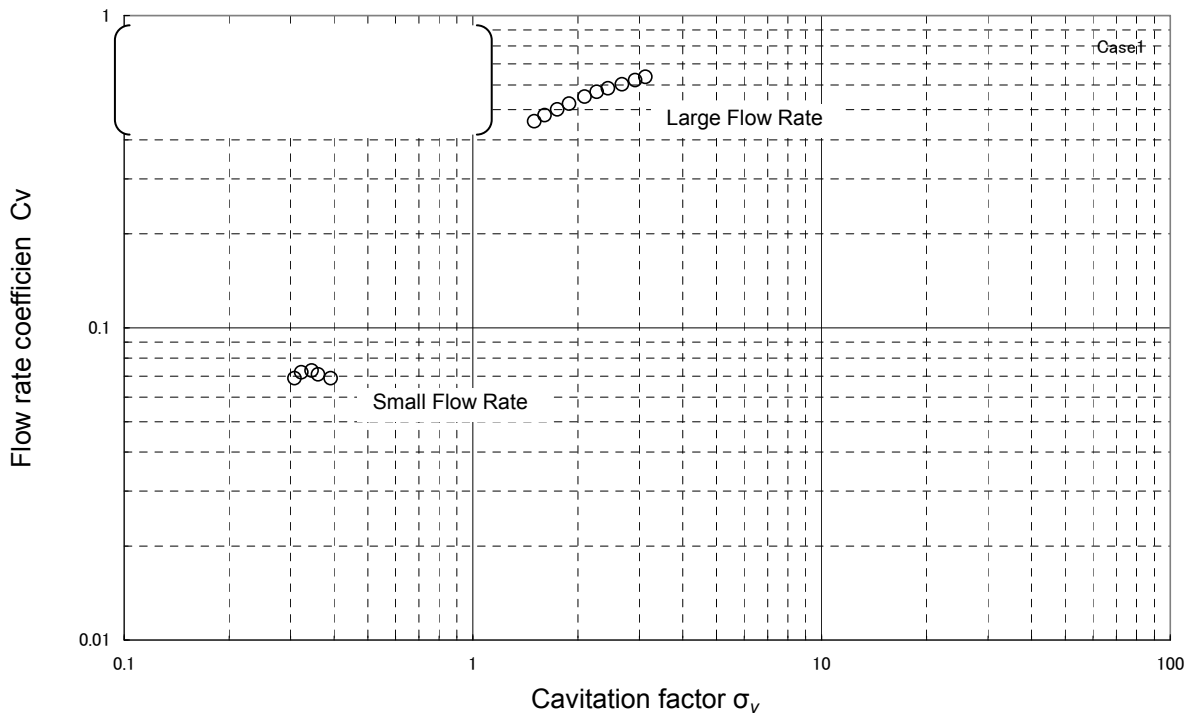
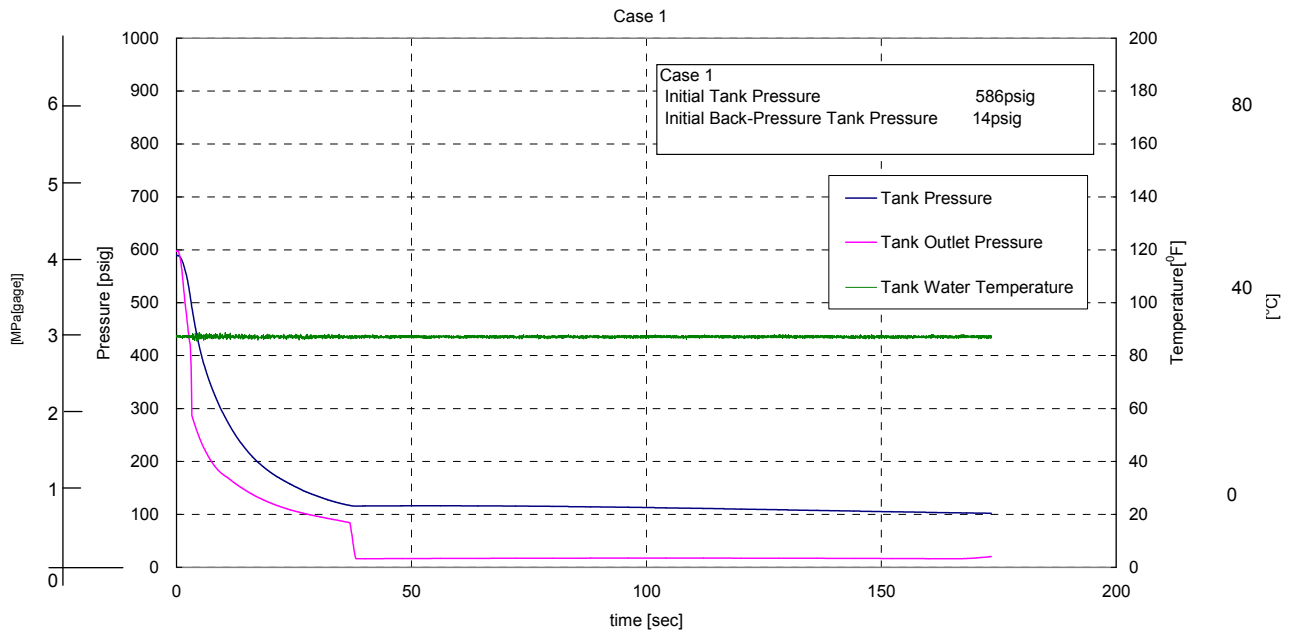


**Fig. 4.2.4-5 (2/2) Full Height 1/2-Scale Test Results (Case 1) 2/2**

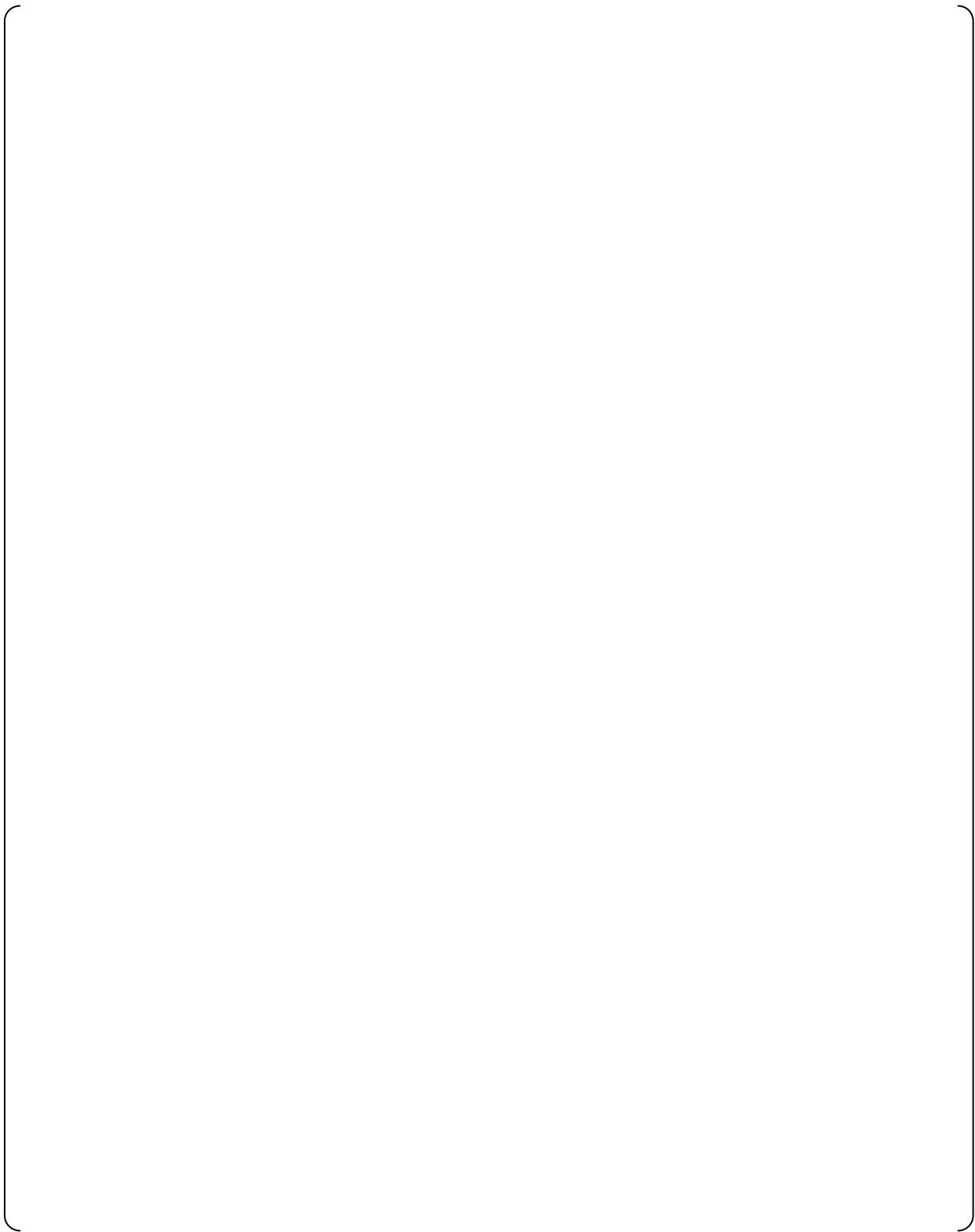


**Fig. 4.2.4-6 (1/2) Full Height 1/2-Scale Test Results (Case 2) 1/2**

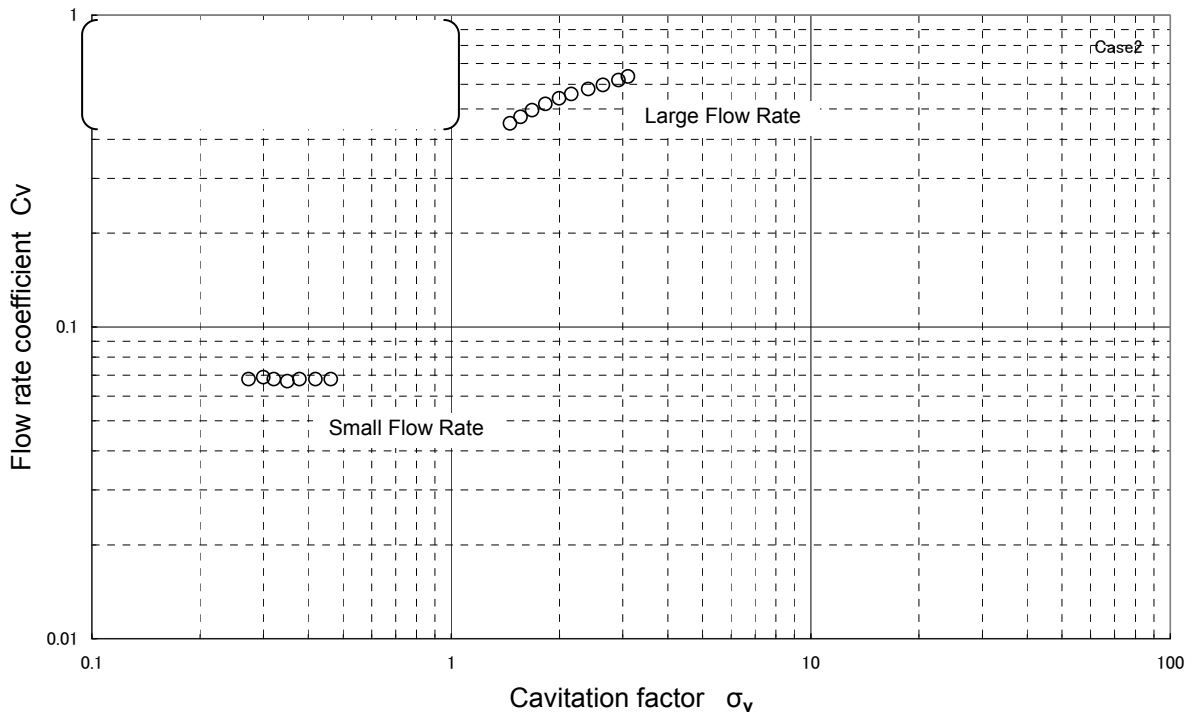
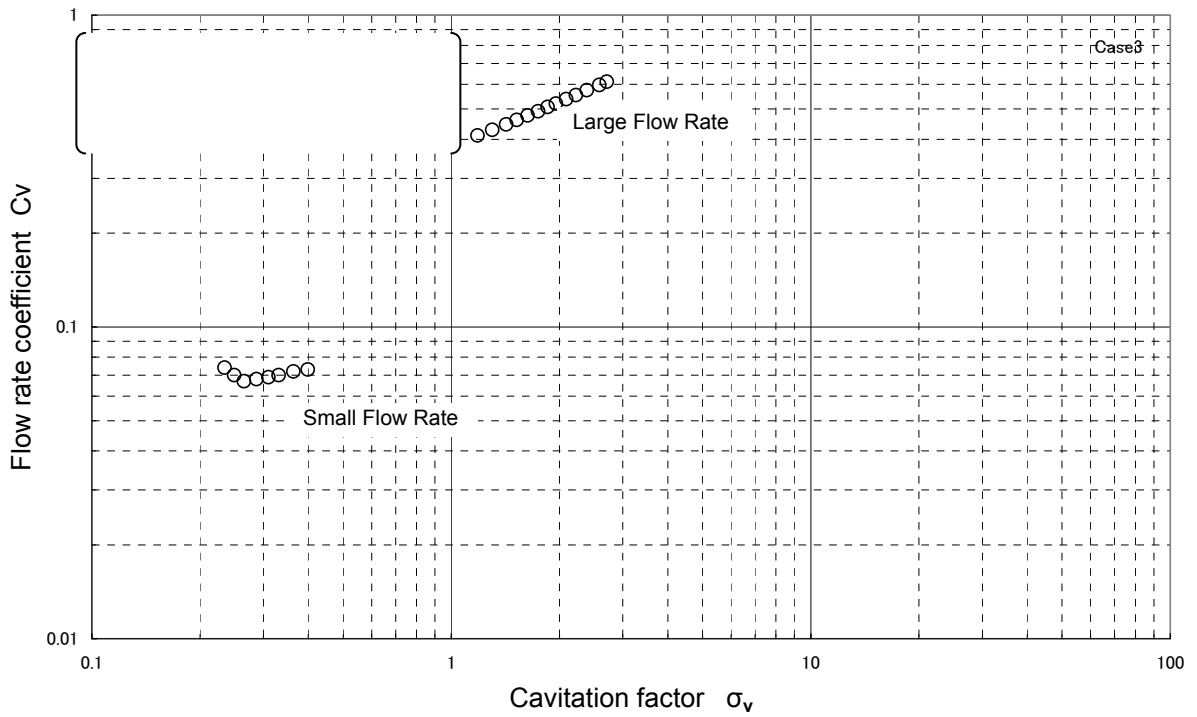


Fig. 4.2.4-6 (2/2) Full Height 1/2-Scale Test Results (Case 2) 2/2



**Fig. 4.2.4-7 (1/2) Full Height 1/2-Scale Test Results (Case 3) 1/2**



**Fig. 4.2.4-7(2/2) Full Height 1/2-Scale Test Results (Case 3) 2/2**

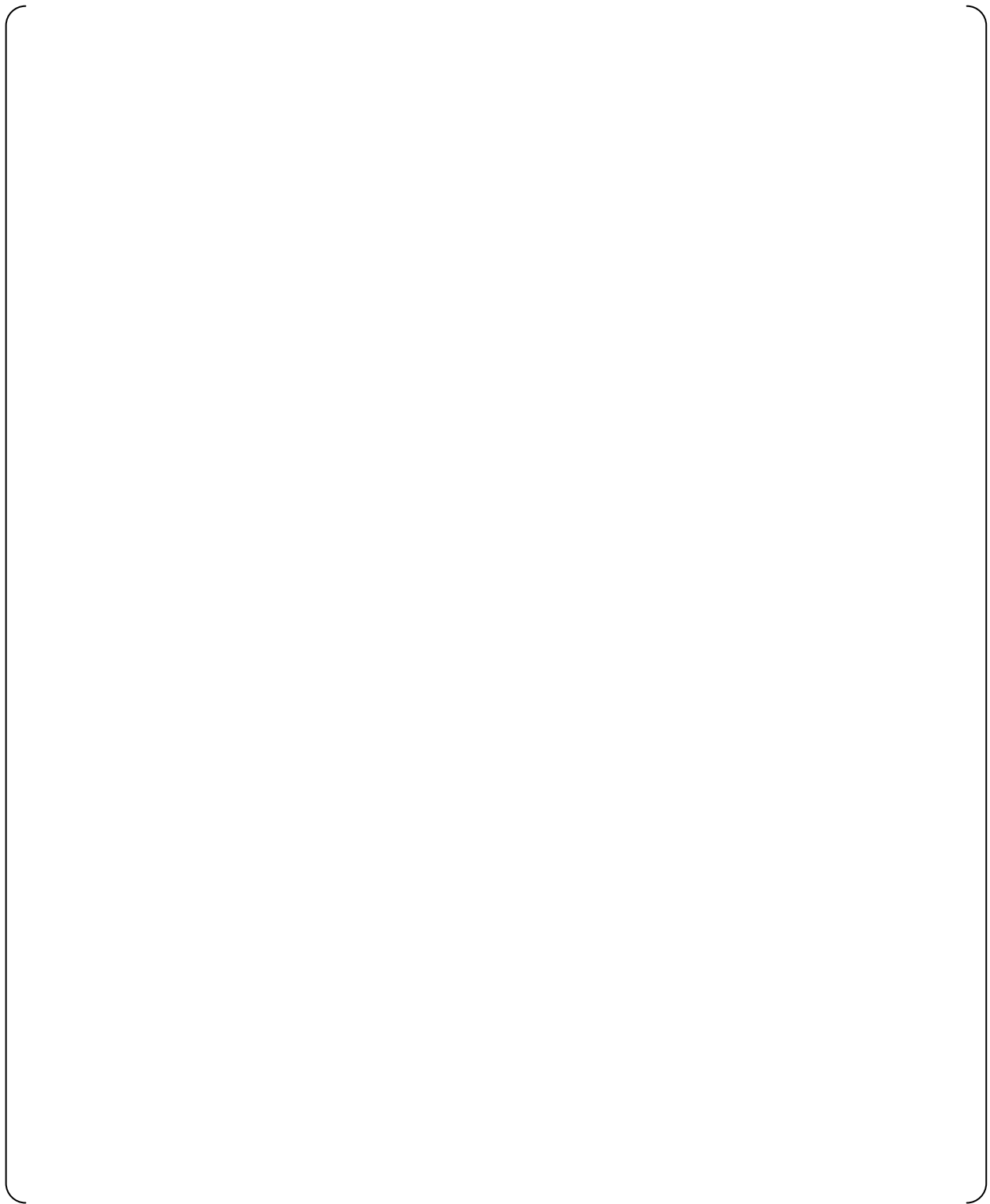


**Fig. 4.2.4-8 (1/2) Full Height 1/2-Scale Test Results (Case 4) 1/2**

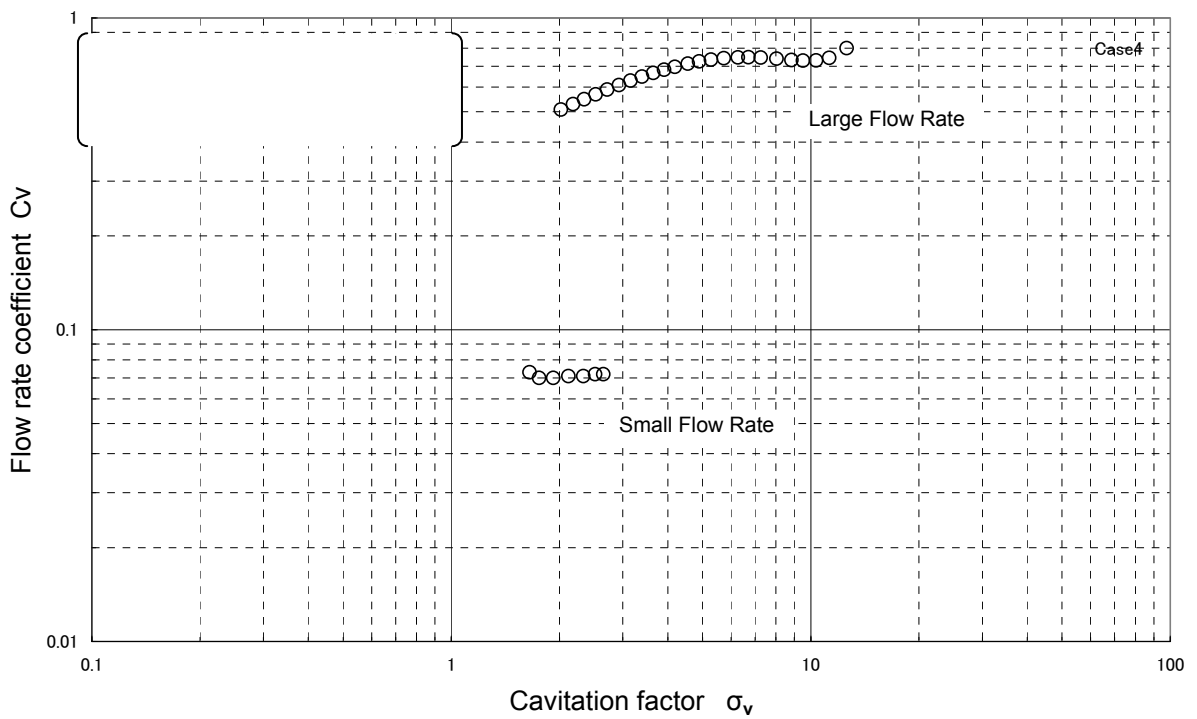
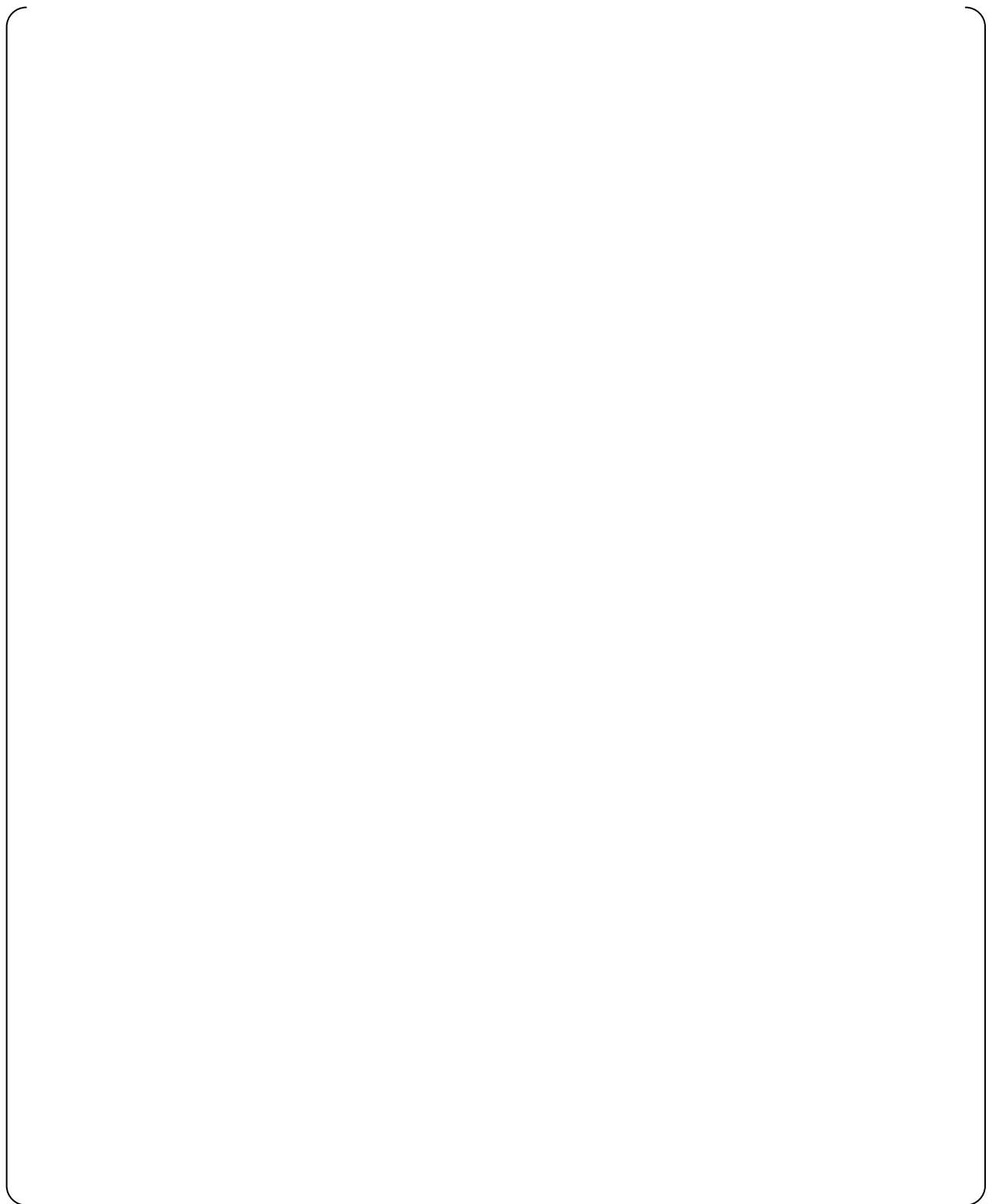
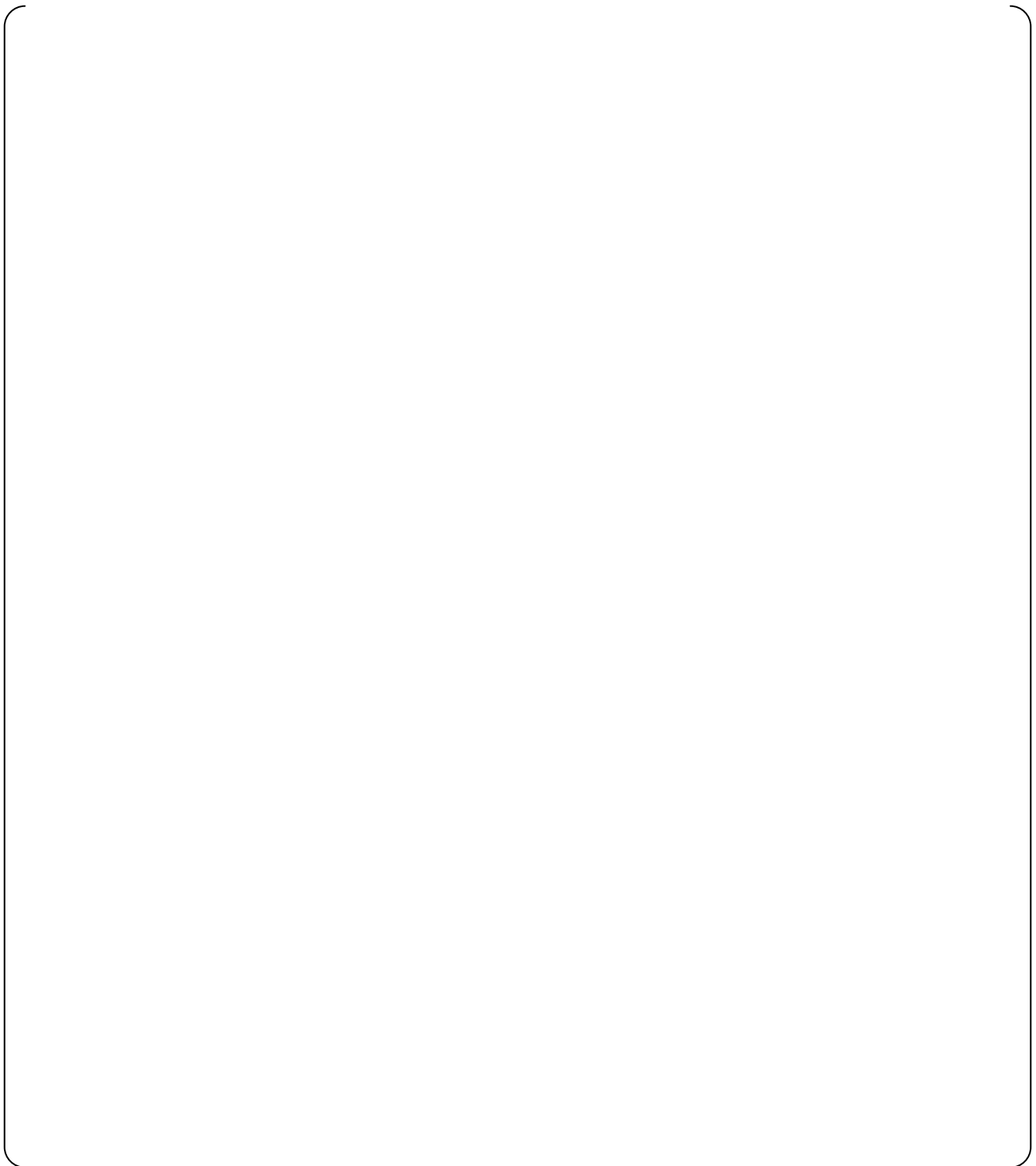


Fig. 4.2.4-8 (2/2) Full Height 1/2-Scale Test Results (Case 4)2/2



**Fig. 4.2.4-9 (1/2) Full Height 1/2-Scale Test Results (Case 5) 1/2**



**Fig. 4.2.4-9 (2/2) Full Height 1/2-Scale Test Results (Case 5) 2/2**

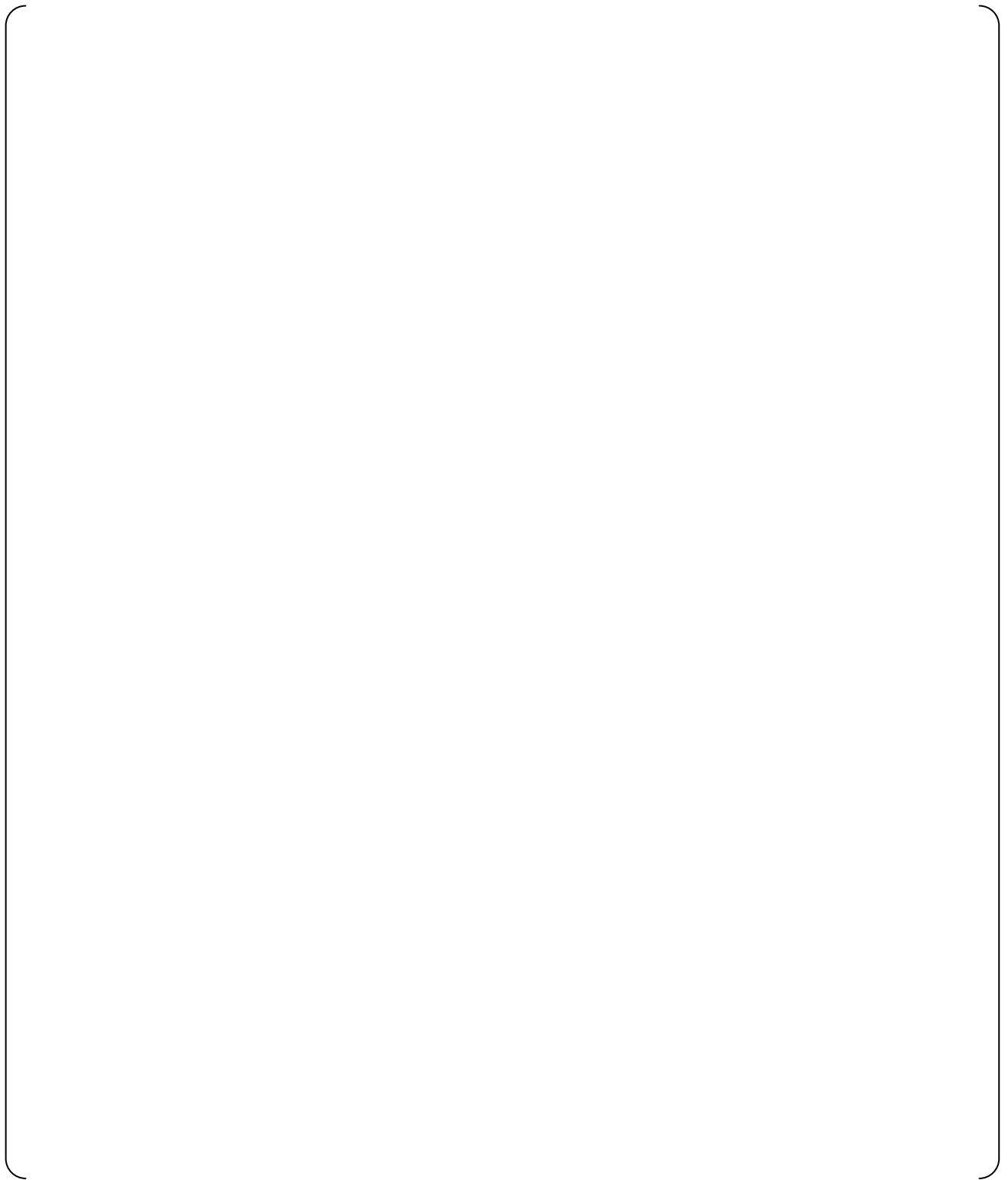


**Fig. 4.2.4-10 (1/2) Full Height 1/2-Scale Test Results (Case 6) 1/2**

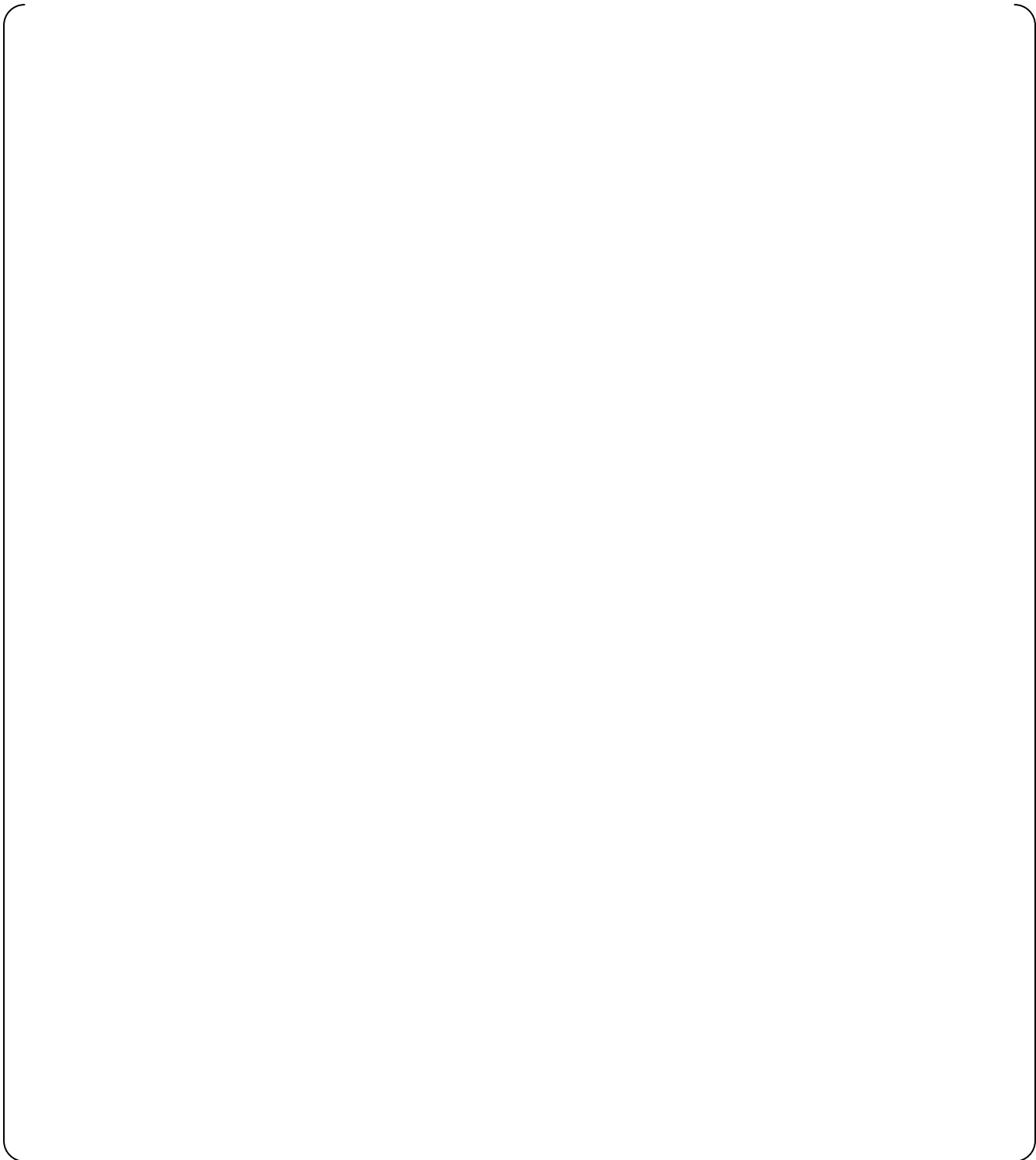


**Fig. 4.2.4-10 (2/2) Full Height 1/2-Scale Test Results (Case 6) 2/2**

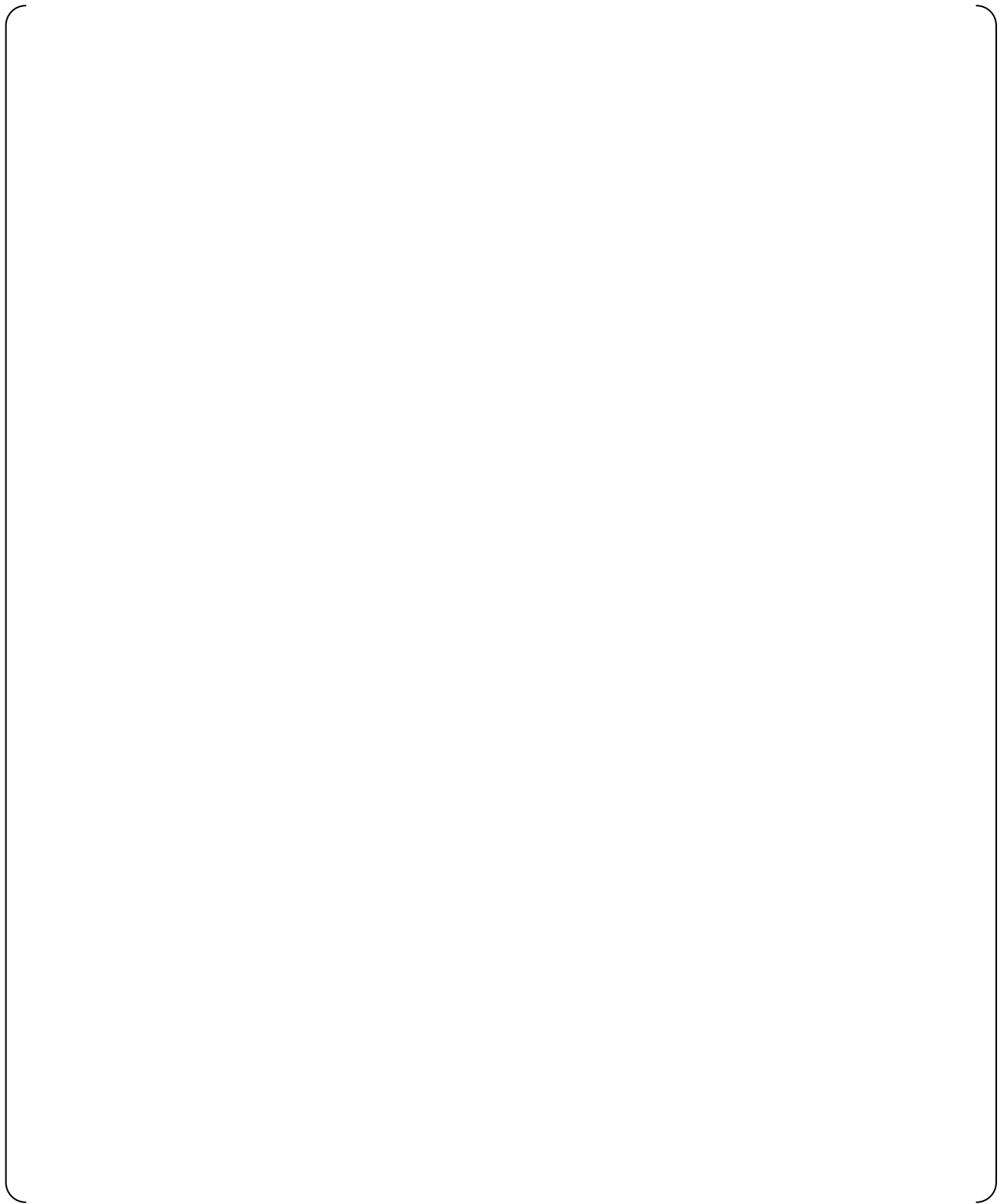


**Fig. 4.2.4-11(1/2) Full Height 1/2-Scale Test Results (Case 7) 1/2**

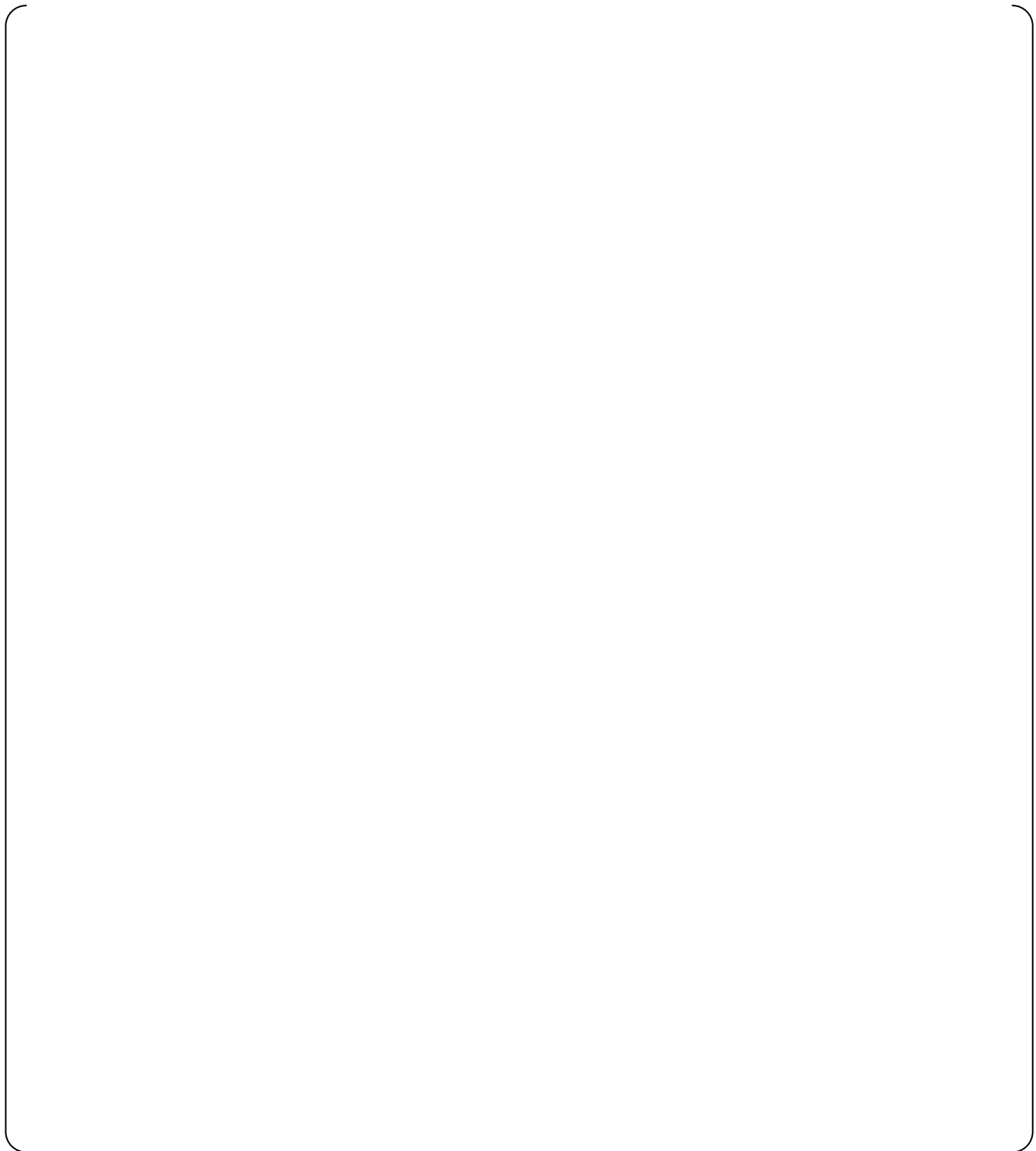


**Fig. 4.2.4-11(2/2) Full Height 1/2-Scale Test Results (Case 7) 2/2**

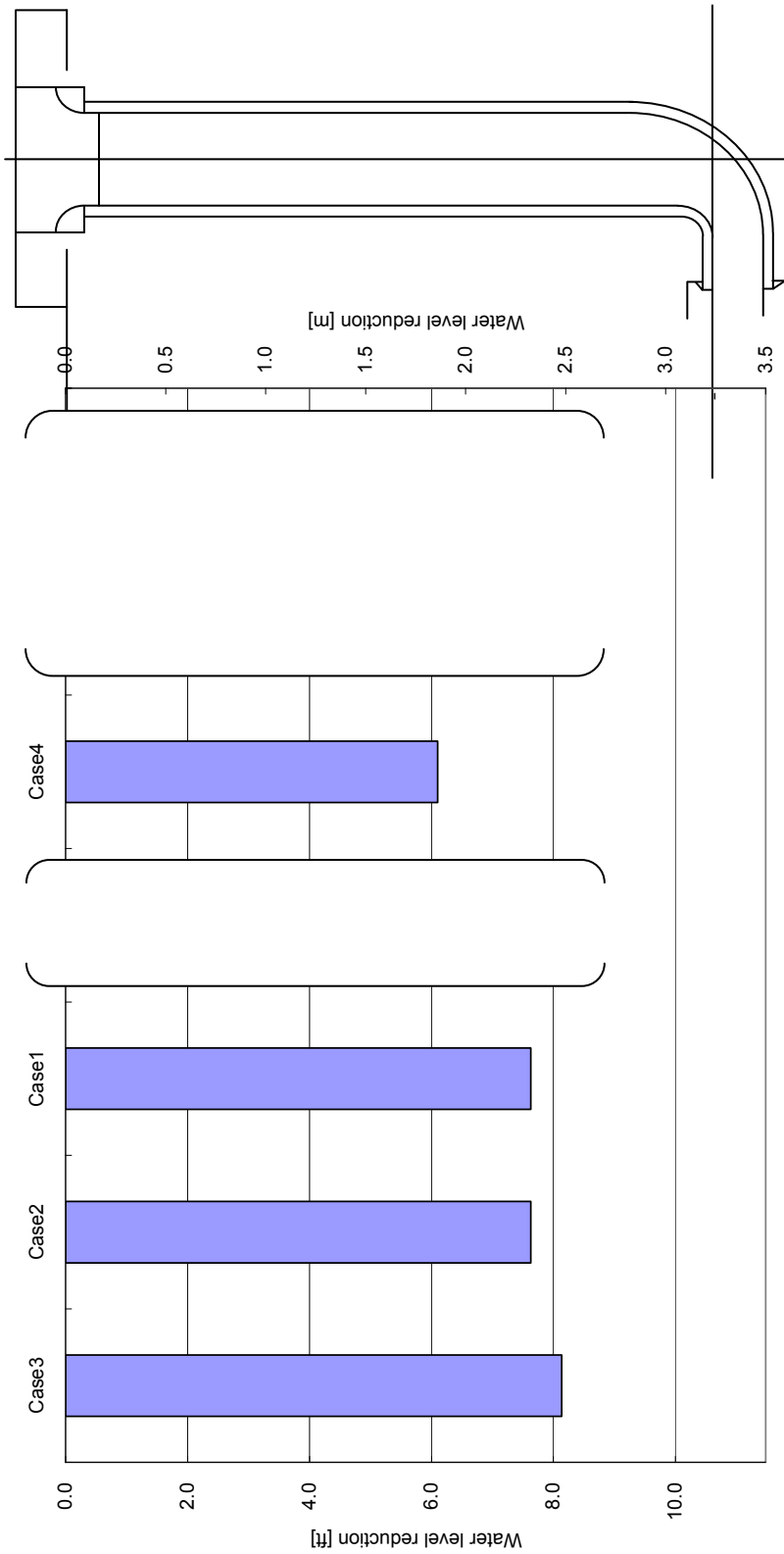
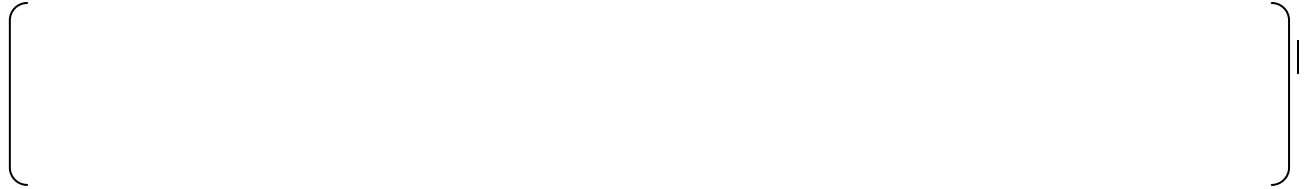


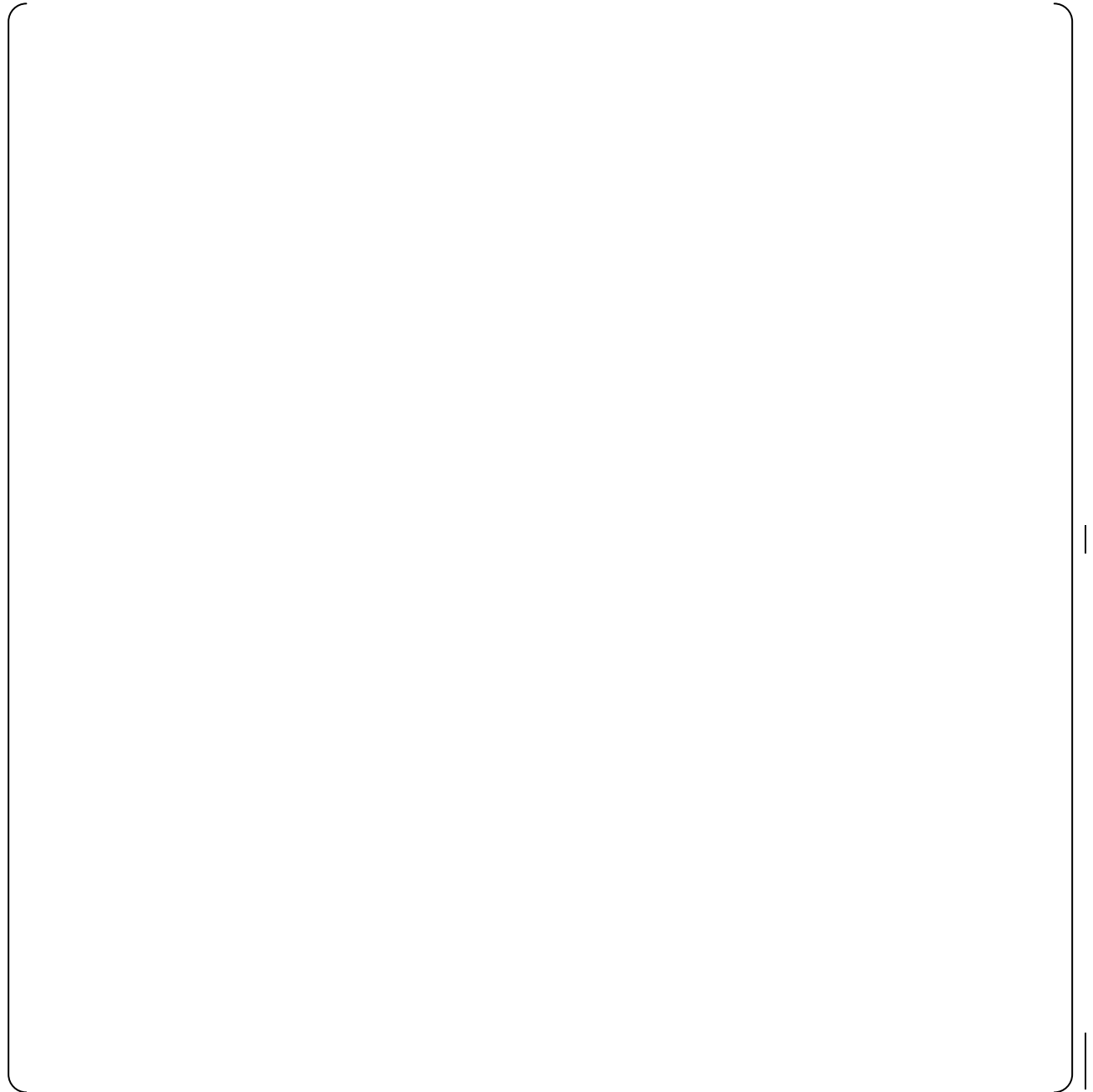
Fig. 4.2.4-12 The Test Results of Water Level Reduction During Flow Rate Switching

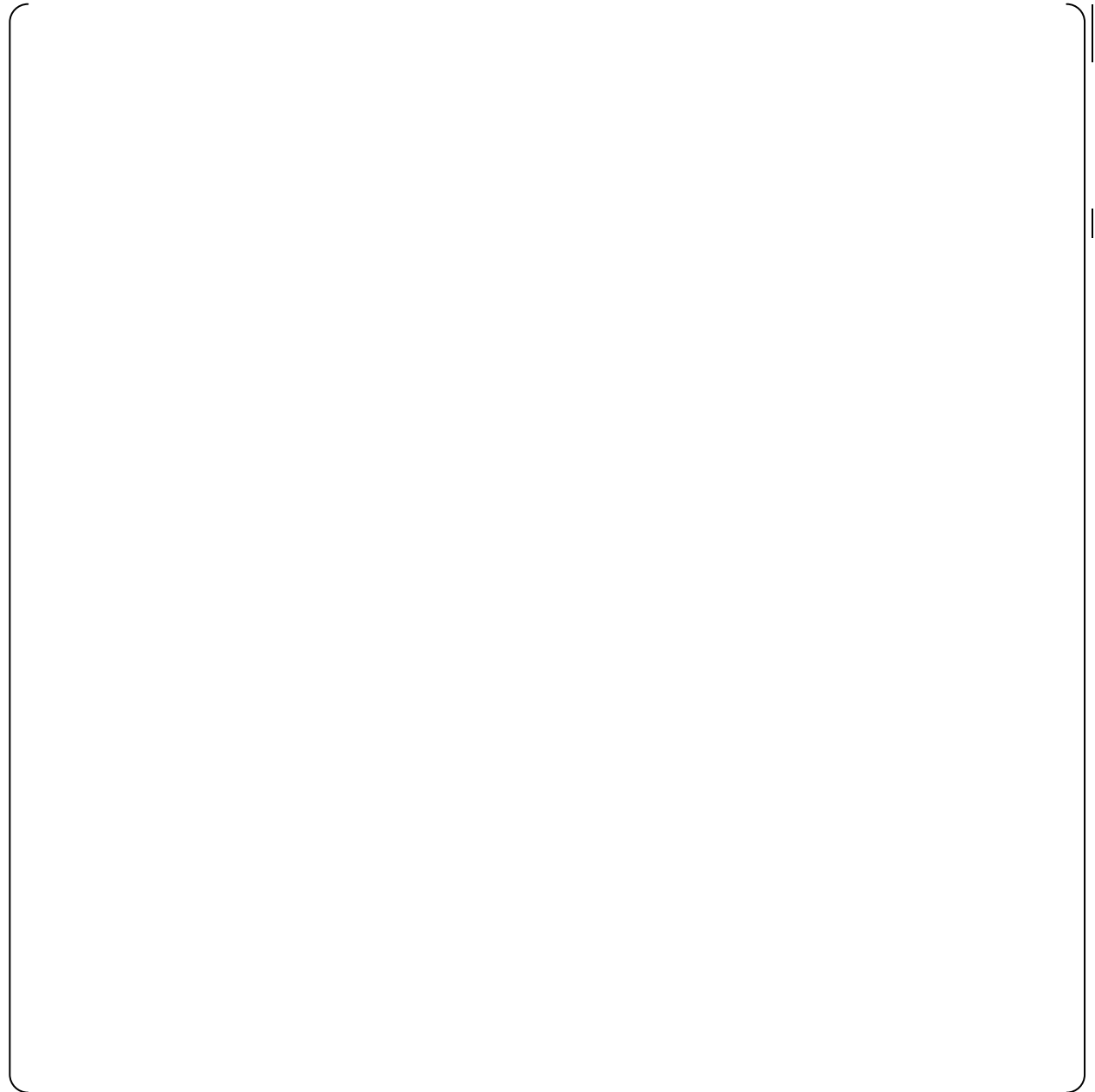
### **4.3 Validity and Scalability of Flow Rate Characteristics**



#### **4.3.1 Large Flow Injection**

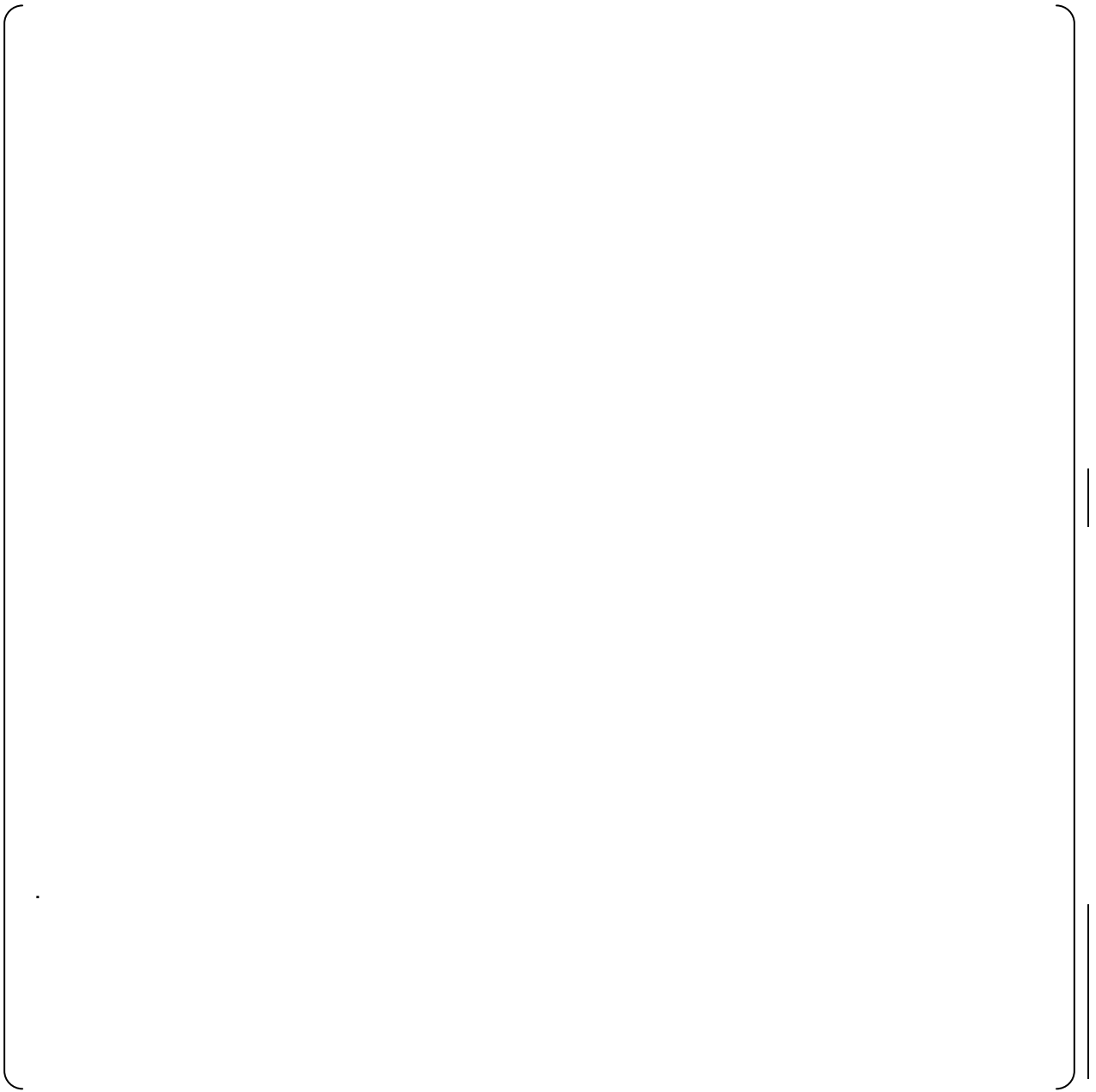
##### **4.3.1.1 Phenomenological Features and Effects on Flow Characteristic**

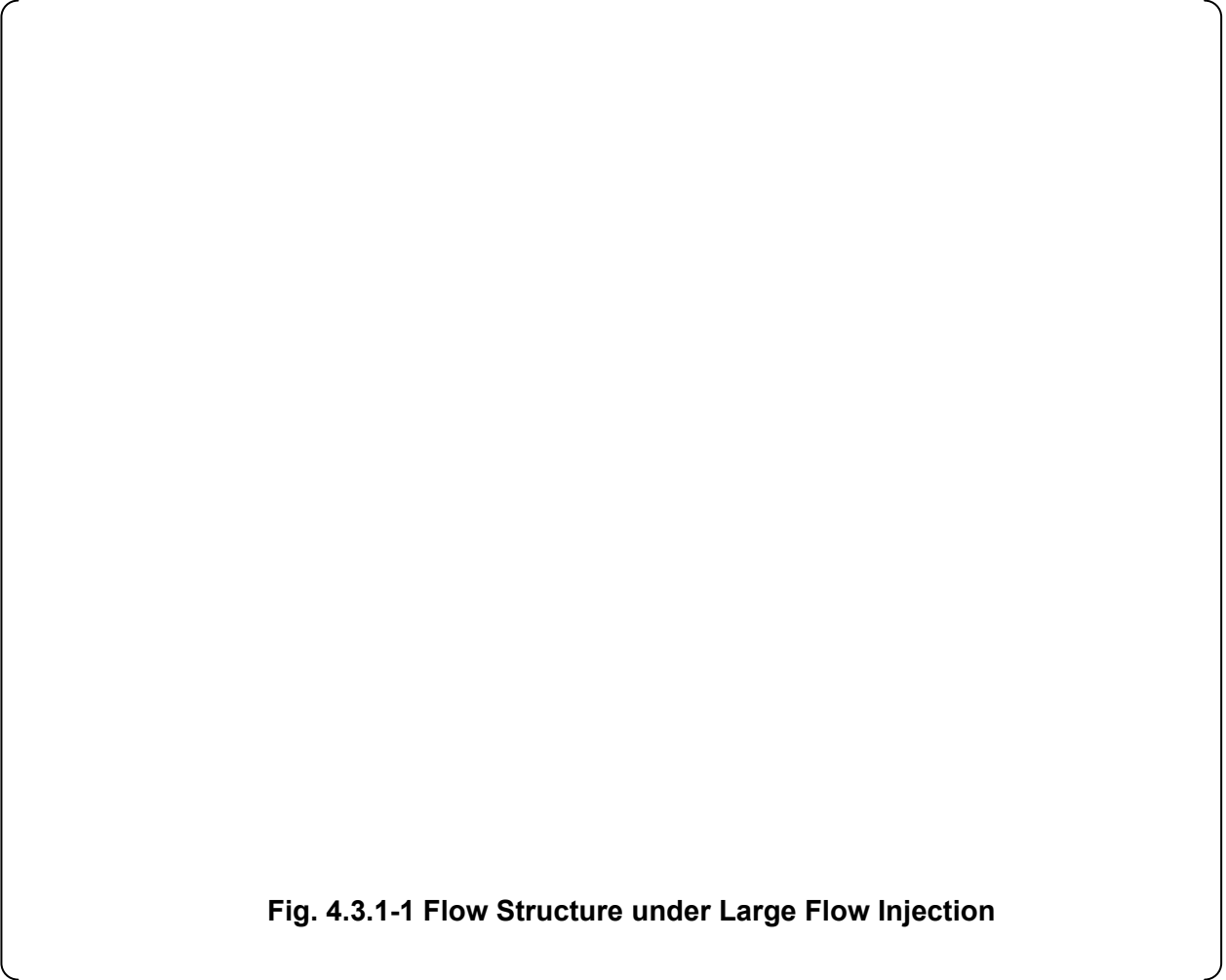




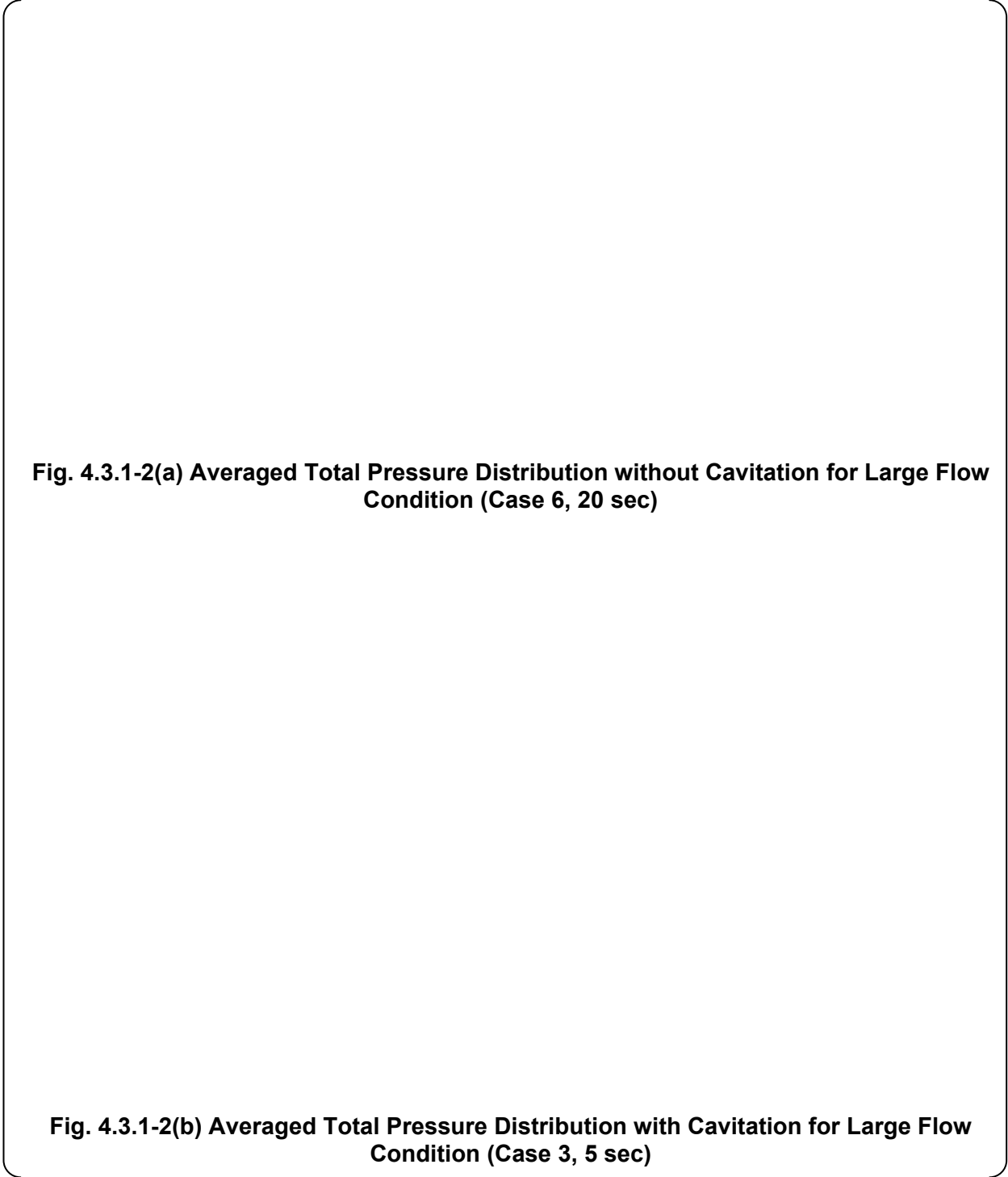
The friction factor  $\lambda$  in particular, is a function of the Reynolds Number. The friction factor becomes less dependent on the Reynolds Number when the Reynolds Number is large, such as the values for the ACC shown in Table 4.3.1-1.

Pressure loss due to the area change also occurs in the outlet nozzle. The loss occurs in the outlet nozzle and is dependent on geometrical shape for contraction and expansion. The contraction and expansion angles, as well as the relative length ( $L/D$ ), are directly scaled between the 1/2 and full-scale ACCs.



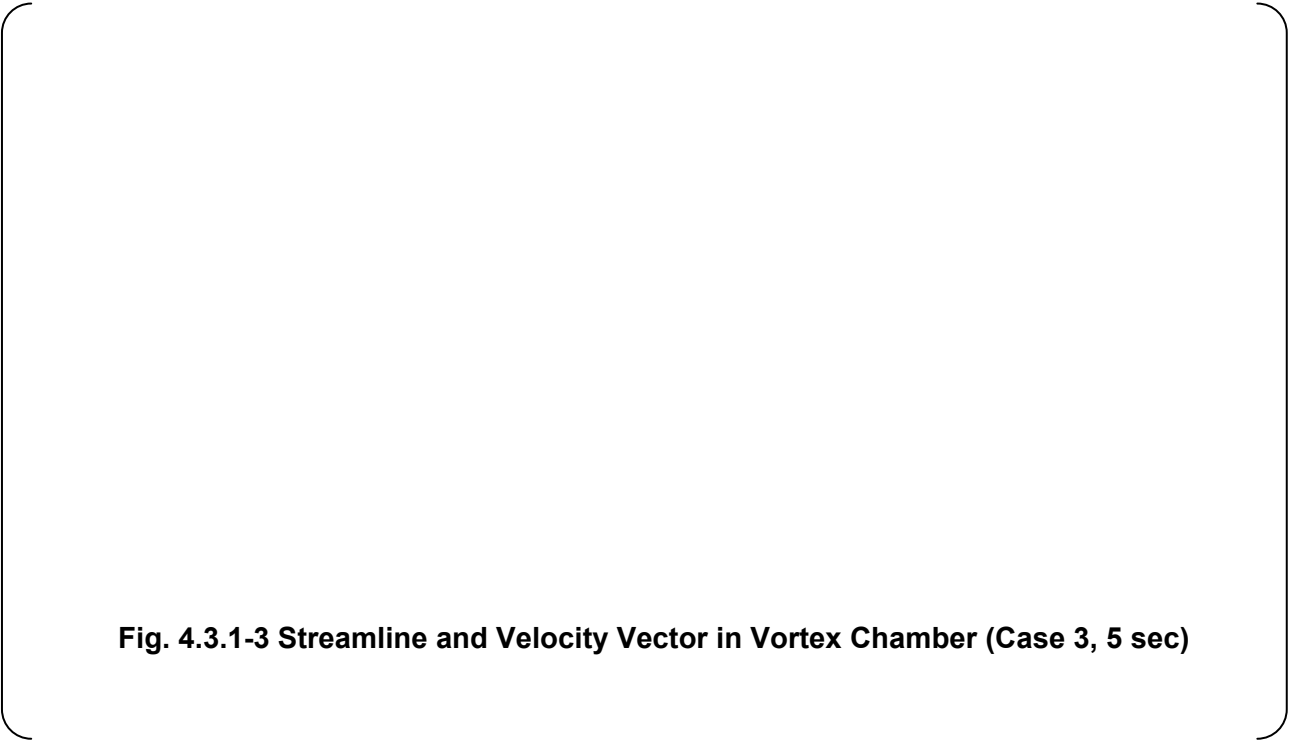


**Fig. 4.3.1-1 Flow Structure under Large Flow Injection**



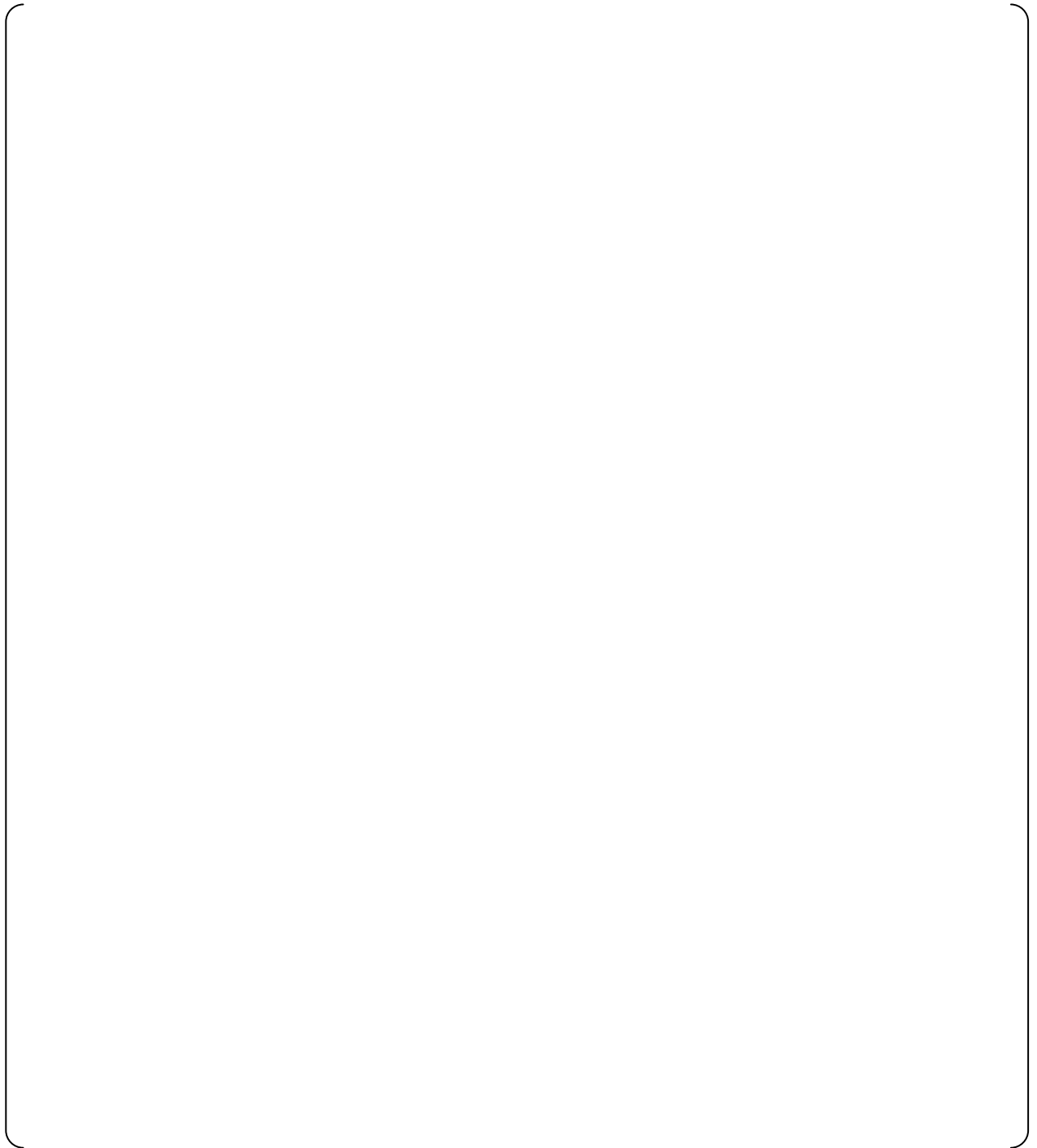
**Fig. 4.3.1-2(a) Averaged Total Pressure Distribution without Cavitation for Large Flow Condition (Case 6, 20 sec)**

**Fig. 4.3.1-2(b) Averaged Total Pressure Distribution with Cavitation for Large Flow Condition (Case 3, 5 sec)**



**Fig. 4.3.1-3 Streamline and Velocity Vector in Vortex Chamber (Case 3, 5 sec)**

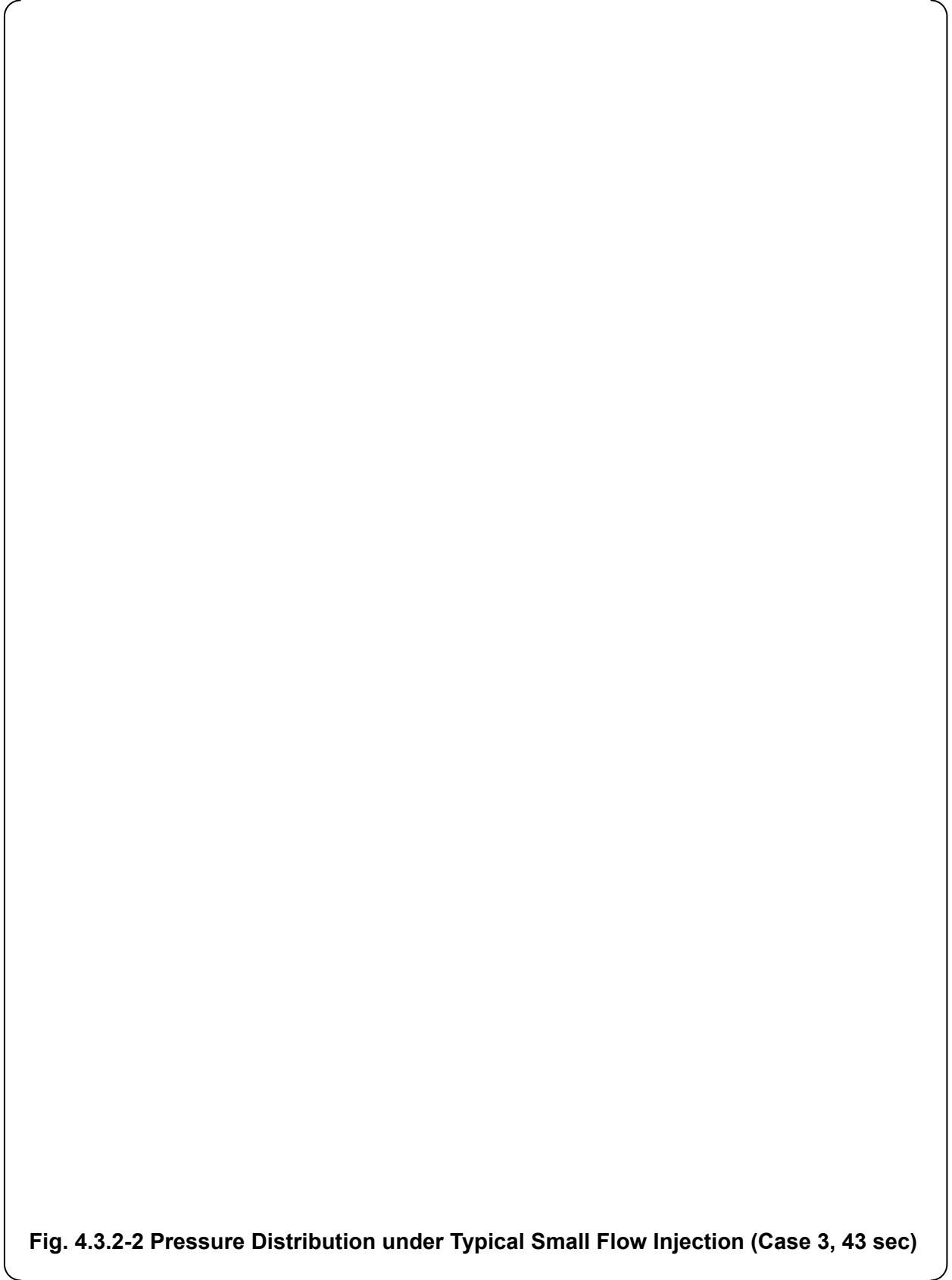
**Table 4.3.1-2 Dimension Comparison between Full Height 1/2-Scale and Full-Scale**



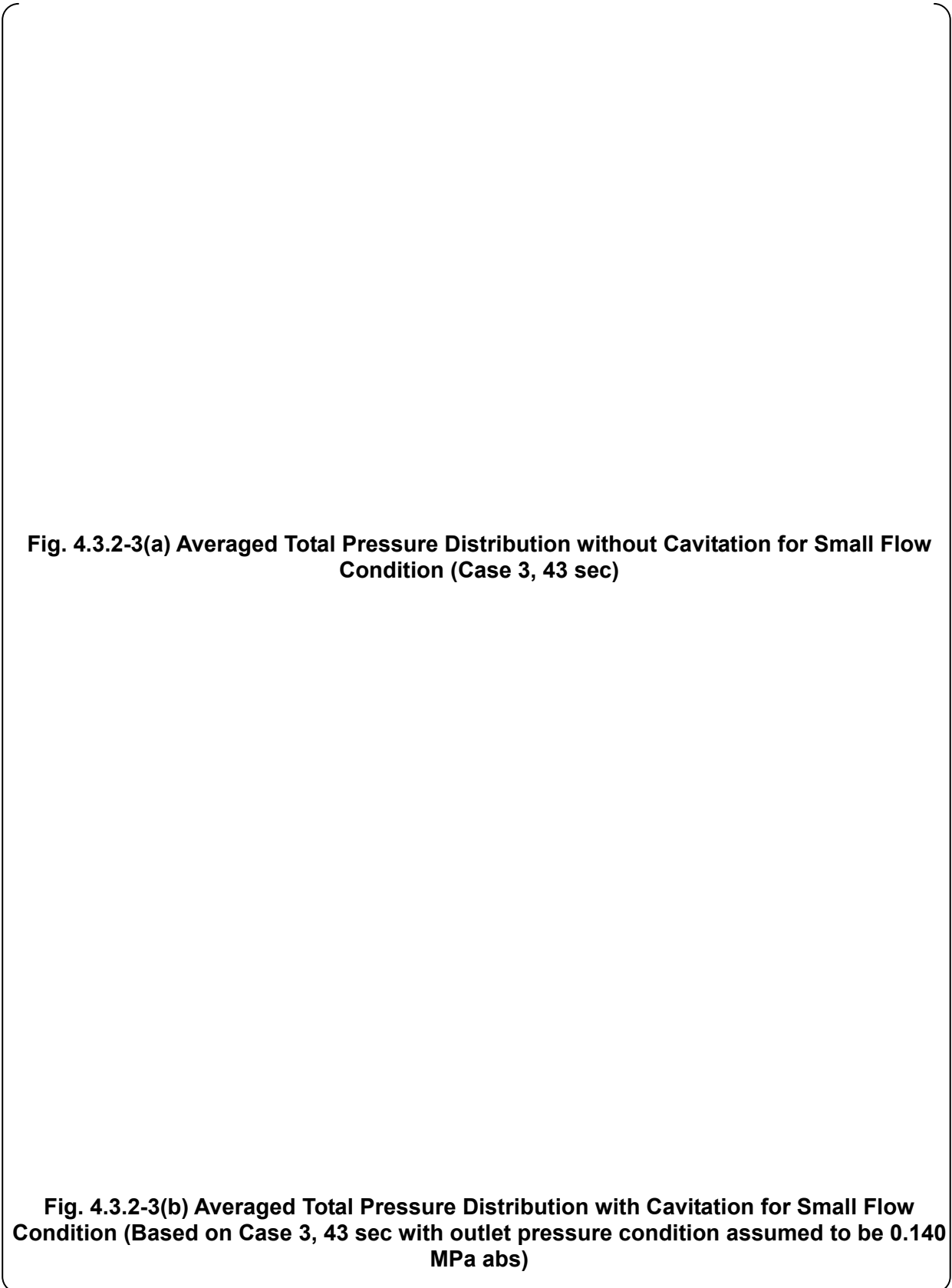
**Fig. 4.3.1-4 Flow Rate Coefficient with Respect to Cavitation Factor of Flow Damper for Full Height 1/2-Scale and 1/5-Scale Models**

### **4.3.2 Small Flow Injection**

**Fig. 4.3.2-1 Flow Structure of Small Flow Phase**

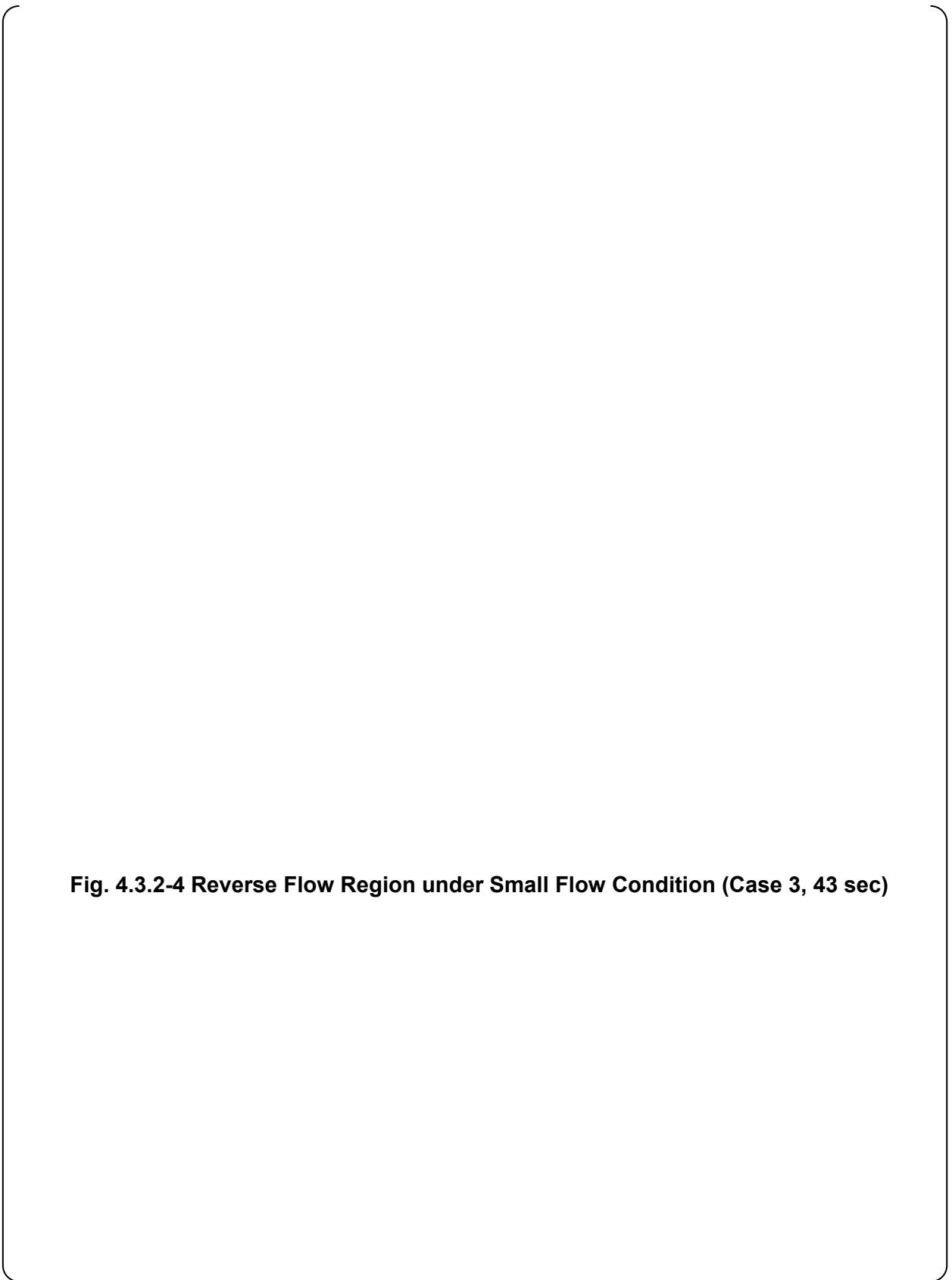


**Fig. 4.3.2-2 Pressure Distribution under Typical Small Flow Injection (Case 3, 43 sec)**

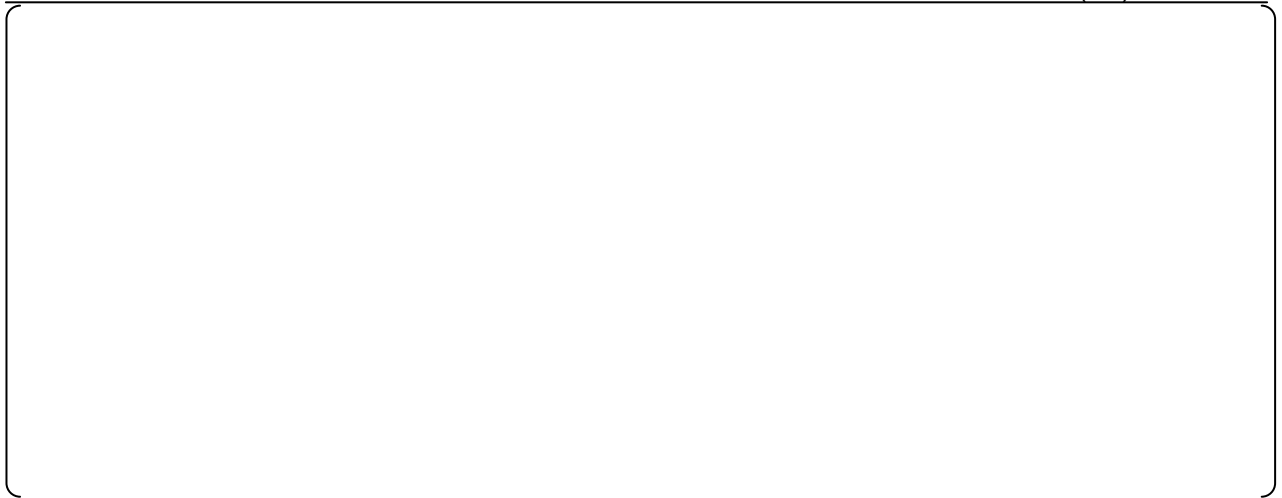


**Fig. 4.3.2-3(a) Averaged Total Pressure Distribution without Cavitation for Small Flow Condition (Case 3, 43 sec)**

**Fig. 4.3.2-3(b) Averaged Total Pressure Distribution with Cavitation for Small Flow Condition (Based on Case 3, 43 sec with outlet pressure condition assumed to be 0.140 MPa abs)**



**Fig. 4.3.2-4 Reverse Flow Region under Small Flow Condition (Case 3, 43 sec)**



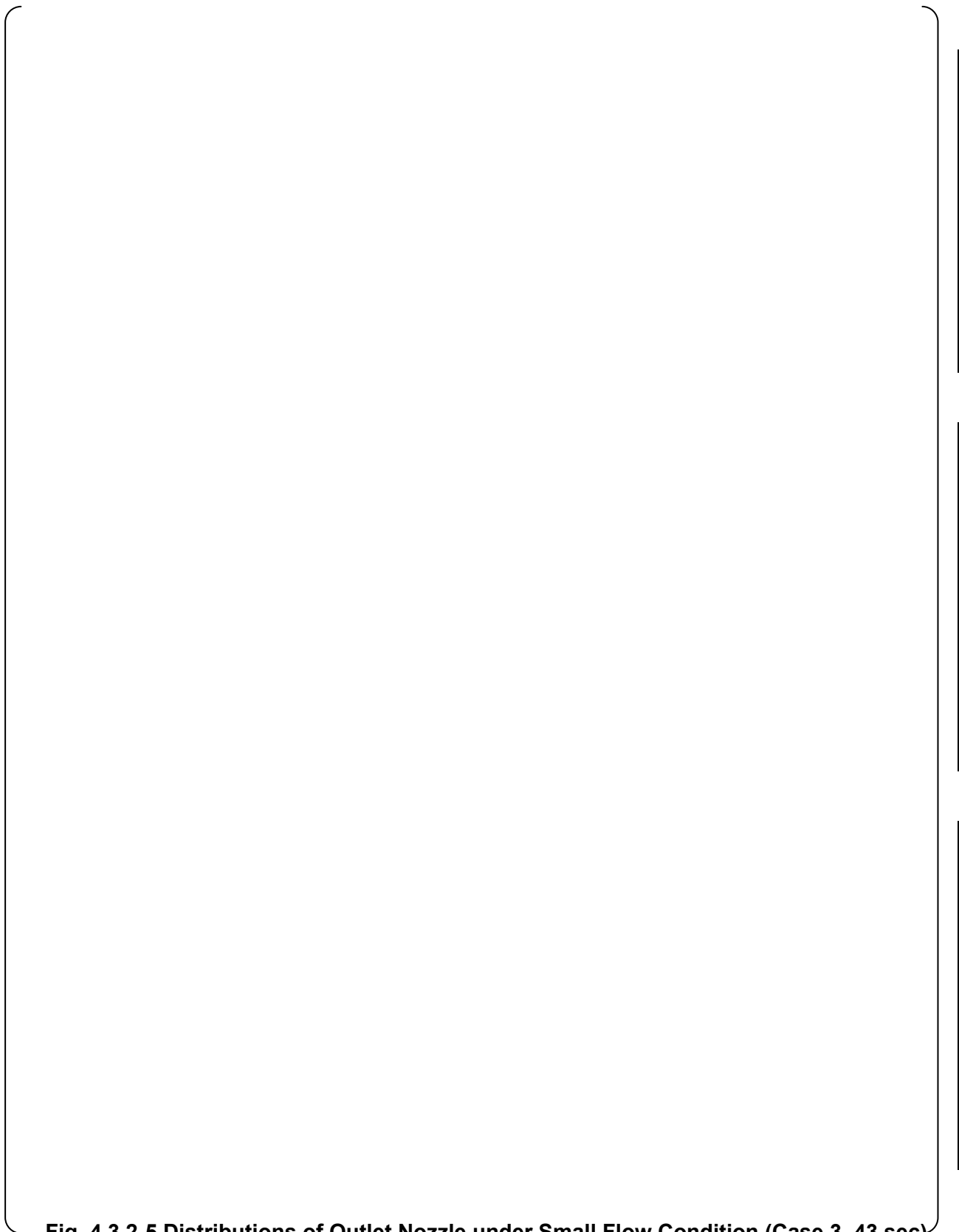
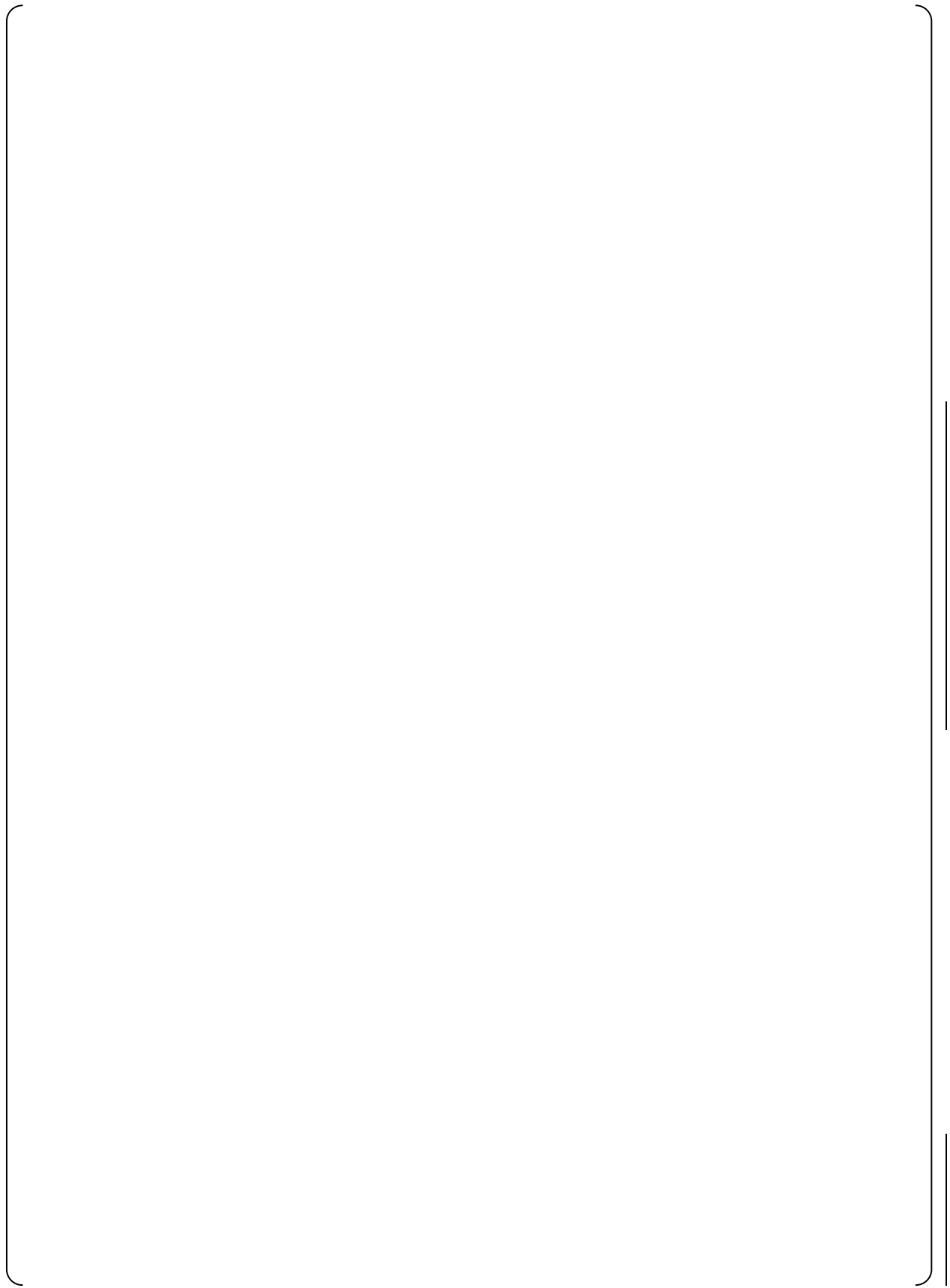


**Fig. 4.3.2-5 Distributions of Outlet Nozzle under Small Flow Condition (Case 3, 43 sec)**





**4.3.2.2 Scalability of Flow Rate Characteristics**

**Table 4.3.2-1 Sample of Input Values and BLC\* for Small Flow Injection**

**Table 4.3.2-2 Swirl Number Comparison between 1/2-Scale and Full-Scale**

**Fig. 4.3.2-6 Comparison of Distributions of Outlet Nozzle under Small Flow Condition (Case 3, 43 sec) between 1/2-scale and full scale CFD**



## **4.4 Quality Assurance of the ACC Test Program**

### **1) General**

The results of the ACC test program, performed from June 1994 to August 1996, are applicable to the US-APWR. These results were reviewed and MHI confirmed that the requirements of the Japanese QA Guideline and QA activities at that time meet the requirements of 10 CFR 50 Appendix B and ASME NQA-1-1994, by comparing the two sets of requirements.

### **2) Procedure of Re-verification**

The ACC test program was re-verified and confirmed to be reliable and accurate for use in the US-APWR. This re-verification was performed by evaluating the following items in accordance with a written procedure.

- (1) Confirmation of Test Procedure
- (2) Evaluation of Test Personnel
- (3) Evaluation of Test Equipment
- (4) Evaluation of Test Procedure (execution)
- (5) Evaluation of Test Results
- (6) Evaluation of Design Personnel Performing the Test

### **3) Results**

It was confirmed that the reliability and accuracy for the ACC test program satisfied the requirements of 10 CFR 50 Appendix B and ASME NQA-1-1994.

The following text describes the re-verification results of the above six items.

#### **(1) Confirmation of Test Procedure**

The ACC test program can be applied to the US-APWR by comparing the test conditions as follows:

- MHI established test conditions for the ACC of the US-APWR consistent with the design requirements for the ACC of the US-APWR.
- MHI compared the previous APWR test conditions with the test conditions established for the US-APWR and confirmed that the previous test conditions are applicable to the US-APWR.
- The test conditions that were compared and confirmed were the following prerequisite conditions for the test:
- Prerequisites: - Adverse conditions (considering operating modes and environments)
  - Configuration
  - Test scope addressed applicable design features

## **(2) Evaluation of Test Personnel**

It was confirmed that the test personnel who had conducted the previous tests satisfied the current required qualifications as follows:

- MHI reviewed the qualifications of the test personnel who had conducted the previous tests against current qualification requirements (NQA-1-1994 2S-1).
- MHI established records documenting this re-verification of the qualifications of the testing personnel.

## **(3) Evaluation of Test Equipment**

It was confirmed that the condition and the accuracy of the test equipment and measurements used during the testing meet current requirements taking into account the test objectives for the US-APWR. The results of this validation were as follows:

- MHI documented the test objectives and test results required for the US-APWR based on the design conditions for the ACC of the APWR.
- Based on this document, MHI established the requirements for the accuracy of test equipment and measurements for the US-APWR.
- MHI determined that the accuracy of the test equipment and measurements used in the ACC test program at that time satisfy the requirements for the US-APWR.

## **(4) Evaluation of Test Procedure (execution)**

It was confirmed that the test procedure used for conducting the ACC tests at that time meets the current requirements as follows:

- MHI documented the design requirements for the US-APWR (i.e., items that must be verified in the test) based on the design conditions for the ACC as used in the US-APWR.
- MHI confirmed that the test procedure used at the time the tests were conducted meets the present requirements and is appropriate. This was done by comparing the items that were to be verified by those tests with the above identified design requirements for the US-APWR to be verified by test.

## **(5) Evaluation of Test Results**

Test results were evaluated by the responsible design organization and it was confirmed that the test results obtained could be applied to the US-APWR.

- MHI documented this evaluation of the applicability of the past test results to the US-APWR.

## **(6) Evaluation of Design Personnel Performing the Test**

Design personnel responsible for the test at that time had participated in the test process from the commencement of test preparations (e.g. test plan, test procedure, test equipments) to the completion of the tests and had both witnessed and evaluated the test results. MHI also confirmed that the design test program was independently reviewed by experienced engineers and that the tests were witnessed by representatives of the utilities that funded the

tests and MHI. Therefore, it was concluded that the test at that time was objective. MHI confirmed that the design personnel had participated in the design of the test plan, test procedure, and test equipment and also in the evaluation of test results from evidence such as meeting minutes, trip reports, and document review reports, etc.

- MHI confirmed based on meeting minutes, trip reports, etc. that meetings concerning the test plan, test procedure, and test equipment had been held with the utilities and that the designs had been reviewed by the utilities and their comments had been incorporated.
- MHI confirmed that the design appropriate personnel of the utilities and MHI had witnessed the actual test.
- MHI confirmed that the design review (e.g. Design Review Board) for the overall review of the test, including the test plan, test procedure, test equipment, and test results, was conducted by independent experienced engineers.

## **5.0 CONCEPT OF THE SAFETY ANALYSIS MODEL**

Section 5 describes how to apply the hydraulic performance measured from the 1/2-scale test results to the full-scale ACC in the safety analysis. The accumulator flow rate is modeled in the safety analyses through parameters such as the characteristic equations of the flow damper and its uncertainty, uncertainty of flow rate switching, and the effect of dissolved nitrogen and scaling effect. According to the methodologies outlined below, these parameters are treated appropriately in the safety analyses.

### **5.1 Flow Rate Characteristics for Safety Analysis**

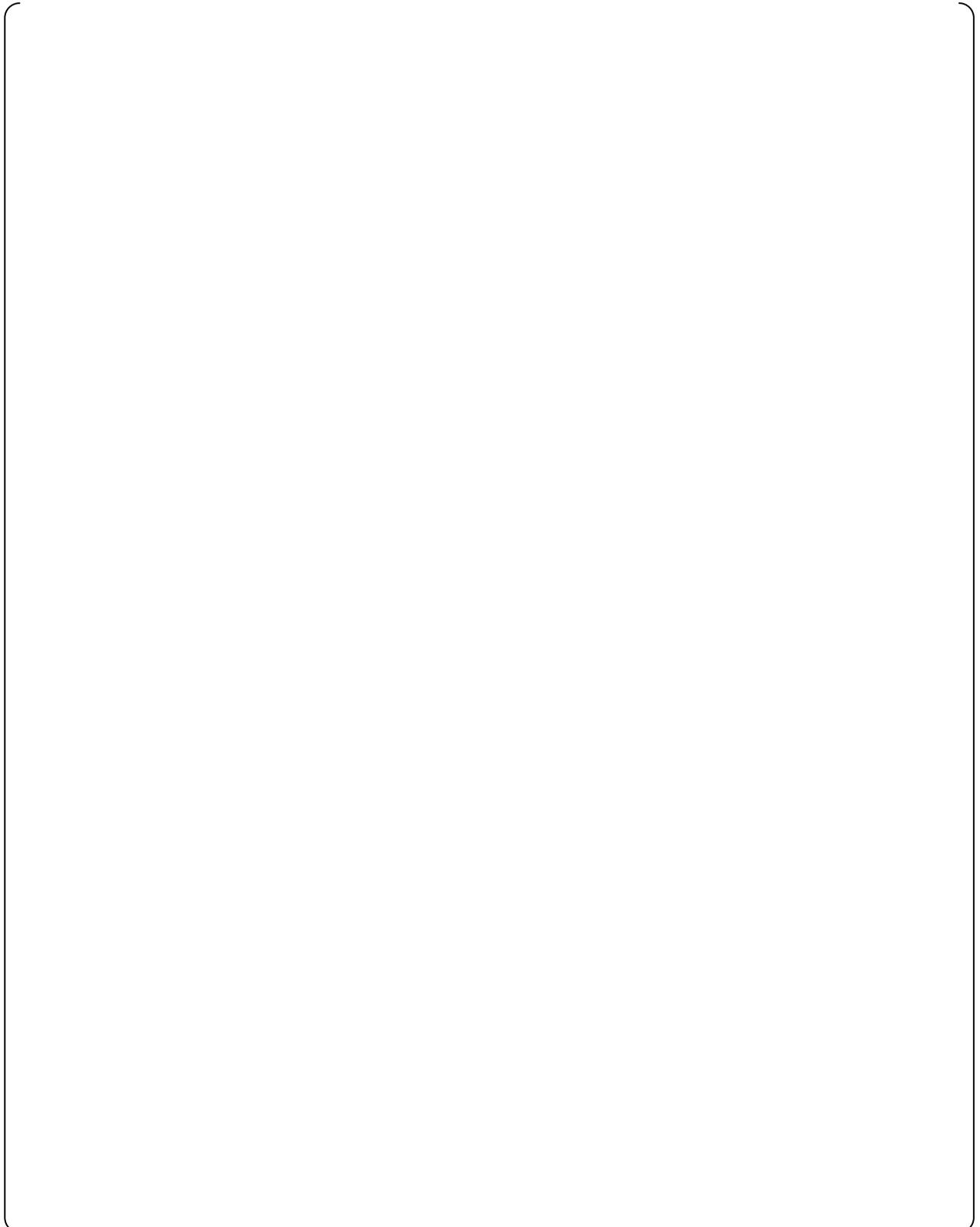
Subsection 5.1 discusses characteristic equations for accumulator flow rates and its uncertainties used in the safety analysis.

#### **5.1.1 Characteristic Equations of Flow Rates for the Safety Analysis**



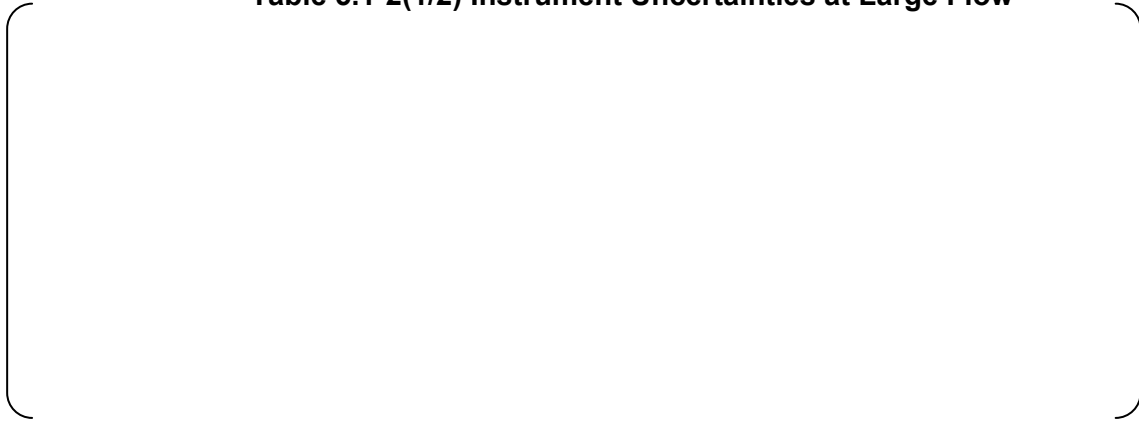
**Fig. 5.1-1 The Flow Characteristics of the Flow Damper**

### 5.1.2 Estimation of Uncertainty of the Characteristic Equations of Flow Rates

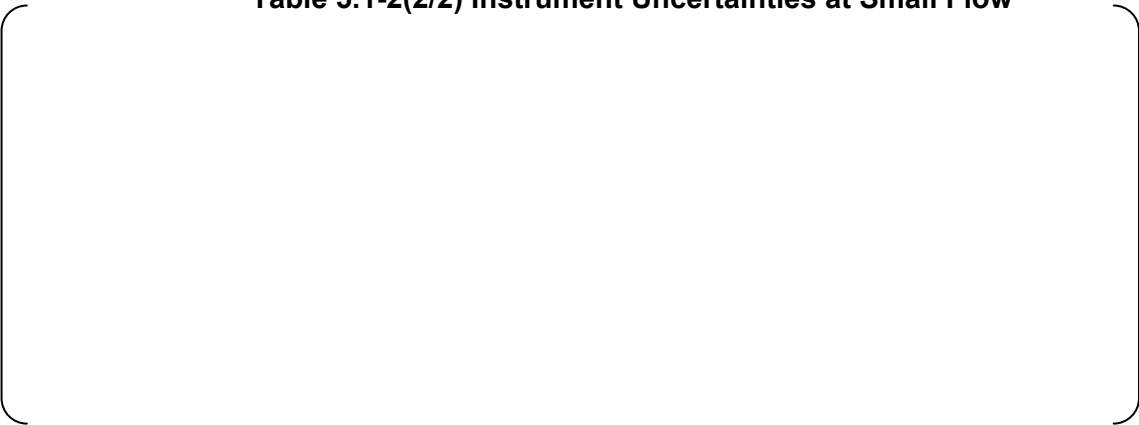


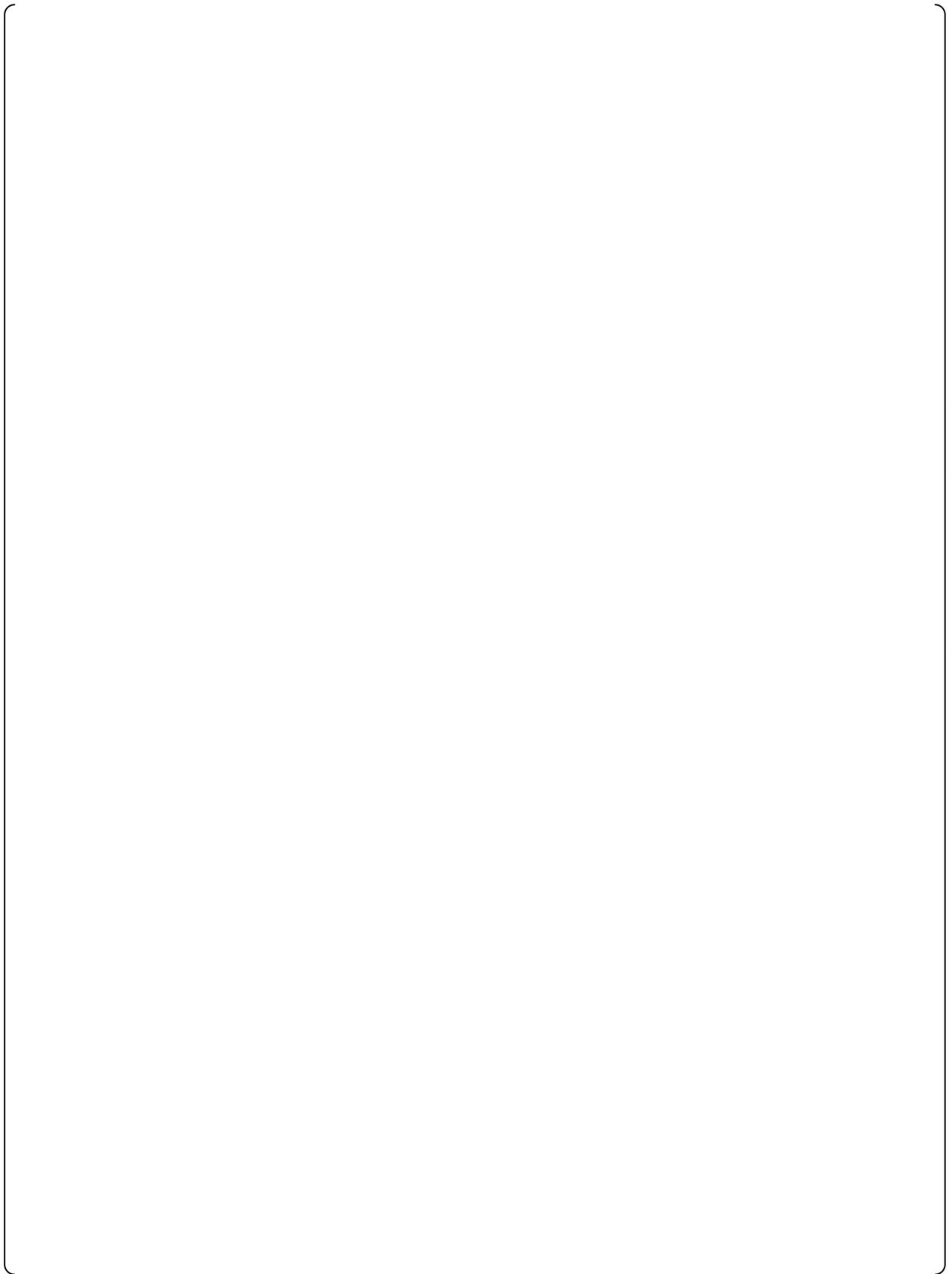
**Table 5.1-1 Dispersion of the Data from the Experimental Equations**

**Table 5.1-2(1/2) Instrument Uncertainties at Large Flow**



**Table 5.1-2(2/2) Instrument Uncertainties at Small Flow**





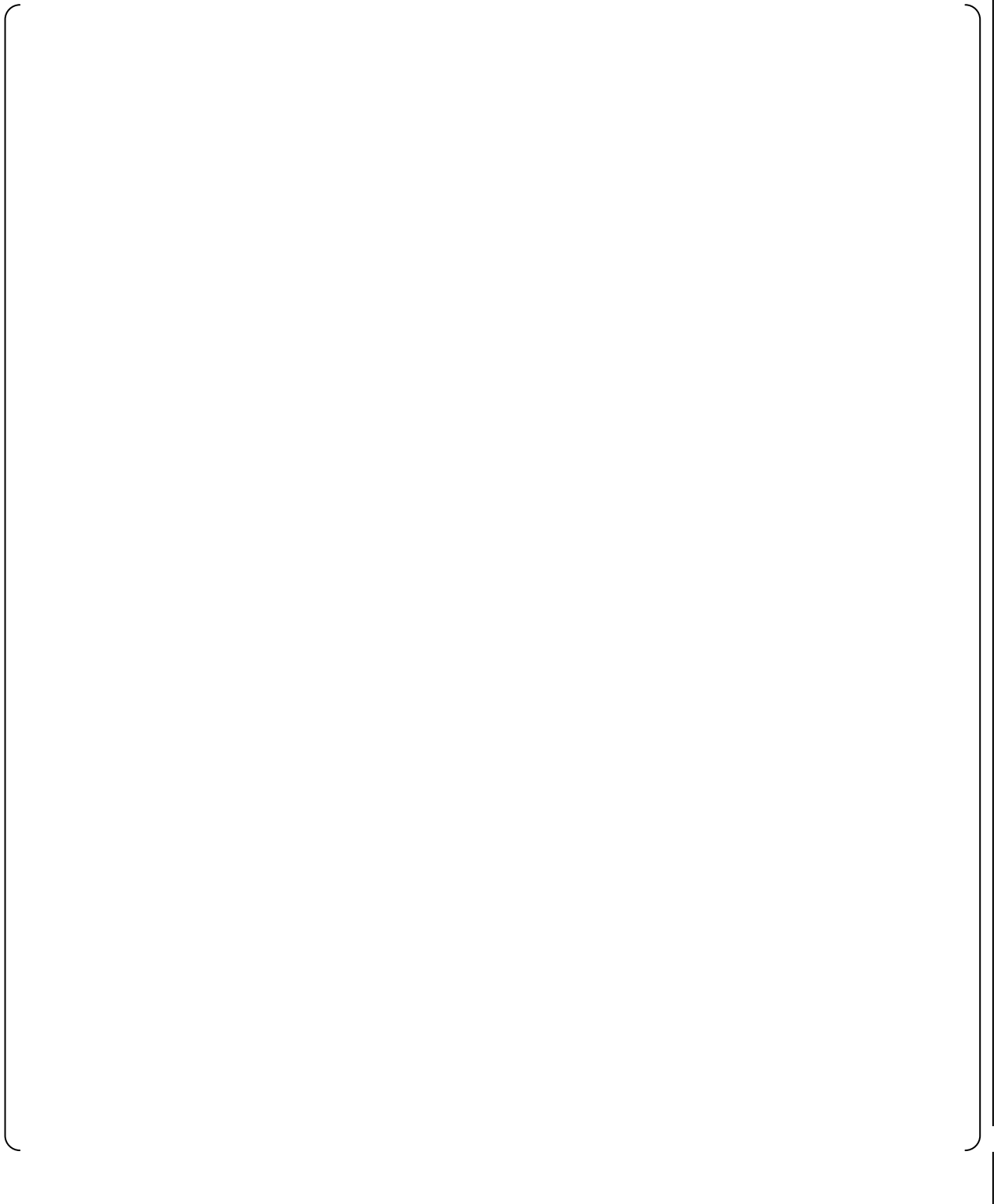


**Table 5.1-3 Total Uncertainty of Flow Rate Coefficient (Experimental Equations) for Safety Analysis of US-APWR**

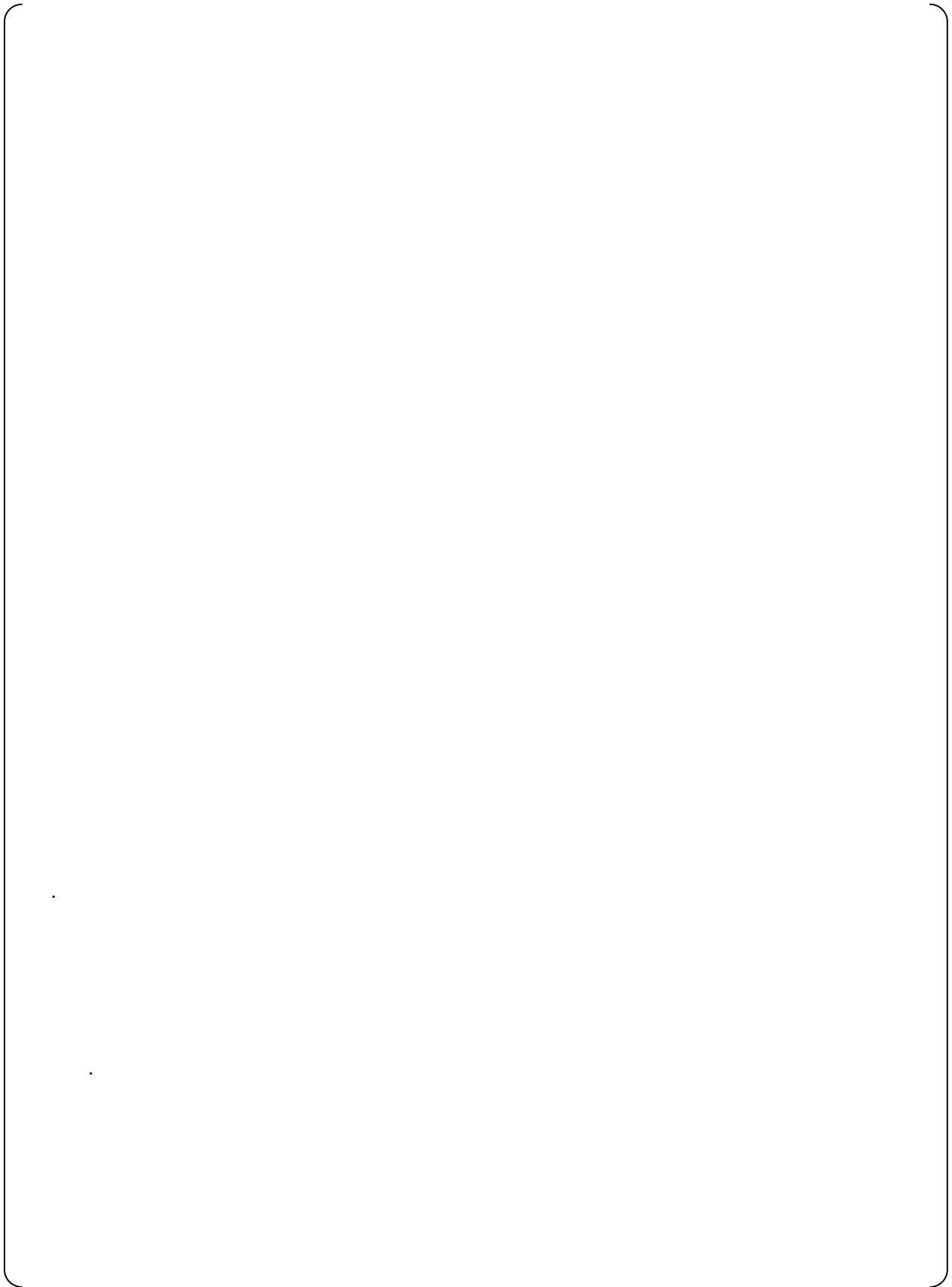
**5.2 Estimation of Potential Uncertainties of Water Level for Switching Flow Rates**

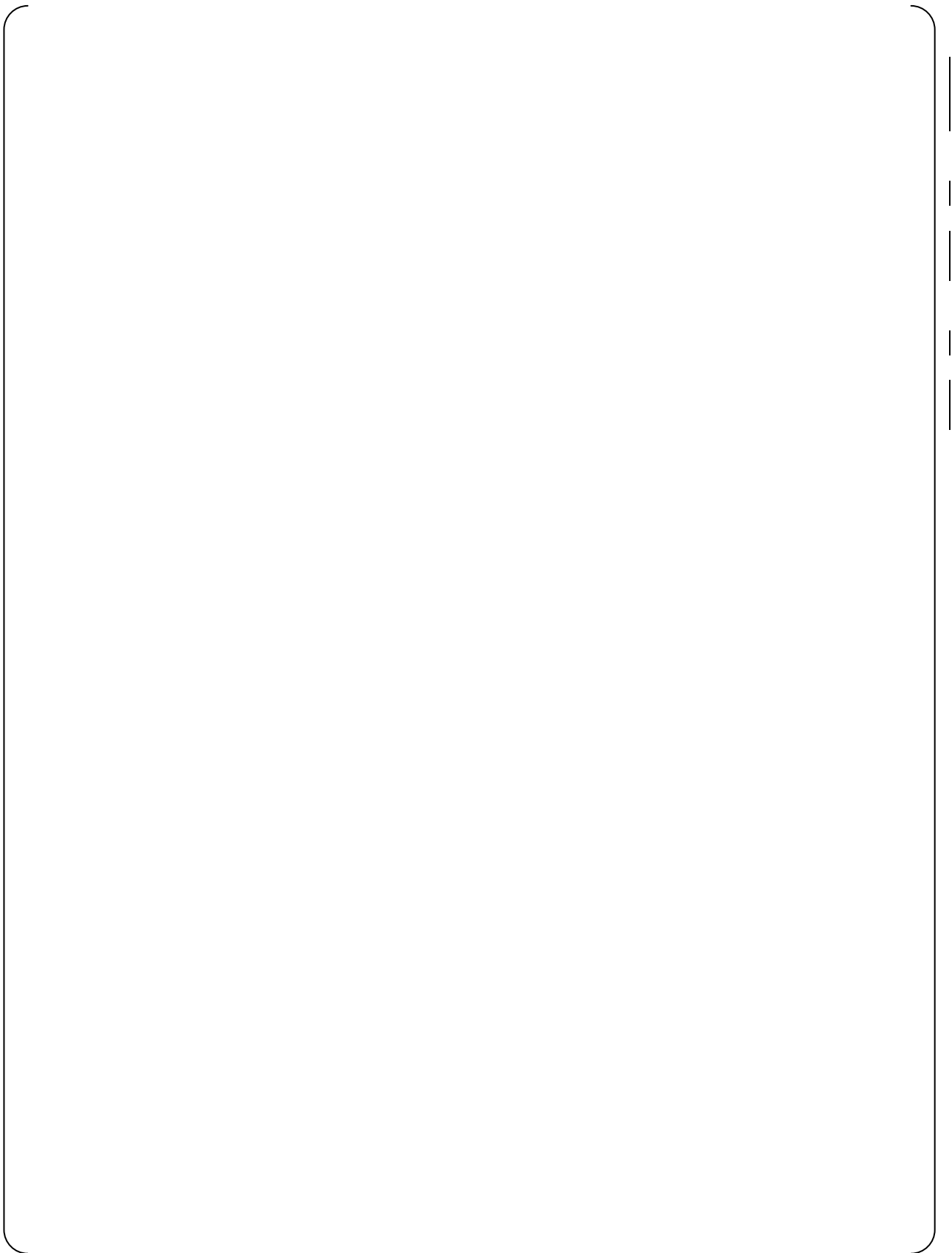
**Table 5.2-1 Uncertainty of Water Level for Switching Flow Rates**

### **5.3 Treatment of Dissolved Nitrogen Gas Effect in the Safety Analysis**

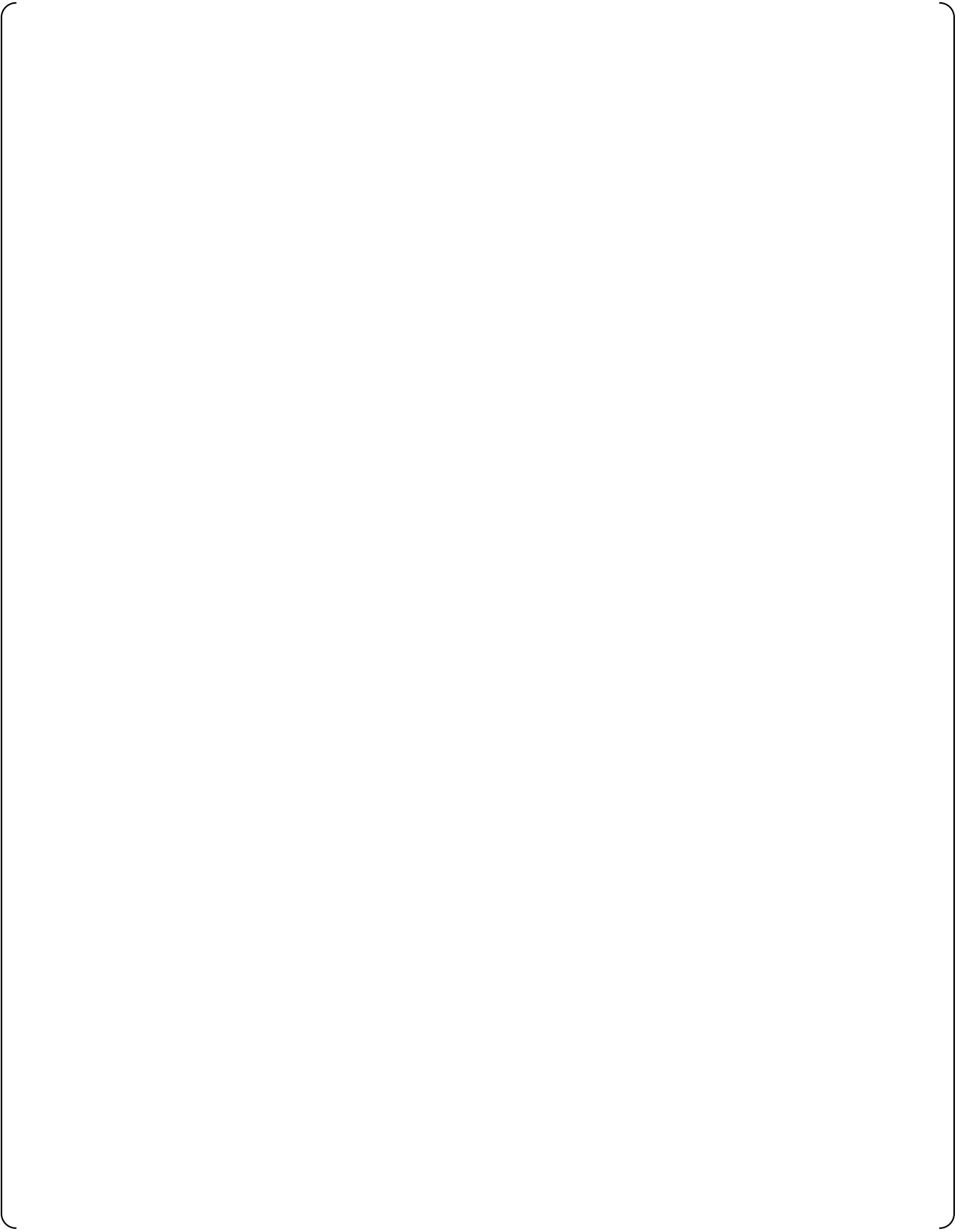
#### **5.4 Estimation of Scaling Effect for Characteristic Equations**

**Table 5.4-1 CFD-evaluated Scaling Effect** <sup>(Ref. 4.3-1)</sup>





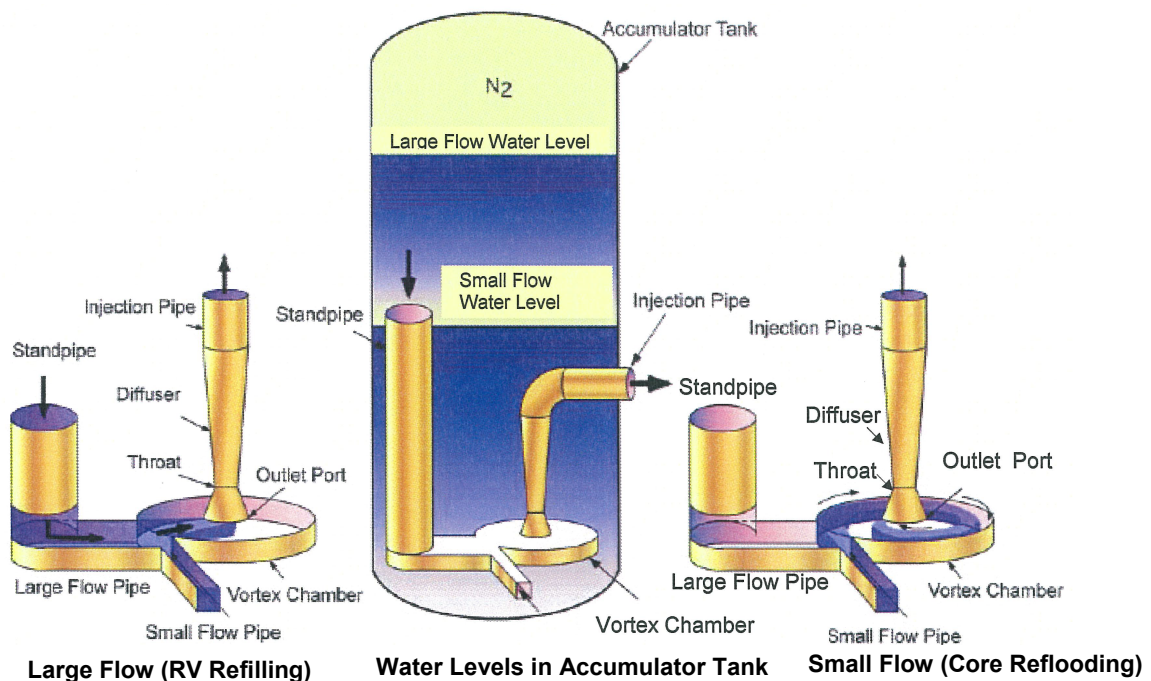
**6.0 CHARACTERISTIC EQUATIONS IN THE PRE-OPERATIONAL TEST**



## 7.0 SUMMARY

The Mitsubishi Heavy Industries, Ltd. Advanced Accumulator (ACC) design will be used in MHI's Advanced Pressurized Water Reactors. The ACC design simplifies the emergency core cooling system design by integrating the short term large flow rate design requirements currently satisfied in conventional pressurized water reactor designs by the combined injection capabilities of the primary system accumulator and the low head safety injection pump into a single passive device, the ACC.

The ACC is a borated water storage tank with a fluidic device that throttles the flow rate of cooling water injected into a reactor vessel from a large to a small flow rate. A conceptual drawing of the ACC is shown below.



The vortex chamber at the inlet of the injection pipe in the accumulator accomplishes the flow rate throttling from large flow to small flow by establishing a vortex (and thus a large pressure drop) at a predetermined accumulator level. The inlet of the standpipe is located at the ACC volume level at which the transition from large to small flow is desired to occur. The ACC is a simple device that achieves precise throttling from a large injection flow rate to a small injection flow rate with no moving parts.

Upon initiation of a large break loss of coolant accident, all short term low head primary coolant injection flow requirements are satisfied by the ACC. Following depletion of the ACC water volume, the long-term ECCS flow requirements are met by the high-head safety injection pumps thus eliminating the need for low head safety injection pumps. The immediate availability of low head flow provided by the ACC upon loss of electrical power coincident with a large break loss of coolant accident provides additional time for actuation of the backup emergency power source.

The design requirements and specifications of the ACC for the US-APWR are the same as that for the APWR. The confirmatory test program for the APWR was successfully conducted as a joint study among five utilities (Japan Atomic Power Co., Hokkaido Electric Power Co., Kansai Electric Power Co., Shikoku Electric Power Co., and Kyushu Electric Power Company) and MHI, from September 1994 to September 1996. The tests confirmed the principles of operation of the flow damper and successfully established the ACC flow characteristics. Specifically, the testing confirmed that:

1. No vortex was formed during large flow and a stable vortex was formed during small flow in the vortex chamber.
2. Sharp flow rate switching occurred without gas entrainment.
3. The flow characteristics of the flow damper can be characterized by dimensionless numbers.

Empirical flow rate coefficients have been developed from the test results and will be used in an integrated thermal hydraulic model of the US-APWR Reactor Coolant and ECCS systems to assure the US-APWR meets or exceeds all US safety standards.

The ACC design is expected to improve the safety of pressurized water reactors by the innovative application of the flow damper to assure the early stage of LOCA injection flow is satisfied by an inherently reliable passive system. This innovation reduces the necessity of relying on maintenance sensitive components such as low head safety injection pumps for assuring LOCA injection flow, provides additional time for actuation of backup emergency power for loss of power coincident with a large break LOCA, and reduces the net maintenance and testing burden by the elimination of low head safety injection pumps from the LOCA mitigation strategy.

## 8.0 REFERENCES

- 4.3-1 Mitsubishi Heavy Industries, Ltd., CFD Analysis for Advanced Accumulator, MUAP-09025-P Revision 3, June 2013.
- 4.3-2 S.S. Fineblum, Vortex Diodes, pp. 48-80, Proceedings of the Fluidic State-of-the-art Symposium Held at Naval Ordnance Laboratory, White Oak, Maryland on 30 September - 3 October, 1974.
- 4.3-3 J. W. Stairmand, Flow patterns in vortex chambers for nuclear duties, Vol. 29, No. 6, pp. 413-418, Nucl. Energy, Dec., 1990
- 4.3-4 I.E.Idelchik, Handbook of Hydraulic Resistance, 3<sup>rd</sup> Edition, Jaico Pub House, 2005
- 4.3-5 W.S.Lewellen, A Review of Confined Vortex Flow, NASA CR-1772, July 1971
  
- 5-1 Mitsubishi Heavy Industries, Ltd., Large Break LOCA Code Applicability Report for US-APWR, MUAP-07011-P
- 5-2 Mitsubishi Heavy Industries, Ltd., Small Break LOCA Methodology for US-APWR, MUAP-07013-P

### Studies on Vortex Behaviors in Flow Diodes

Flow in vortex diodes is similar to flow in the vortex chamber of the flow damper for small flow injection. Papers with regard to vortex diodes are useful to investigate the vortex behaviors for small flow injection in the vortex chamber of the flow damper. J. W. Stairmand described the flow patterns and dominant mechanisms in a vortex chamber (Ref. 4.3-3). S. S. Fineblum reported his excellent experimental results on various geometries of vortex diodes in 1974 (Ref. 4.3-2). This section provides the summaries of these reports.

#### 1. Summary of Qualitative Investigation

J.W. Stairmand indicated that the dominant mechanism for flow in a vortex chamber is the conservation of angular momentum. In other words, he notes that the dominant mechanism for flow in a vortex chamber is the conservation of circulation. The flow pattern in a vortex chamber consists of a free vortex region in the periphery where the circulation is conserved and a forced vortex region in the central part where a significant pressure drop occurs. Therefore in the design of fluidic devices, it is important to clarify at what point the transition from free to forced vortex occurs. Stairmand used the model that was first applied to the vortex valve by Wormley. This model assumes axisymmetry and uses the momentum integral method of solving the boundary layer equations. This identifies a developing flow region ( $r > r_c$ ) and a developed flow region ( $r < r_c$ ). In the developing flow region, the circulation is conserved; in the developed flow region, flow is restricted by the boundary layer and the circulation is not conserved. Predictions for the distribution of swirl velocity in the vortex chamber exhibit a variety of forms to characterize the free and forced vortex modes. A modified boundary layer coefficient ( $BLC^*$ ) as shown below, was found to largely determine which form is taken.

$$BLC^* = \frac{2AfS^*}{Re^{*0.25}}$$

where

$$A = \frac{R}{h}$$

$$Re^* = \frac{v_i(h/2)}{\nu}$$

$$S^* = \frac{w_i}{v_i}$$

$f$ : Friction factor for flow over the equivalent flat plate

$Re^*$ : Reynolds number

$A$ : Aspect ratio between the radius of the vortex chamber  $R$  and the height of the vortex chamber  $h$

$\nu$ : Kinematic viscosity

$S^*$ : Swirl number in the vortex chamber

$v_i$ : The value of the radial velocity  $v$  at  $r = R$

$w_i$ : The value of the tangential velocity  $w$  at  $r = R$

Wormley's theory has been used to predict the circulation distribution shown in dimensionless form in Fig. A-1. From this diagram it is clear that when  $BLC^*$  is 0.25 or less, the flow in the vortex chamber conserves circulation. When  $BLC^*$  is greater than 0.25, the

flow structure changes to a forced vortex at some critical radius. As  $BLC^*$  is increased, the extent of this central forced vortex increases until it occupies most of the vortex chamber ( $BLC^* = 2$ ).

The pressure profiles across the chamber are shown in dimensionless form in Fig. A-2. For  $BLC^*$  less than 1, the pressure profiles are substantially determined by inertial effects and an inviscid analysis is appropriate. Thus it seems that the viscosity effect is weak when  $BLC^*$  is 1 or less.

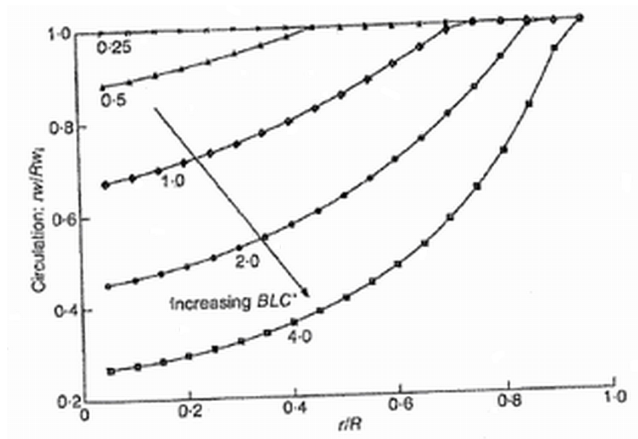


Fig. A-1 Calculated circulation distribution (Ref 4.3-3)

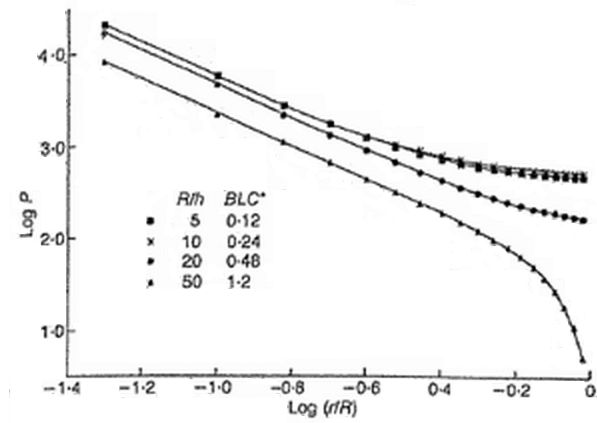


Fig. A-2 Calculated pressure profile (Ref 4.3-3)

## 2. Summary of Quantitative Investigations

### 1) Experiments

The vortex chambers used in his experiments varied in diameter,  $D$ , from 1.58 to 3.25 inches (40 to 82.6 mm) and in length,  $L$ , (equivalent to height of the vortex chamber,  $H$ , for the ACC) from 0.188 to 1.0 inches (4.78 to 25.4 mm). The nozzles varied in width from 0.016 to 0.4275 inches (0.4 to 11.1 mm), and the outlet varied in diameter from 0.179 to 0.394 inches (4.6 to 10.0 mm). The maximum available pressure,  $p$ , and flow,  $Q$ , were 100 psi ( $6.90 \times 10^5$  N/m<sup>2</sup>) and 6 gpm ( $3.79 \times 10^{-4}$  m<sup>3</sup>/sec). It is not clearly mentioned in the paper, but gas or air appeared to be the working fluid because of the large tangential velocities of the diodes. If the working fluid was air at 305 K in temperature, the maximum dimensionless flow rate (equivalent to Reynolds number)  $q^* = Q/(2\pi H\nu)$ , is from 82 to 440.  $\nu$  is the kinematic viscosity of the fluid.

### 2) Vortex Pressure Drop Coefficient

The pressure drop coefficient  $K$  is defined as:

$$K = \frac{P_o - P_i}{\frac{\rho}{2} V_N^2} = \frac{1}{n} (1 - R^{2n})$$

where  $R$  is the ratio of the outer-to-inner radii of vortex diodes,  $R = r_i/r_o$ ,  $r_i$  the radius of the vortex chamber,  $r_o$  the radius of the outlet port, and  $n$  the vortex exponent. The exponent,  $n$ , varies between -1 (forced vortex) and 1 (free vortex).

The tangential velocity,  $V$ , at an arbitral radius,  $r$ , is assumed to have the form:

$$V = V_N \left( \frac{r_i}{r} \right)^n,$$

where  $V_N$  is the tangential velocity from the nozzle.

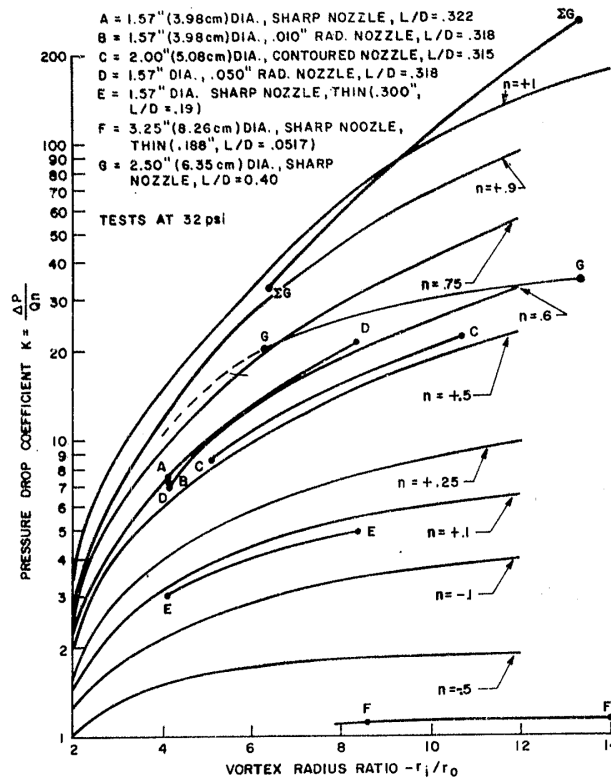


**Fig. A-3 Test Results: Total Pressure Drop Coefficient across Diode Versus Radius Ratio (Ref. 4.3-2)**

The variation of the pressure drop coefficient,  $K$ , with respect to the ratio of radii,  $R$ , is shown in Fig. A-3. Lines of computed  $K$  versus  $R$  with constant values  $n$  are plotted for comparison. The results of Fineblum show that for most vortex chambers the effective vortex exponent is approximately constant. The vortex exponent,  $n$ , should be chosen as an effective  $n$  to express the fact that many modes of flow in the vortex chamber result in a specific pressure drop and that the resulting pressure drop coefficient is a function of  $R$ . Therefore,  $n$  is an average correlation quantity rather than a true vortex exponent indicating the exact mode of vortex flow. The real flow in the vortex chamber is three dimensional due to the growth of boundary layers on the walls, which cannot be expressed by Eq. (2). Therefore, the vortex exponent " $n$ " cannot be theoretically determined, but has to be experimentally determined.

### 3) Effect of Height-to-Diameter Ratio

For very thin diodes the boundary layers on its disk walls will completely fill the chamber. As the height increases, the available distance free of the boundary layers increases. Once this free distance is much greater than the boundary layer, further increase in  $L/D$  is not beneficial.

The average vortex exponent,  $n$ , increases with  $L/D$  as seen in Fig.A-4. It supports the fact mentioned above. In the cases of the vortex diodes, the vortex exponent,  $n$ , becomes relatively insensitive to any increase above  $L/D=0.35$ . The insensitivity limit must depend on viscosity. If viscosity effect is smaller, thickness of the boundary layer on the wall in the vortex chamber must be thinner to give a smaller insensitivity  $L/D$  limit.

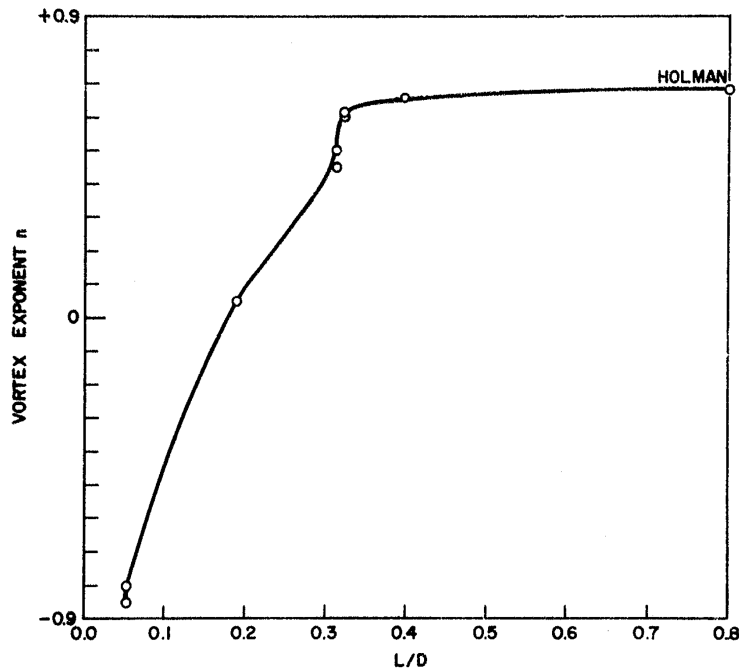


**Fig. A-4 Variation of Vortex Exponent,  $n$ , with respect to Ratio of Vortex Height to Diameter (Ref. 4.3-2)**

#### 4) Vortex Generated Pressure Drop in Outlet Tube

Fineblum stated that, "In most cases, the pressure drop measured across the outlet tube was relatively insignificant. However, at very high values of vortex radius ratio and vortex pressure drop coefficient, the pressure drop through the outlet tube is a major portion of the total." In this case, the pressure drop in the tube immediately downstream of the vortex chamber contributes significantly to the vortex generated pressure drop. It is important to note that the swirl flow in the outlet tube originates in the vortex chamber. This means that the pressure loss from swirl flow in the outlet tube is controlled by the vortex in the vortex chamber. Strictly speaking, the dynamic pressure converted from static pressure in the vortex chamber is lost in the outlet tube, if there is no static pressure recovery.